Journal of Marine Engineering & Technology

ISSN: 2046-4177 (Print) 2056-8487 (Online) Journal homepage: www.tandfonline.com/journals/tmar20

A CFD investigation on scale effects of open and ducted propellers

Vittorio Gallotti & Stefano Gaggero

To cite this article: Vittorio Gallotti & Stefano Gaggero (20 Mar 2026): A CFD investigation on scale effects of open and ducted propellers, Journal of Marine Engineering & Technology, DOI: 10.1080/20464177.2026.2647616

To link to this article: https://doi.org/10.1080/20464177.2026.2647616

Published online: 20 Mar 2026.

JOURNAL OF MARINE ENGINEERING & TECHNOLOGY
https://doi.org/10.1080/20464177.2026.2647616

A CFD investigation on scale effects of open and ducted propellers

Vittorio Gallotti and Stefano Gaggero

Department of Electrical, Electronic, Telecommunications Engineering and Naval Architecture, University of Genoa, Genoa, Italy

ABSTRACT

A systematic numerical investigation on the scale effects on the open water performance of open and ducted propellers is proposed. To this aim, two well-known open propellers, the conventional VP1304 and the tip-raked P1727 from the PPTC benchmark, and one ducted propeller in an accelerating nozzle and one ducted propeller in a decelerating nozzle, both from the BESST EU Project, are considered in the study. Results are obtained with the aid of RANSE-based simulations, using Star-CCM+ (open and ducted propellers) and OpenFOAM (open propeller only). Both are employed with the adoption of fully turbulent (model-scale and full-scale) and transition-sensitive (model-scale) turbulence models. A systematic variation of the model-scale rates of revolution (i.e. model-scale Reynolds number), encompassing usual values of towing tank and cavitation tunnel experiments, as well as the ambient turbulence intensity influencing turbulent boundary layer onset, are addressed for relatively large ranges of loading conditions for a complete overview of the phenomena influencing model-scale performance and scaling trends. Calculations show scale effects that are substantially different (higher, sometimes opposite) from those suggested by ITTC procedures and a non-negligible dependency on the flow conditions (in other words, the choice of the numerical model, initial values of calculations and loading conditions) that could make the definition of a scaling procedure, based on numerical calculations only, a very complex task.

ARTICLE HISTORY
Received 5 October 2025
Accepted 14 March 2026

KEYWORDS
Propeller scale effect; PPTC test case; ducted propellers; transition sensitive turbulence models; CFD; RANSE; propeller model-scale performance; propeller full-scale performance; laminar to turbulent boundary layer transition;

Introduction

The prediction of full-scale propeller performance is a critical aspect of naval architecture. The design and optimisation of marine propulsion systems require accurate full-scale predictions of propeller efficiency, thrust, and cavitation characteristics for the wide range of operating conditions the ship may encounter during her life. As such, the ability to extrapolate data from model-scale experiments to full-scale applications has long been a focus of research and development in the field. Traditionally, model-scale experiments plus analytically or statistically extrapolation methods formed the basis for such predictions since the size and speed limitations of the experimental facilities prevent Reynolds number similarity in model-scale, while propeller performance is significantly affected by Reynolds-related scaling phenomena. In contrast to ship models, the application of turbulence stimulation to model propellers was always omitted (Hughes and Allan 1951) even if it could serve as a valuable tool for a better understanding (and a simple scaling) of the model- to full-scale variations of the flow regime (Kerkvliet et al. 2024; Schuiling et al. 2024). Different Reynolds numbers mean different boundary layer regimes (laminar or transitional boundary layer at model-scale, fully turbulent at full-scale), completely different risks of flow separation and, definitely for the design or the optimisation process, different, and sometimes unexpected, performance of the propulsors in full-scale (Kuiper 1978, 1981). Despite the controlled conditions under which model tests are performed to gather in the towing tank or at the cavitation tunnel all the relevant data, the scaling process introduces several uncertainties that can have a non-negligible impact on the estimated full-scale performance. This was earlier pointed out by van Lammeren (1939), who argued that the propeller efficiency can either increase or decrease with an increase of the Reynolds number as a consequence of the complex interactions between blade geometry, model-scale Reynolds number and loading conditions of the propeller, preventing definitive conclusions on full-scale performance without a deep understanding of the occurring boundary layer nature at both model - and full-scale.

The absence of a commonly accepted and reliable scaling methodology applicable to any type of propellers is a consequence of this complexity. The most widely adopted methodology is the one proposed by the International Towing Tank Committee in its 1978 guideline (ITTC 1978). The main idea behind this procedure, following the original work by Allan et al. (1951) and extended by Meyne (1968) to the B-series propeller, is the equivalence of the scaling effects a propeller is subjected to with those of one characteristic section of its blade, at $r/R = 0.7$ (or 0.75). The full-scale performance is derived only from the changes in the drag coefficient of the sectional hydrofoil, corrected to full-scale using the proportional dependency of the drag coefficient with the friction coefficient of the flat plate. This scaling approach completely ignores the influence of the Reynolds number on sectional pressure drag and lift, which are assumed to be only dependent on angle of attack and shape of the equivalent profile. To overcome some of the limitations of the ITTC-suggested methodology, Streckwall et al. (2013) made use of a similar concept of equivalent 2D sections to realise a strip/chordwise method where the influence of the viscous regime on the propeller performance is obtained by accounting for the local Reynolds number along the blade sectional chord at any radial position on the blade. The integration of the local (laminar and/or turbulent) skin friction coefficient along the chord is used to compute the sectional drag, permitting a simple and straightforward scaling to ship scale of the (frictional) performance of the propeller while also taking into

CONTACT Stefano Gaggero stefano.gaggero@unige.it Department of Electric, Electronics, Telecommunications Engineering and Naval Architecture, University of Genoa, Via Montallegro, 1, Genoa 16145, Italy

account the blade outline and the radial pitch distribution (Streckwall et al. 2013). This methodology, extended to deal with tip-modified propellers, is the standard extrapolation procedure applied at the HSVA. Similar 'strip' methodologies were developed in the case of Contracted and Tip Loaded (CLT) propellers (González-Adalid et al. 2016, 2018). Also in this case, the objective was to more accurately account for the markedly different load distributions characteristic of these propulsors, which, through substantially different gradients of the pressure distribution, modify the local flow regime and the associated viscous interaction mechanisms. Recently, some attempts have been made to define a scaling approach for ducted propellers (Bhattacharyya et al. 2015, 2016a, 2016b) using systematic numerical analyses on a set of different ducts and blade pitch settings, since very limited studies, focused mainly on the flow features modifications on the nozzle due to different loading, were the only ones available (Falcao de Campos 1983).

An extended survey of these semi-empirical and practical scaling methodologies and associated boundary layer issues is given in Helma (2016), Helma et al. (2018) and Schuiling et al. (2024). The overall picture is that of a complexity of phenomena associated with differences in the propeller boundary layer regime between model - and full-scale (and related effects) that are still unresolved. The full-scale dominance of turbulent boundary layer drastically changes the performance also in terms of lift, which is an aspect typically not addressed by the commonly adopted scaling approaches. The laminar boundary layer, which is predominantly encountered at model scale, is highly susceptible to separation under adverse pressure gradients, resulting in a significant increase in pressure drag. More broadly, the momentum deficit associated with different boundary-layer regimes not only alters the frictional forces but also strongly affects the overall pressure distribution and associated forces. This occurrence, closely related to propeller design and operational conditions, is neglected as well in the 'equivalent section' based scaling methodologies (ITTC 1978, 2014, 2017a). The mutual influence of these phenomena, moreover, contributes to the inconstancy of the full-scale extrapolations, which may be more pronounced or even divergent from case to case or from functioning condition to functioning condition.

The recent trends in ship design and operations, together with the development of modern CFD based design and analysis tools, moreover, bring back the attention back to this field of research. Following the need for low fuel consumption, most of the modern propellers are designed for high efficiency and slow steaming, preferring smaller blade area ratios. If a direct full-scale design of these geometries using viscous CFD codes is, by now, the standard procedure, it is the model-scale validation that brought attention to the discrepancies that may rise from the very different nature of the flow fields, and to the need of appropriate and well-calibrated CFD analyses. At the same time, any attempt to assess the scale effects only through numerical simulations rises several uncertainties given the state of the art and the contradictory results available in literature for what concerns, mainly, the prediction of the complex model-scale phenomena in transitional flow regimes. For sure, the advancements in computational fluid dynamics and numerical modelling have significantly contributed to bridging the gap between model-scale and full-scale performance predictions, accounting for complex phenomena such as laminar-to-turbulent transition, its dependency on blade geometry and loading. Systematic numerical campaigns evidenced trends not accounted in usual semi-empirical/analytical scaling approaches, such as, in some cases, the dominance of scaling effects of thrust rather than of torque (Baltazar et al. 2021), or the influence of details like blunt or sharp trailing edge (Brown et al. 2014; Rubino and Abdel-Maksoud 2024). As paint tests, transition sensitive numerical models permitted to assess the onset and the extent of transition as well as the resulting changes in skin friction, pressure distribution, and trailing wake features. At the same time, this number of results shed light on possible sources of uncertainties and inconsistencies related to numerical calculations, and in particular to the tuning of the calibration parameters of the transition sensitive turbulence models which, in most cases, are correlation-based approaches and then dependent on local and free-stream conditions.

Müller et al. (2009) proposed, among the first, numerical calculations of model-scale propellers employing the γ -Re_θ local correlation transition model of Langtry and Menter (2009). Rijpkema et al. (2015) conducted detailed analyses of the effect of Reynolds number on propeller performance predictions in open-water conditions, spanning from laminar flow ($\mathrm{Re} = 10^4$) to full-scale ($\mathrm{Re} = 10^7$) Reynolds numbers. Similar investigations were proposed by Grlj et al. (2022) who studied the scale effects on open-water propeller performance for Reynolds numbers ranging from 1.3×10^6–3.3×10^8. Both compared experimental model-scale results with numerical results using the *SST k-ω* turbulence model, with and without the LCTM γ -Re_θ transition model, showing the early transition to the turbulent boundary layer ($\mathrm{Re} < 10^4$; as noted by Eça and Hoekstra 2008) of the standard *SST k-ω* model together with a very limited transition length that makes the model inappropriate for calculating the performance of propellers operating in the transition regime. Hasuike et al. (2017) evidenced, by a combination of numerical calculations and paint tests, the predominant laminar nature of the boundary layer in both open water and self-propulsion tests for a family of small blade area propellers and, consequently, the need to integrate these phenomena in calculations to account for the extensive separation region at the trailing edge in the evaluation of the performance. Li et al. (2019) conducted open-water tests on several propeller designs at both low – and high model-scale Reynolds numbers, combining model/paint tests with numerical calculations using a transition sensitive turbulence model. Their analyses permitted them to recognise a predominant (separated at the trailing edge) laminar flow at very low Reynolds numbers and a mix of phenomena: laminar, transitional, and turbulent flow, for the range of Reynolds numbers typical of model-scale open water tests. The outcome of their analyses was a two-step procedure for full-scale self-propulsion extrapolations, using a low-Reynolds number open water test of the propeller performance for analysing the model-scale self-propulsion experiments and a high-Reynolds open water experiment to perform the full-scale extrapolation. A similar behaviour, i.e. the mostly laminar nature of the flow on propeller blades in model-scale self-propulsion tests, despite the common belief in earlier transition and dominance of the turbulent boundary layer due to the turbulence generated by the hull, was observed in Schuiling et al. (2024), whose experiments confirmed the findings of Hasuike et al. (2017) and Lücke and Streckwall (2017). Shin and Andersen (2017) evidenced the larger scale effects in the case of tip-modified propellers because of the increase in the thrust coefficient in full-scale thanks to a weaker/nullified separation of the flow at the trailing edge, while Moran-Guerrero et al. (2018) included the cross-flow effects, rarely employed due to a lack of extensive validation with paint tests, for the analysis of the scale effects of CLT-type propellers. Rubino and Abdel-Maksoud (2014) used both fully turbulent and transition sensitive calculations to predict the scale effects on two tip-modified propellers (one with the tip pointing towards the suction side, resembling Kappel-like geometries, one with the tip pointing towards the pressure side, resembling the CLT concept). They reported that the occurrence of flow separation at model scale exhibited a non-negligible sensitivity to the pressure distributions, which were in turn modified by the different rake designs. The use of the γ -Re_θ model, whose adoption made the discrepancies with experiments in model-scale almost negligible when compared to the results of fully turbulent simulations, almost nullified the scale effects on efficiency, resulting in a contradiction with those of Shin and Andersen (2017) for similar tip-raked geometries. This was due to a simultaneous balance (increase or decrease) of both thrust and torque from model - to full-scale. Compared to the ITTC scaling method, the results of numerical analyses were only qualitatively in agreement, and some major causes of the differences were identified in the lack of scaling laws for flow phenomena associated with blunt trailing edges and associated vortices at different Reynolds regimes. Similar discrepancies with respect to the ITTC methodology were also observed by Grlj et al. (2022). Their results indicated a substantial reduction of the scale effects when the transition model is applied for model-scale numerical predictions. In their calculations, anyhow, scale effects remained substantially higher than those computed using the ITTC 1978 performance prediction method.

The need for scaling approaches applicable to ducted propellers, whose complex nozzle–propeller interactions, vortex shedding, and separation phenomena prevent the use of the simpler ITTC methodology, have motivated similar numerical campaigns. The most recent results are those of Bhattacharyya et al. (2016a, 2016b) who considered controllable pitch propellers working inside different types of nozzles to derive, only based on numerical calculations, a dedicated scaling approach. The first attempt to address by numerical calculations the scale effects of ducted propellers was, indeed, that of Abdel-Maksoud and Heinke (2002), followed by the calculations of Krasilnikov et al. (2007). Both worked on the relatively old geometries of the KA-series propellers, evidencing a lower torque coefficient in full scale and then a higher scale effect compared to that commonly observed on open propellers (Baltazar et al. 2021; Kerkvliet et al. 2024). The recent work of Bhattacharyya et al. (2016b) also investigated the role of tip loading of modern blade geometries by changing the pitch of the CPP blades employed in their study. They observed decreasing scale effects on propeller efficiency with the increase of the blade pitch for all the functioning conditions under investigation. The blade thrust, in particular, showed discordant model- to full-scale trends depending on the loading, and a more pronounced Reynolds effect on the thrust of the duct (increasing from model – to full-scale), itself dependent on the loading condition of the blade, was identified. Krasilnikov et al. (2007), in this respect, evidenced only a slight increase in duct thrust, particularly appreciable in lightly loaded conditions where the risk of flow separation at model-scale for the typical Nozzle 19A duct shape of their calculations is higher.

If, on one side, this abundance of analyses evidenced the improvements provided by these numerical approaches for model-scale predictions, on the other hand, some peculiarities, as well as some of their limitations, emerged clearly. In parallel to scale effect predictions, indeed, several investigations on the sensitivity of laminar-to-turbulent sensitive models were carried out. Gaggero and Villa (2018) and Gaggero (2022a, 2022b) analysed the influence of different turbulence intensity levels at the propeller plane on the predicted onset of transition and performance of the propeller. Calculations were proposed using two different transition-sensitive turbulence models (the k-k_L-ω of Walters and Leylek 2002 and the γ -Re_θ of Langtry and Menter 2009) and two different CFD solvers (OpenFOAM and StarCCM+). The VP1304 propeller from the PPTC Test Case (Barkmann et al. 2011) was considered for comparison and a very high sensitivity to the turbulence intensity was observed. An arbitrary value of turbulence intensity level equal to 1% permitted a good match of measured open water model-scale performance. The same intensity level in proximity of the propeller was assumed by Rubino and Abdel-Maksoud (2024) based only on qualitative comparisons with experiments. Their simulations, in any case, pointed out a less relevant influence of turbulent intensity on the overall propeller characteristics. The outcomes of their calculations have shown, indeed, a negligible variation of thrust and torque as a consequence of a variation of the turbulence level from 0.5 to 1.5%: the highest variations induced by the different turbulence levels were associated with friction forces (maximum change of 11%), whose contribution to the total performance of the propeller is minimal if compared to the pressure contribution. The results of Baltazar et al. (2023) and Kerkvliet et al. (2024), instead, highlighted again a stronger dependency of propeller performance on the turbulence intensity level. Only a systematic comparison with paint tests allowed for the identification, for the specific case under investigation, of a tuned value of turbulence intensity level equal to 1.35%, perfectly matching the onset of transition on both the pressure and the suction side of the propeller. This very high sensitivity of the numerical model explained the significant comparison errors observed by Baltazar et al. (2021) for advance ratios near the design condition, where the prevalence of transitional flow at model-scale needs to be accounted accurately.

Using the turbulence-intensity level as a tuning parameter also raised concerns about the robustness of transition – sensitive turbulence models. When the turbulence intensity (and the eddy viscosity ratio) is adjusted to match a target turbulence level at a reference location, the corresponding inlet turbulent quantities may become physically unrealistic. This issue becomes especially evident when inlet tuning is used in lieu of introducing localised turbulent – kinetic – energy source terms in confined regions upstream of the propeller. Such a procedure may compromise the physical consistency of the modelled turbulence field and adversely influence the predicted onset and evolution of laminar–turbulent transition. In particular, imposing non-physical inflow specifications, dictated solely by operating conditions or by attempts to match observations and trends, may introduce inconsistencies in the upstream flow. As a result, the reliability of transition-sensitive formulations becomes questionable under such artificially constrained boundary conditions. In this respect, Lopes (2021) evidenced the risk of an altered laminar regime on the propeller blades when excessively high values of eddy viscosity ratio are employed to counteract the decay of turbulence intensity. Gaggero and Villa (2018) compared the resulting turbulence intensities in correspondence of the expected transition zone of the ERCOFTAC flat plate obtained by a change of the turbulence intensity and the eddy viscosity ratio at inlet. They, instead, observed a minimal dependence of the onset of turbulent boundary layer (at constant turbulence intensity level at the flat plate leading edge) by the slope of the decay curve. In the case of ducted propellers, the few available simulations using transition sensitive models were carried out with substantially higher values of turbulence intensity (5%), further raising concerns about the appropriate calibration of this parameter.

Inspired by the previous research, this paper proposes a further numerical study on the scale effects, i.e. on model – and full-scale performance, of open and ducted propellers operating in very different regimes by employing fully turbulent (*SST* k-ω) and transition sensitive (γ -Re_θ) models. Model-scale performance is collected for ranges of advance coefficient spanning from highly to lightly loaded conditions, at several rates of revolution to comparatively study the dependence of transition on loading and Reynolds number. Given the sensitivity to turbulence quantities, calculations are repeated for different levels of turbulence intensity in order to provide a complete overview of the influence of this ‘tuning’ parameter of the turbulence model. The aim is to disentangle the extensive discussions and often contradictory conclusions reported in previous studies. This is achieved through the systematic nature of the proposed simulations, which are not restricted to a single operating condition or geometry and are performed using computational domains, meshes, and numerical schemes that are topologically consistent across all

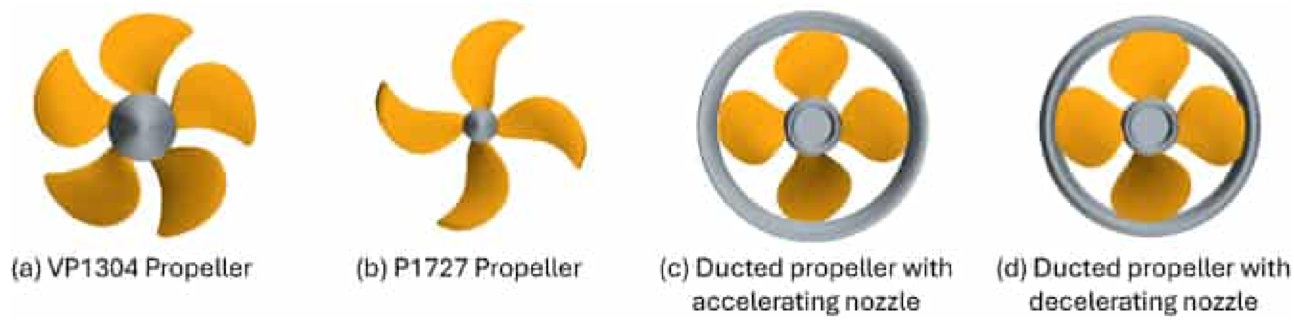

Figure 1. Overview of the open and ducted propellers selected for the analyses.

cases. To ease the repeatability, the selected open propellers are those from the 'Workshop on propeller performances' (Barkmann et al. 2011), recently adopted also by ITTC for benchmarking purposes. Ducted propellers derive instead from the research activities of the EU-funded BESST project (Gaggero et al. 2012). Compared to the old KA-series, they are modern designs. One of the two is a propulsor operating in a decelerating nozzle, which is a geometry never addressed in literature for what concerns the influence of such geometry (and related pressure fields) on transition and scale effects. Different CFD codes, namely StarCCM + (Siemens 2021) and OpenFOAM v8.0 (The OpenFOAM Foundation 2020) are used to furthermore discuss possible differences ascribable to the flow solvers.

Test cases and functioning conditions

Four different propulsors were considered for the study: two open propellers and two ducted propulsors. Open propellers are those adopted by the Workshop on propeller performances held at the 2nd Symposium on Marine Propulsors and developed by SVA Potsdam (Barkmann et al. 2011). The first, VP1304, is a conventional, five-bladed, right-handed, controllable pitch propeller designed in 1998. The second (P1727) is an unconventional geometry recently developed for the 'Tip Rake' research project. It is a four-bladed, right-handed, fixed pitch propeller that has a fixed chord at the tip and a rake at the tip towards the pressure side, similar to the 'new generation CLT propellers' developed by González-Adalid et al. (2016) and Gaggero et al. (2016). Both were already considered for assessing the reliability of CFD based scaling procedures by the ITTC Propulsion Committee (ITTC 2017b). Model-scale measurements (thrust and torque at several advance coefficients, without artificial turbulence stimulation in towing tank or cavitation tunnel tests) are available from SVA as a part of the ITTC benchmark (ITTC 2017c, 2024). An overview of their geometries is given in Figure 1. Main geometrical characteristics are summarised in Table 1.

Ducted propellers were developed in the framework of the EU-funded project BESST (Breakthrough in European Ship and Shipbuilding Technologies, European Community's Seventh Framework Programme FP7/2007-2013). The first (Figure 1c) is a propulsor equipped with an accelerating duct (a standard Nozzle 19A) to operate, like any of these kinds of propulsors, at a very reduced advance coefficient. The second (Figure 1d) was designed for a naval unit, and since the focus of the application was on the reduction of the radiated noise by postponing the cavitation inception, a custom decelerating nozzle was preferred. For the same reason of cavitation postponement, the blade tip is significantly unloaded by a non-negligible reduction in pitch and chord, at least compared to traditional KA ducted propulsors, which have an almost constant pitch from midspan to tip, and the maximum value of the chord exactly at the tip. Both are brass model-scale propellers operating in nozzles realised in Perspex. No artificial transition triggering or leading-edge boundary-layer tripping devices were applied on either component, neither on the blades nor on the nozzle. Validation data come from towing-tank experiments conducted at SVA, while cavitation-tunnel measurements were performed at the University of Genoa.

The design point, due to the nature of the application, is for a relatively high advance coefficient ($J = V/nD$ greater than 1, where n is the rate of revolution in rotations per second and D the propeller diameter). Both propulsors are four-bladed, right-handed, controllable pitch propellers, whose geometries and main characteristics are listed in Table 2.

To thoroughly investigate scale effects and the influence of model-scale Reynolds number and turbulence levels on the extrapolation process itself, these four propellers underwent a systematic analysis campaign, encompassing several advance coefficients, model-scale rates of revolutions and levels of turbulence intensity estimated in correspondence with the propeller plane. The simulations were performed at several advance coefficients to address the influence of propeller loading on the propeller blade flow features and, consequently, on the scaling process. Different rates of revolutions were considered as well to investigate how model-scale Reynolds numbers affect predictions and relative scaling effect. For the conventional

Table 1. Main geometrical characteristics of VP1304 and P1727 (data in brackets refer to full-scale).

	VP1304	P1727
D [mm]	250 (3000)	238.6(7500)
$P/D_{r/R=0.7}$	1.635	0.8406
$P/D_{average}$	1.5675	0.8191
$c/D_{r/R=0.7}$	0.4166	0.23633
Thickness/$c_{r/R=0.7}$	0.0425	0.058
Skew at tip [deg.]	18.8	25.68
Blade Area Ratio	0.779	0.444
Number of blades	5	4

Table 2. Main geometrical characteristics of the accelerating and the decelerating ducted propellers (data in brackets refer to full-scale).

	Accelerating ducted propeller	Decelerating ducted propeller
D [mm]	230 (3000)	230 (3000)
$P/D_{r/R=0.7}$	1.5658	1.3545
$P/D_{average}$	1.3899	1.2151
$c/D_{r/R=0.7}$	0.491	0.498
Thickness/$c_{r/R=0.7}$	0.0265	0.0266
Skew at tip [deg.]	3.5	3.5
Blade Area Ratio	0.689	0.725
Number of blades	4	4

VP1304, this corresponds approximately to Reynolds numbers spanning from 4.410^5–1.0310^6 at the design advance coefficient. The range is reduced from 2.510^5–5.810^5 in the case of the P1727 geometry as a consequence of its very low expanded area ratio. Ducted propellers are tested in a range of Reynolds numbers between $4.0\ 10^5$ and 1.0510^6.

Any combination of advance coefficient and rate of revolution was furthermore repeated at different levels of turbulence intensity on the propeller plane, achieved for any functioning conditions through a calibrated choice of turbulence intensity and eddy viscosity ratio at the inlet. Given the sensitivity of the transition model to this parameter (Gaggero, 2022a; Kerkvliet et al. 2024), and the very different performance (and relative scale effects) achievable on model-scale by minor modification of the boundary layer regime and induced separation, an investigation on the different numerical results achievable by tuning the turbulence intensity was deemed necessary for the thoroughness of the investigation. At the same time, different turbulence intensity levels combined with varying Reynolds numbers broaden the range of boundary-layer regimes that develop over the blades at model scale, providing a more comprehensive (even if numerical) understanding of the phenomena influencing the extrapolation to full-scale. Gaggero (2022a) and Rubino and Abdel-Maksoud (2024) both employed a 1% turbulence intensity at the propeller plane with satisfactory results in terms of comparative errors with model-scale measurements and, in Rubino and Abdel-Maksoud (2024), also with paint tests. Kerkvliet et al. (2024) identified a value of 1.35% for *Tu* as the best-balanced value for comparisons with experiments. Higher levels of turbulence usually resulted in earlier onset of transition and predicted performance comparable to that of the fully turbulent case. The adopted range of variations was selected based on these results: from a minimum of 1% to a maximum of 1.8%, to include in the current study the most typical values reported in the literature. This serves a two – fold objective. Turbulence intensity is typically treated as a tuning parameter in most (semi – empirical) correlation – based, transition – sensitive turbulence models. Literature results consistently show improved agreement with experiments when adopting values slightly higher than those measured during tests. In this sense, the comparison among four different propellers provides, first, further evidence of the role and influence of this parameter on the accuracy of numerical predictions, enabling a broader generalisation of the tuning process. Second, although the selected values of turbulence intensity could be not completely consistent with the experimental measurements, simulations carried out at different turbulence intensity levels allow the inclusion of multiple laminar/turbulent model-scale scenarios in the performance-scaling analysis. This makes it possible to discuss how the relative prevalence of phenomena closely tied to friction and viscous/inviscid interactions, such as changes in suction on the blade back and flow separation, may affect model-scale performance and the associated extrapolation to full-scale conditions. To this aim, the turbulence intensity levels at the propeller plane were tuned by changing the inlet parameters of turbulent intensity and eddy viscosity ratio based on the decay estimated from the resolution of the *SST* k-ω transport equations in the simplified case of steady, uniform flow without diffusion and cross-flow. Given the dimensions of the computational domain and the functioning conditions under investigation, it was possible to achieve the desired values of intensity using not excessively high values of eddy viscosity and inlet turbulence. This is the easiest approach, without the need to counteract the destruction terms of k and ω in the *SST* k-ω equations by modifying the equations themselves (by adding source terms), which instead is the method preferred by Lopes (2021), Kerkvliet et al. (2024), Rubino and Abdel-Maksoud (2024), to avoid the need for extremely high values of eddy viscosity when the inlet boundary is far from the propeller plane. Current calculations (VP1304) employed inlet turbulence values never higher than 3% and an eddy viscosity ratio at maximum equal to 250 in the worst case (highest propeller rate of revolution, then highest undisturbed velocity, for the desired turbulence level at the propeller plane equal to 1.8%). The most representative cases (design speed and functioning, intermediate turbulence level) can be obtained with eddy viscosity ratios of about 100. Based on the preliminary experience reported in Gaggero and Villa (2018), these combinations of turbulence quantities are not expected to significantly affect the reliability of the calculations. Anyhow, dedicated simulations performed to extend the findings obtained with the k-k_L-ω turbulence model on the ERCOFTAC T3A flat-plate test case (Gaggero and Villa 2018) and to further confirm the robustness of this approach in a more complex scenario are discussed in the following section. For the fully turbulent simulations (model- and full-scale), default values of the parameters ($Tu = 1\%$ at the inlet, eddy viscosity ratio equal to 10) were assumed since no appreciable influence on the predicted fully turbulent performance, except a faster smearing of the trailing vortical wake features (Gaggero and Villa 2018; Rubino and Abdel-Maksoud 2024), was reported in the literature.

Mathematical and numerical models

Turbulence and transition modelling

All the calculations presented in the paper are based on RANS equations solved using StarCCM + v16.04 (Siemens 2021) and OpenFOAM v8.0 (The OpenFOAM Foundation 2020). Cell-centered collocated variables and face-based implementation are used in a finite volume framework by both the solvers. This allows arbitrary cell shapes and unstructured grids. The solution is obtained using a segregated method that employs a SIMPLE approach for the velocity-pressure coupling. The ‘consistent’ implementation of the algorithm is used in OpenFOAM. Convective fluxes are solved using second-order upwind schemes. For OpenFOAM calculations, first-order accurate schemes were preferred for the turbulent quantities. Turbulence closure is addressed in two ways. Fully turbulent analyses (model – and, of course, full-scale) are carried out using the *SST* k-ω turbulence model (Menter 1994). Laminar-to-turbulent boundary layer transition in model-scale, instead, is addressed by the transition sensitive γ -Re_θ model (Langtry and Menter 2009).

The *SST* k-ω model is, de facto, the standard two-equation turbulence closure model for RANSE calculations, where one equation is dedicated to turbulence kinetic energy k and another to the specific dissipation rate ω. In the inner part of the boundary layer, it adopts a conventional k-ω model formulation, allowing the *SST* version to be applicable all the way down to the wall within the viscous sublayer without requiring additional damping functions. As the flow transitions to the free stream, the model behaviour resembles that of a k-ϵ model, then mitigating the original k-ω model sensitivity to inlet free-stream turbulent quantities. Simultaneously, this adaptation enhances boundary layer predictions under adverse pressure gradients (Menter 1994). The general formulation of the transport equations for k and ω is as follows:

$$
\begin{aligned}
\boldsymbol{U}\frac{\partial k}{\partial \boldsymbol{x}} &= P_k - D_k + \frac{\partial}{\partial \boldsymbol{x}}\left[(\nu + \sigma_k \nu_T)\frac{\partial k}{\partial \boldsymbol{x}}\right] \\
\boldsymbol{U}\frac{\partial \omega}{\partial \boldsymbol{x}} &= P_\omega - D_\omega + \frac{\partial}{\partial \boldsymbol{x}}\left[(\nu + \sigma_\omega \nu_T)\frac{\partial \omega}{\partial \boldsymbol{x}}\right] + 2(1 - F_1)\frac{\sigma_{\omega 2}}{\omega}\frac{\partial k}{\partial \boldsymbol{x}}\frac{\partial \omega}{\partial \boldsymbol{x}}
\end{aligned}
\tag{1}
$$

where P_k, D_k, P_ω and D_ω are the production and the dissipation terms for k and ω respectively. The kinematic eddy viscosity is given by:

$$\nu_T = \frac{a_1 k}{\max(a_1\omega,\ SF_2)} \tag{2}$$

and S is the strain-rate magnitude, F_1 and F_2 are two auxiliary functions, and a_1, σ_k, σ_ω and $\sigma_{\omega 2}$ are the constants of the model.

The *SST* version implemented in OpenFOAM is based on the work of Menter et al. (2003), incorporating modifications to the production term of turbulence kinetic energy. Detailed information on blending functions and constants used in the model can be found in Menter and Esch (2001) and Menter et al. (2003). Details of the implementation of the model in OpenFOAM are provided by The OpenFOAM Foundation (2020). On the other hand, StarCCM + utilizes the original formulation by Menter (1994) along with the constitutive relationship proposed by Spalart (2000) and Hellsten (2005). Further details regarding this implementation and the constants adopted in the model can be found in Siemens (2021).

The γ-Re_θ model belongs to the category of local correlation-based transition models, designed to leverage experimental correlations between free-stream turbulence, local pressure gradient, and transition momentum thickness Reynolds number for assessing the occurrence and location of boundary layer transition. Traditional correlation methods faced challenges in comparing actual momentum-thickness Reynolds numbers to transition values due to difficulties in defining boundary layer edges in unstructured meshes and three-dimensional calculations. Menter et al. (2002) introduced an innovative approach to circumvent the need for non-local information to compute momentum thickness, but the initial formulation lacked robustness. In a subsequent development by Menter et al. (2006), this approach was refined to eliminate the need for non-local analyses with the use of two transport equations:

$$\begin{aligned} \frac{\partial(\boldsymbol{U}\gamma)}{\partial \boldsymbol{x}} &= P_\gamma - E_\gamma + \frac{\partial}{\partial \boldsymbol{x}}\left[\left(\nu + \frac{\nu_T}{\sigma_f}\right)\frac{\partial \gamma}{\partial \boldsymbol{x}}\right] \\ \frac{\partial(\boldsymbol{U}\overline{Re_{\theta t}})}{\partial \boldsymbol{x}} &= P_{\theta t} + \frac{\partial}{\partial \boldsymbol{x}}\left[\sigma_{\theta t}(\nu + \nu_T)\frac{\partial(\overline{Re_{\theta t}})}{\partial \boldsymbol{x}}\right] \end{aligned} \tag{3}$$

The first equation represents an intermittency equation utilised to trigger transition in the *SST k-ω* model because the production and destruction terms of turbulent kinetic energy are made dependent on the intermittency itself. The terms P_γ (production) and E_γ (re-laminarization), along with model constants, are described in Langtry and Menter (2009). This approach avoids the critical limitation of traditional correlation-based methods (i.e. dependency on non-local quantities) by using the relationship between transition momentum thickness and strain-rate Reynolds number, which instead is a local quantity easily derivable also in the case of unstructured/arbitrary shaped meshes. Additionally, the model accounts for separation-induced transition through intermittency.

The second equation is a transport equation for the local transition onset momentum-thickness Reynolds number, $Re_{\theta t}$, involving only the production term $P_{\theta t}$. This equation incorporates empirical correlations for the transition onset, transferring information from the freestream into the boundary layer. $Re_{\theta t}$ is computed using the freestream empirical correlations (since pressure gradients and turbulence intensity are defined for the freestream) and then diffused into the boundary layer. This method allows including the influence of non-local phenomena such as changes in turbulence intensity or freestream velocity outside the boundary layer. Details regarding model implementations and constants are provided in Langtry and Menter (2009) and Menter et al. (2006).

Computational domain and boundary conditions

The computational domain and boundary conditions were maintained identical for the four cases under investigation. A single blade passage, exploiting the propeller periodicity and periodic boundary conditions, was used (Figure 2). Open propellers were modelled with the front hub cap and the shaft downstream (Figure 2). Ducted propellers adopted the 'reverse POT' configuration, with the shaft in front of the propeller. Based on a preliminary influence analysis, the inlet was placed $3D$ in front of the propeller. This choice is dictated by the need to counteract the decay of turbulence intensity through the computational domain setup. This positioning minimises the influence of the boundary on the predicted propeller performance (lightly to moderately loaded cases) while allowing the use of inlet eddy viscosity and turbulence intensity values that are not excessively high, as discussed in the previous section. Outlet is $9D$ behind the propeller plane, and the external cylindrical surface is $5D$ far from the shaft, in accordance with ITTC suggestions (sectional area of the domain over area of the propeller disk ratio higher than 100).

Boundary conditions are applied consistently with the type of simulations, which is steady-state and employs the Moving Reference Frame approach. Only at bollard pull (or in very lightly loaded conditions) does the adoption of this numerical setup may pose some issues for the accuracy of computed results. Recently, Bhattacharyya et al. (2016b) evidenced, in the case of ducted propellers, some non-negligible differences in the flow features at bollard pull on the external surface of the duct. Steady-state solutions showed a smaller separation extent compared to unsteady calculations. An exacerbation of these differences was observed in the case of fuller and blunter nozzle profiles, where the interactions with shedding trailing vortices are stronger. Given the range of advance coefficients under investigation, and the type of geometries, in current simulations it was deemed not necessary to switch to an unsteady analysis using sliding or overlapping meshes.

Mesh sensitivity analysis

Prior to any analyses and comparisons with the available experiments, a grid sensitivity analysis was carried out to examine the uncertainties associated with the spatial discretisation of the problem. The study was limited to the VP1304 and the P1727 propellers, using StarCCM+ and its native unstructured polyhedral meshing tool. Meshes of ducted propellers (StarCCM+) have been realised following the guidelines, in terms of local mesh refinements and prism layers arrangement, deduced from the results of the open propellers.

The meshes for open propeller simulations using OpenFOAM were selected on the basis of the grid refinement studies already carried out in Gaggero (2022a, 2022b). Despite the type of cells (hexa-dominant grids were preferred for OpenFOAM calculations), the total cell count, local surface and volume refinements, as well as the prism layer total thickness and number of layers of the grid that best balance accuracy and computational efficiency were not substantially different from those derived using StarCCM+. An overview of the reference grids (StarCCM+), from which the coarser and finer meshes for the grid sensitivity study were derived, is given in Figure 3.

For VP1304, the reference mesh consists of about 4 million cells, uniformly scaled (obviously with the exception of the prism layers) to obtain simulations suitable for the convergence study, ranging from 1.5 (coarser) to 11 (finest) million cells. The average surface mesh size corresponds to 0.5% (1.25 mm) of the reference length (propeller diameter D), while highly curved zones are discretized with cells having an average dimension of 0.05%D, for a total of about 140,000 surface cells per blade. The number of prism layers

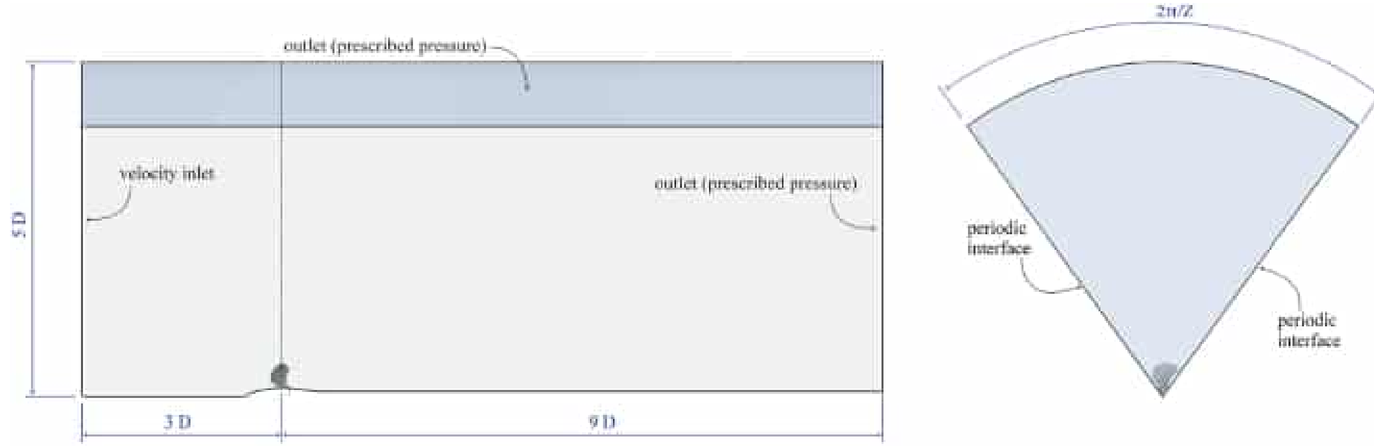

Figure 2. Computational domain for open and ducted propeller analysis.

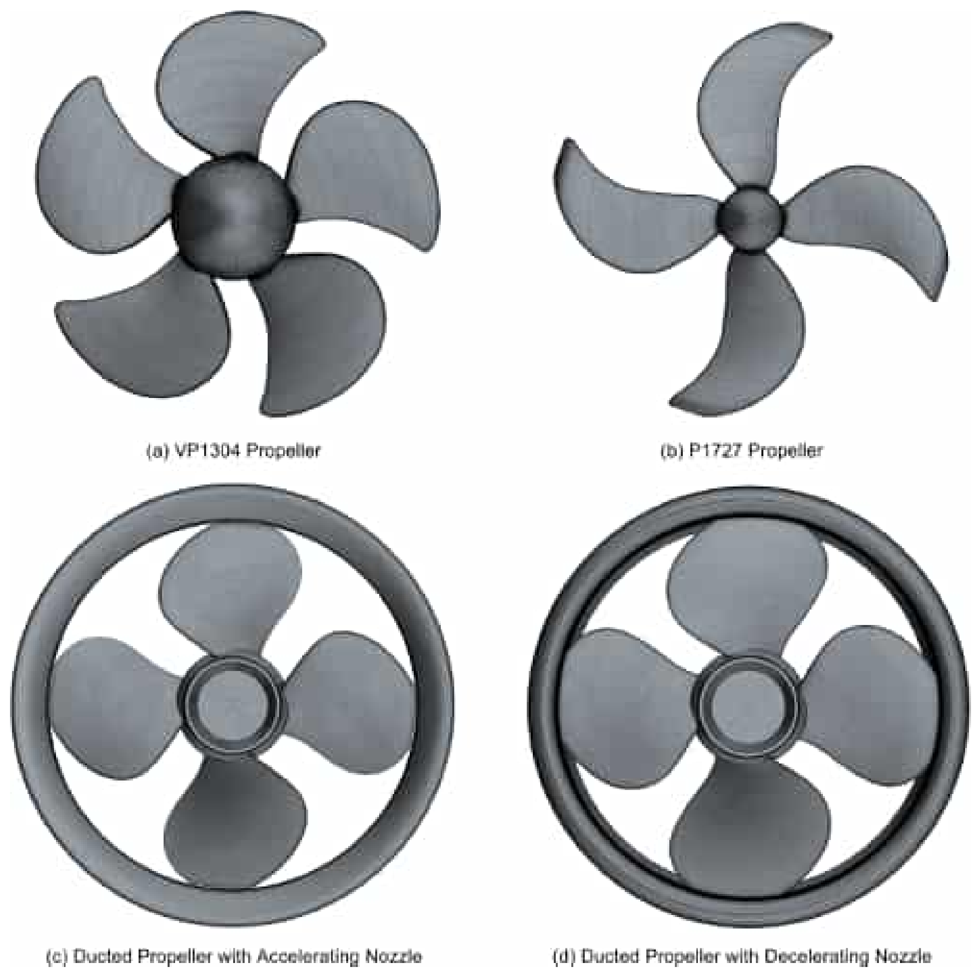

Figure 3. Surface meshes (reference grid arrangement, StarCCM+) for the open and ducted propellers under investigation.

is fixed at 25, and at the design functioning ($J = 1.2$, $rps = 15$, lowest turbulence intensity level, as per Table 3), it provides an averaged non-dimensional wall distance calculated using the transition sensitive turbulence model equal to 0.4. Local maxima at the leading edge do not exceed 1.5. Given the reliability of the model also for slightly higher values of $y+$ with respect to the canonical value of 1 (Gaggero and Villa 2018), the setup of the prism layers seems appropriate. P1727 is similarly discretized. The reference grid counts about 3.8 million cells. Coarsest and finest grids range from 1.1 to 10.8 million elements. Average and minimum surface dimensions are set equal to those of the VP1304 case. Due to the different blade shape, this choice leads to about 98,000 surface cells per blade. The number of prism layers is reduced to 20 as a consequence of the different range of functioning conditions investigated in the study. However, the value of the non-dimensional wall distance is maintained, on average, lower than 0.3. At the leading edge, where the prism layer cells have lower quality, the maximum $y+$ reaches 2, but only on very few cells.

Table 3. Tested conditions.

	VP1304	P1727	Accelerating Duct.	Decelerating Duct.
J	0.6; 0.8; 1.0; 1.2∗; 1.4	0.1; 0.3; 0.5∗; 0.7; 0.9	0.2; 0.4; 0.6; 0.8; 1.0	0.6; 0.8; 1.0∗; 1.2
rps (model-scale)	7.5; 10; 12.5; 15∗∗; 17.5	9; 12; 15; 18∗∗; 21	7.5; 10; 12.5; 15∗∗; 17.5	7.5; 10; 12.5; 15∗∗; 17.5
rps (full-scale)	4.33	3.21	4.17	4.17
Turbulence intensity level (*Tu* [%]) at the propeller plane (model-scale)	1.0%; 1.4%; 1.8%; fully turbulent			

∗design point (approximately), ∗∗rps of model-scale experiments by SVA.

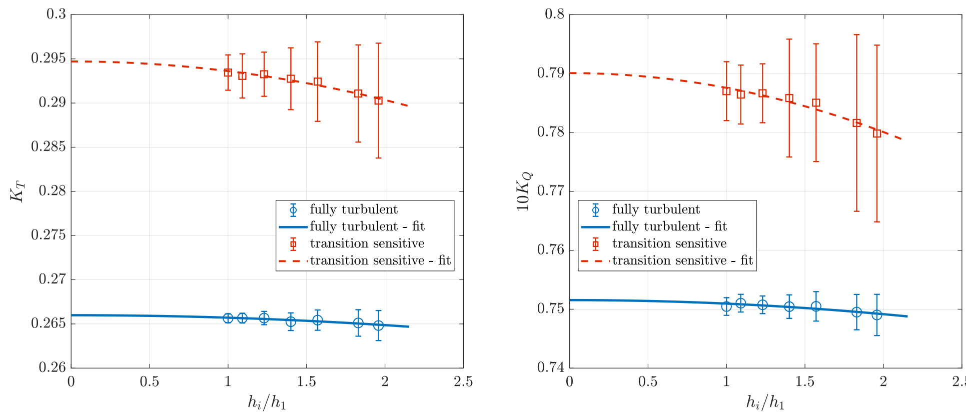

(a) $K_T - J = 1.2$ (b) $10K_Q - J = 1.2$

Figure 4. Grid sensitivity study and estimated numerical uncertainty for the VP1304 propeller. Comparison between fully turbulent and transition sensitive turbulence models ($Tu = 1\%$) in model-scale at design advance coefficient ($J = 1.2$).

The assessment of the discretization uncertainty is provided by the procedure proposed by Eça and Hoekstra (2014) using the tool made available by MARIN. Computed data at different grid densities are collected as a function of the 'relative step size' (ore refinement ratio), defined as the cubic root of the ratio between the cell count of the finest grid (N_1) and the cell count of the current grid (N_i) of the simulations ($h_i/h_1 = (N_1/N_i)^{1/3}$). The quantity of interest, as a function of the refinement ratio, is then approximated with power series expansions (eventually using fixed exponents and different coefficients in case anomalous behaviour is detected) in the least square sense to identify the exact (extrapolated to an infinite number of cells) solution and the observed order of convergence. Safety factors are used to determine, based on the discretization error (i.e. the difference between the exact solution and the value of the quantity of interest with the current mesh), the numerical uncertainty associated with any grid.

Results of calculations, repeated using the fully turbulent and the transition-sensitive turbulence models (model-scale, at the design advance coefficient, rate of revolution equal respectively to 15 and 18 *rps*, turbulence intensity level *Tu* for the transition-sensitive model at the propeller plane set equal to 1%), are shown in Figures 4 and 5. The analyses confirm the outcomes of several similar investigations available in the literature. However, they are useful to guide towards the choice of the most balanced grid setup for the systematic simulations proposed in the paper. Fully turbulent calculations exhibit very good 2nd order convergence for both the quantities under investigation (thrust coefficient, $K_T = T/\rho n^2 D^4$, and torque coefficient,$^{KQ = Q/\rho n2}D^5$, where T and Q are respectively the delivered thrust and the absorbed torque, ρ the water density, n the propeller rate of revolution) in the case of VP1304 and 2nd (thrust) and mixed 1st / 2nd (torque) order convergence for the P1727. With the transition-sensitive model, again a 2nd order convergence is achieved for the VP1304. Compared to the fully turbulent case, the discretization error is doubled (from – 0.3% to – 0.66% for the thrust, from – 0.15% to – 0.55% for the torque) and, consequently, the uncertainty which, from values almost lower than 1% at any grid size in the fully turbulent case, reaches 4% in the worst (coarser) case of calculations based on the transition-sensitive model.

P1727 suffers a bit more from the use of the transition sensitive model in terms of convergence trends. Second-order convergence is predicted concerning the thrust, while only a linear trend characterises the torque. The discretization error, which is very low in the case of fully turbulent analyses (on average 0.1% for thrust, 1.4% for torque), sensibly increases when using the γ-Re_θ model, up to 1% and 1.7% respectively. The numerical uncertainty rises to 3% (K_T) and 5% (K_Q) when using the reference grid from a modest 0.5% and 1.8% observed in the fully turbulent calculations. These numbers are not substantially different from those of previous calculations on the same propeller geometries, but using different CFD solvers (Gaggero 2022a) or from similar cases available in the literature (Kerkvliet et al. 2024; Rubino and Abdel-Maksoud 2024). The unstructured grid type seems to have the highest (negative) influence on the convergence trends. Kerkvliet et al. (2024) and Baltazar et al. (2021), when using block-structured grids, were indeed able to reduce the numerical uncertainties, but at the cost of using high-quality computational grids up to 100 million cells (entire propeller). For some functioning conditions, their calculations exhibited only linear trends too, and were characterised by substantially higher values of uncertainty in the case of transition sensitive simulations, confirming the high sensitivity of the laminar to turbulent transition model to the spatial resolution in the flow direction, especially when a severe risk of separation is recognised as in the cases with very low turbulence intensity. This trend is clearly observable in the distribution of the skin friction coefficient in Figure 6. Also for the VP1304, which is less affected, from the point of view of global performance, by numerical uncertainty, a non-monotonic trend of the portion of the blade under transition/turbulent flow is visible. Qualitatively, the phenomenon of transition is captured very similarly, but the extension of the fully developed turbulent boundary layer seems to have a minimum exactly for the reference mesh, with the finer grid results being more similar to those from the coarse grid. On the basis of these results, and also having in mind the need for systematic calculations

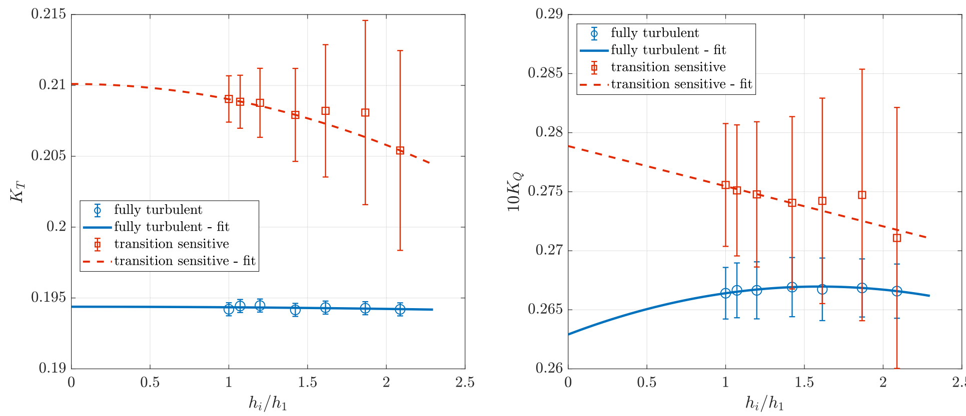

(a) $K_T - J = 0.5$ (b) $10K_Q - J = 0.5$

Figure 5. Grid sensitivity study and estimated numerical uncertainty for the P1727 propeller. Comparison between fully turbulent and transition sensitive ($Tu = 1\%$) turbulence models in model-scale at design advance coefficient ($J = 0.5$).

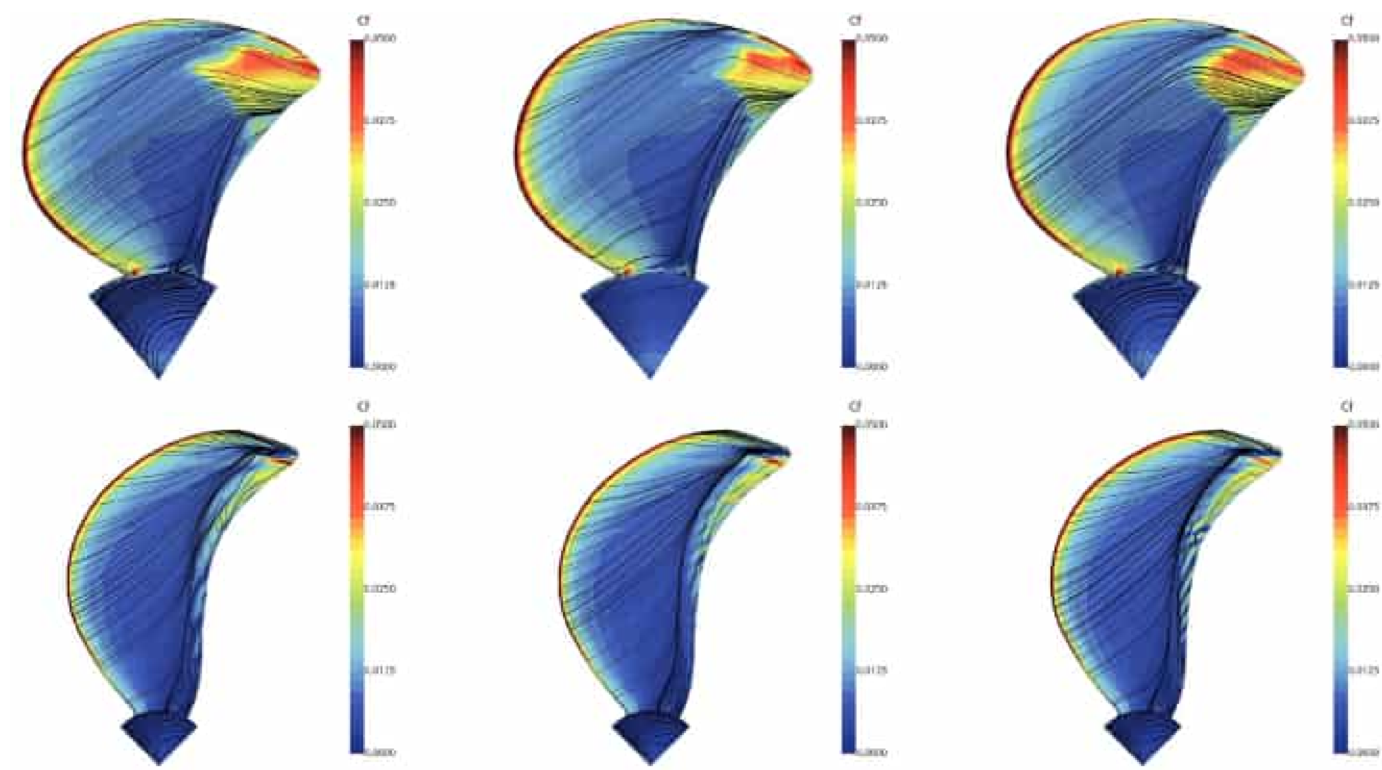

(a) Coarsest grid (b) Reference grid (c) Finest grid

Figure 6. Influence of the grid density (skin friction coefficient distribution and surface streamlines) on the predicted laminar to turbulent boundary layer transition, turbulence intensity level of 1% at the design advance coefficient. Calculations using StarCCM+. Top: VP1304 propeller ($J = 1.2$). Bottom: P1727 propeller ($J = 0.5$).

at several loading conditions, turbulence intensity levels and rates of revolutions, the reference grid can be considered accurate enough for the simulations.

As a further confirmation of the reliability of the selected grid density, Figure 7 shows the predicted skin friction coefficient and streamlines computed using OpenFOAM and the mesh arrangement devised in Gaggero (2022a) but adapted to the current computational domain. For VP1304, the total cell count was about 5.1 million hexa-dominant cells, arranged with a variable number of prism layers (maximum of 26) on a surface mesh having average and minimum dimensions respectively equal to 0.4% and 0.08% of the reference length (propeller diameter). P1727 adopted the same relative dimensions on the blade/hub boundaries, but the total cell number counts about 4.5 million elements due to the different blade shape. The number of prism layers was adapted to the different functioning conditions, which corresponds to 23 layers. In both cases, the non-dimensional wall distance was maintained well below 1 (on average, 0.4).

OpenFOAM calculations compare very well with the results of StarCCM+. The transition to the turbulent boundary layer is predicted very similarly, in any case, within the 'uncertainty' associable to the grid differences observed in Figure 6. Streamlines show the very same radial dominance, typical of the laminar boundary layer, on most of the suction side of the blade, and the flow separation, identified by the clustering of the streamlines at the trailing edge, is almost identical.

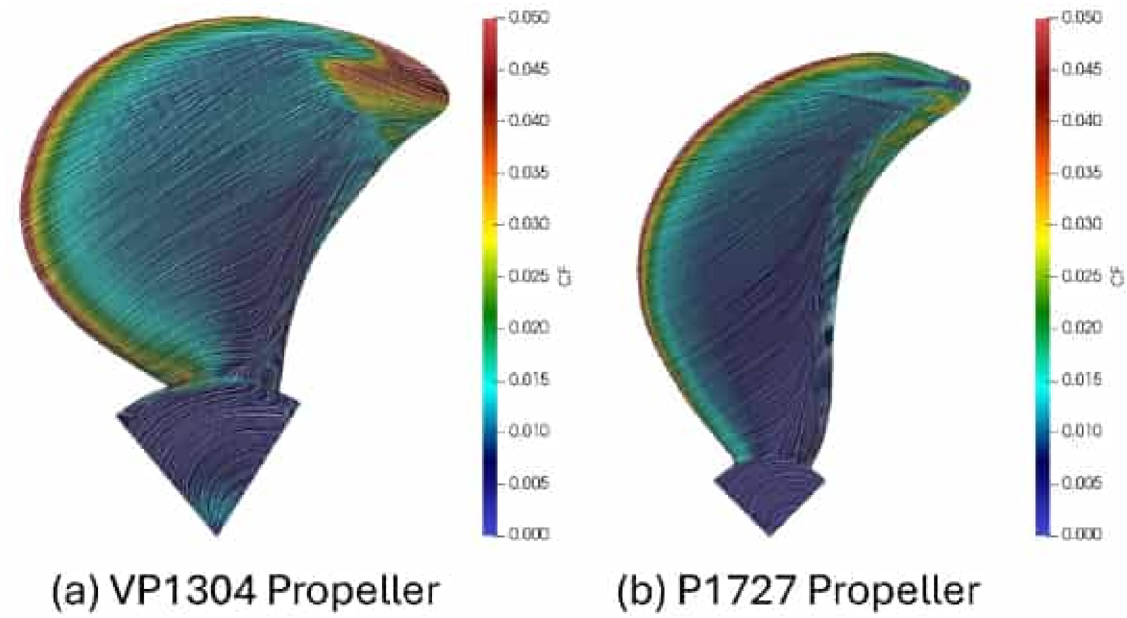

Figure 7. Predicted laminar to turbulent boundary layer transition (skin friction coefficient distribution and surface streamlines) using OpenFOAM. Turbulence intensity level of 1% at the design advance coefficient ($J = 0.5$).

The computational meshes for the ducted propellers appear very similar to those realised for VP1304 and P1727. In this case only StarCCM + calculations are proposed, and the meshes are based on the typical polyhedral cell discretization available within this solver. The parameters for surface and volumetric refinements follow the setup of the open propellers. Using again the propeller diameter as the reference length, average and minimum mesh surface sizes were set respectively equal to 0.5% and 0.05%. An identical discretization is adopted for the nozzle. The number of prism layers was set equal to 25, ensuring, at a representative functioning condition (design advance coefficient, 15 *rps*), an averaged value of $y+$ not greater than 0.3.

For the full-scale simulations, no particular studies were carried out. Computational grids were simply scaled from model-scale calculations, while maintaining the relative dimensions of cells and the zonal refinements. The only modification concerned the definition of the prism layer cells, which were modified to realise a full-scale $y+$ of approximately 40. This value is acceptable given the use of blended low- and high-Reynolds-number wall functions in both StarCCM+ and OpenFOAM. Such an assumption is common practice, as no or only extremely limited and thus negligible laminar boundary layer (strictly requiring wall-resolved meshes) is expected at full scale. At full scale, the impact of a wall-resolved boundary layer is minimal, as resolving or modelling it through wall functions primarily influences frictional forces, which contribute only marginally at high Reynolds numbers. Under full-scale conditions, pressure forces dominate and are far less sensitive to the specifics of boundary-layer resolution (i.e. wall-resolved versus wall-modelled) than in model-scale configurations, due to the proportionally thinner boundary layer. This further supports the suitability of modelling boundary-layer phenomena through wall-function approaches in the present context, also in light of the recent calculations by Rubino and Abdel-Maksoud (2024), which have shown differences between wall-resolved and wall-modelled simulations lower than 1%, and are completely acceptable for the type of analyses. The use of wall-resolved meshes, on the other hand, would have required further refinements to adapt $x+$ and $z+$ values of the cells, which would have increased significantly due to the higher aspect ratio at constant surface grid dimensions. Moreover, at full scale, a generally lower sensitivity to turbulence modelling and overall lower numerical uncertainties were observed by Eça et al. (2023), sustaining the choice of not performing dedicated grid sensitivity studies for full-scale calculations.

Sensitivity to turbulence quantities

The influence of inlet quantities on the onset of transition, and then on the reliability (and influence) of tuning inlet parameters to achieve the desired turbulence intensity on the propeller plane was studied by means of two dedicated analyses. The first applies to fully turbulent calculations using the *SST k-ω*; the second addresses the transition sensitive γ -Re_θ turbulence model in a way similar to what has already been done in Gaggero and Villa (2018) for the ERCOFTAC T3A flat plate test case and for a propeller test case using the k-k_L-ω model. In that study, it was demonstrated that, due to the numerical decay of turbulence intensity, the accurate prediction of transition onset on the flat plate depends primarily on the ability to enforce the correct level of turbulence intensity at a reference location. It was also shown that both transition and the resulting performance, expressed through the skin – friction coefficient distribution, are only marginally influenced by the specific quantities set at the inlet (turbulence intensity and eddy – viscosity ratio) to achieve that turbulence level, as well as by the local decay of turbulent quantities within the transition region, which itself depends on the inlet combination of turbulence intensity and eddy – viscosity ratio. For propellers, the same study showed that the fully turbulent model provides very similar performance predictions, within less than 1% deviation in the worst case, almost independently of the selected turbulence quantities (with inlet turbulence intensity up to 10% and an eddy – viscosity ratio of 1000). The only noticeable effect concerns the diffusion of the propeller wake, which becomes appreciably faster when very high eddy – viscosity ratios are prescribed. Since all transition – sensitive simulations presented in this work rely on tuning inlet parameters, rather than sustaining turbulence levels through dedicated turbulent – kinetic – energy source terms applied upstream of

Table 4. Fully turbulent performance (StarCCM+) of the VP1304 as a function of turbulence quantities at the design advance coefficient (J = 1.2).

Tu at inlet	μ_T/μ	*Tu* at propeller plane	K_T	$10K_Q$
1%	10	0.43%	0.2653	0.7505
2%	50	0.95%	0.2652	0.7506
3%	100	1.36%	0.2650	0.7507
5%	500	2.84%	0.2655	0.7532
10%	1000	4.32%	0.2667	0.7563

Table 5. Transition sensitive performance (StarCCM+) of the VP1304 as a function of turbulence quantities at the design advance coefficient (J = 1.2).

Tu at inlet	μ_T/μ	*Tu* at propeller plane	K_T	$10K_Q$
1.25%	113	1%	0.2927	0.7859
1.50%	75	1%	0.2927	0.7857
2.00%	57	1%	0.2927	0.7858
3.00%	51	1%	0.2929	0.7864

the propeller, the verification of the robustness of this approach, particularly when employing the γ -Re_θ model and in the specific case of propeller flows, is of paramount importance.

To this aim, VP1304, already addressed for the grid sensitivity study, is considered. Addressed fully turbulent simulations cover a wide range of inlet turbulence intensities, from 1% to 10%, and eddy–viscosity ratios between 10 and 1000 (Table 4). Transition-sensitive simulations span a narrower range of turbulence intensities, from 1.25% to 3%. In the latter case, to ensure a consistent turbulence level (1% in present analyses) at the reference location, namely, the propeller plane, the corresponding eddy–viscosity ratios were adjusted accordingly, resulting in values between 51 and 113 (Table 5).

The sensitivity to turbulence quantities seems minimal. As seen in previous analyses, predicted performance in fully turbulent conditions is barely influenced by the choice of turbulence intensity and viscosity ratio: compared to the default choice ($Tu = 1\%$, $\mu_T/\mu = 10$), differences are less than 0.1% for all the combinations with the exception of the extreme case ($Tu = 10\%$, $\mu_T/\mu = 1000$) that leads in any case to an acceptable deviation not larger than 0.5%.

The laminar to turbulent transition (at identical turbulence intensity on a reference location) seen in Figure 8 and monitored through the corresponding performances of Table 5, is minimally affected by the inlet parameters as well. Transition to the turbulent boundary layer, observed in the previous calculations (Figure 6) only at the tip of the blade, is consistently predicted throughout the selected range of parameters, and differences in the onset of the turbulent boundary layer are hardly appreciable from the skin friction distributions. The consistency of predictions is confirmed by the values of thrust and torque coefficients that, with respect to the reference configuration (*Tu* at inlet equal to 2%, eddy viscosity ratio of 57) already employed for the grid sensitivity study of Figure 6, shows deviations always lower than 0.1%. These results confirm the outcomes of the flat plate test case using the k-k_L-ω turbulence model (Gaggero and Villa 2018). The onset of turbulent boundary layer predicted by the γ -Re_θ model appears to depend primarily on the local turbulence intensity. Once transition has taken place, the subsequent decay of turbulence has a negligible effect, largely because the limited spatial extent of the blade results in very similar decay rates in the transition region regardless of the inlet conditions. Likewise, within reasonably broad limits, the specific choice of inlet parameters used to achieve the prescribed turbulence intensity at the reference location has only a minor influence on the transition behaviour and on the resulting propeller performance. This supports the conclusion that, given the present computational domain configuration, calibrating inlet quantities is as effective as sustaining turbulence by introducing dedicated turbulent kinetic energy source terms upstream of the propeller in the RANS equations when the objective is to reproduce a target turbulence intensity.

Open propellers: VP1304 and P1727

The analysis of the performance of VP1304 and P1727 concerns the model-scale predictions at the nominal rate of revolution of experiments ($rps = 15$) to discuss, among others, the influence of the turbulence intensity level on the model-scale boundary layer transition and then on the resulting thrust and torque. For these two literature propellers, no paint tests are available for direct comparisons with predicted blade streamlines. The discussion on the role of turbulence intensity, as well as any conclusions on the most appropriate tuning of this parameter (see, for instance, Kerkvliet et al. 2024), is then only qualitative. It relies solely on the relative comparison between calculations and on the agreement with the open water performance measured at the towing tank.

The comparison with experiments for VP1304 is given in Figure 9 and Table 6. Corresponding skin friction distributions (design advance coefficient of 1.2, StarCCM + calculations) are shown in Figure 10.

At the lowest turbulence intensity of 1%, only a spot of fully developed turbulent boundary layer, corresponding to the local increase of the skin friction coefficient, is present at the tip of the blade. Limiting streamlines have the expected radial orientation which denotes the predominant laminar nature of the boundary layer on most of the suction side. At the blade trailing edge, there is the typical confluence of streamlines, which indicates laminar flow separation. The combination of these effects, together with the different viscous-inviscid interaction for the pressure distributions, explains the highest values of thrust and torque in Figure 9, even if their relationship is not linear. The reduction of friction, associated with the laminar nature of the flow (see the differences in the shear-related thrust coefficient at the design advance coefficient between transition sensitive models at different turbulence intensity, i.e. different extension of laminar boundary layer, or with fully turbulent flow of Figure 12) contributes to the increase of thrust. Both thrust and torque, moreover, increase (in most cases, mainly) as a consequence of a different pressure distribution on the blade rather than by a modification of the shear forces, as seen in Figure 11, where a correlation between the nature of the boundary layer (i.e. skin friction distributions) and the pressure at the trailing edge can be established. The interaction with a dominant laminar boundary layer results in flatter pressure distributions at the trailing edge (evidenced, for instance, also in Shin and Andersen 2017; Gaggero and Villa 2018; Gaggero, 2022a; Rubino and Abdel-Maksoud 2024; Khraisat et al. 2023) and consequently higher forces associated with higher suction on the back of the blade. Laminar separation, fostered by the very low level of turbulence intensity and the low Reynolds number, further exaggerates the suction on the back of the blade and the related increase of (pressure) force in model scale. From model-scale, fully turbulent simulations to model-scale, transition-sensitive calculations with $Tu = 1\%$, there is an increase in the thrust coefficient of about 2.1% (reference to the model-scale fully turbulent value, using StarCCM+, but results are almost identical if OpenFOAM data are considered) ascribable to the reduction of the friction contribution (more than halved with respect to the fully turbulent case, see the corresponding skin friction values in Figure 11(b and d) for the intermediate turbulence intensity) granted by the dominant laminar boundary layer. But the total increment of thrust seen at model-scale when using the transition sensitive model reaches 10% only thanks to the contribution of the different pressure component due to a different coupling with the boundary

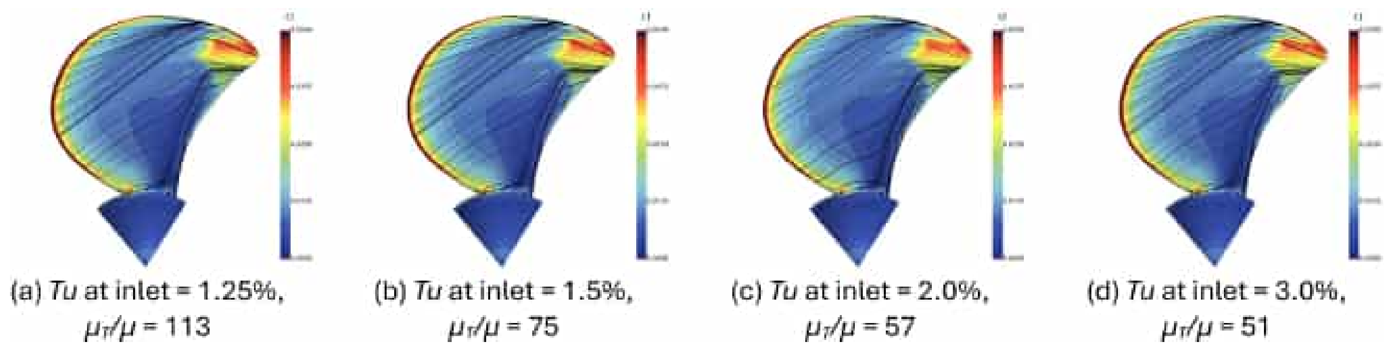

Figure 8. Influence of turbulent quantities at inlet on the onset of transition through skin friction coefficient distribution and surface streamlines. Turbulence intensity level at the propeller plane of 1% at the design advance coefficient. Calculations using StarCCM + for VP1304.

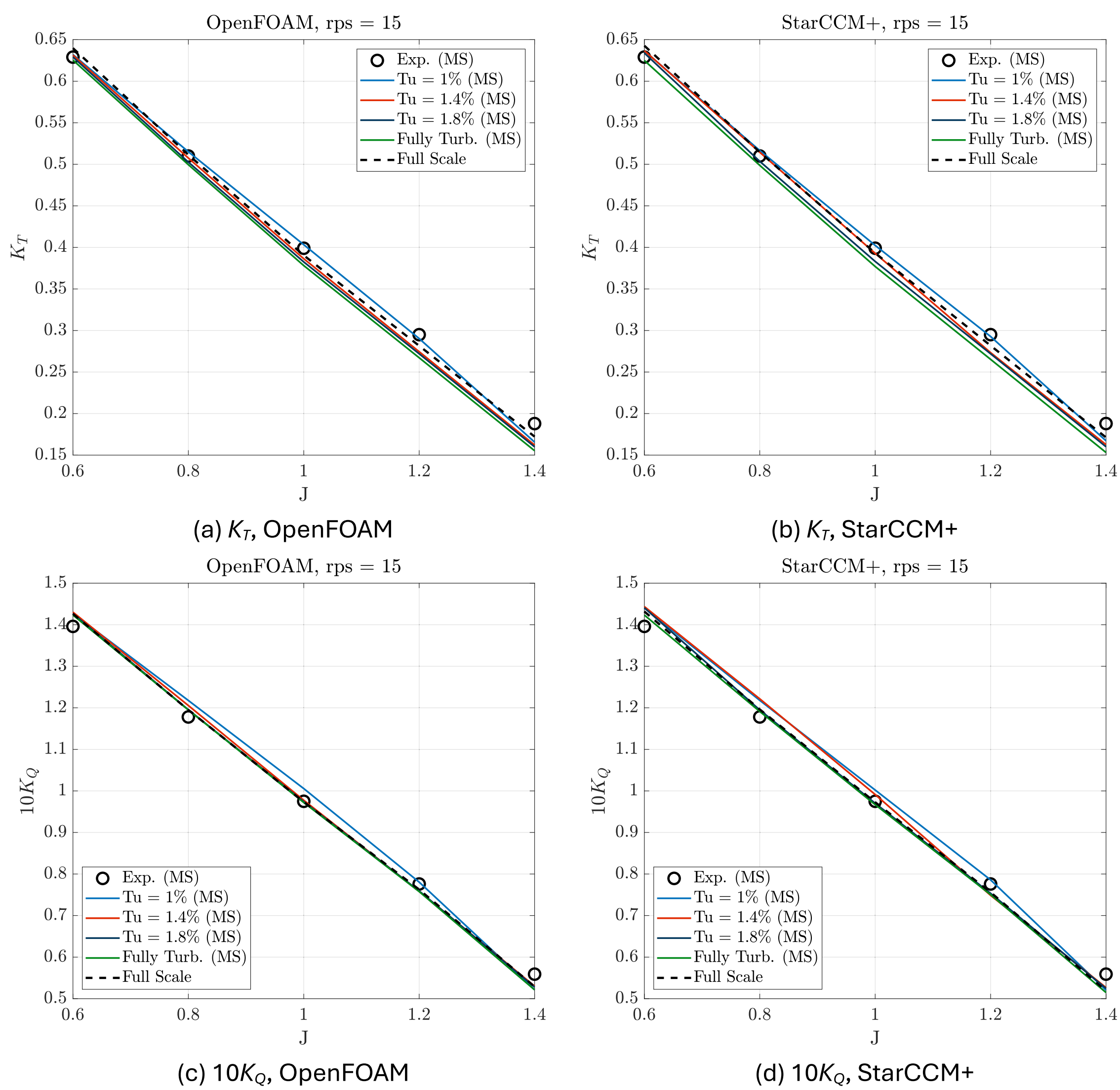

Figure 9. Model-scale open water propeller performance of VP1304. Comparison of different turbulence models and turbulence intensities using OpenFOAM (left) and StarCCM + (right) with model-scale experiments (15 *rps*).

layer, which is clearly appreciable in the higher values of suction of Figure 11(a,c).

Boundary layer interaction with the pressure distribution and flow separation influences torque as well: a reduction (about 4%) of the friction component of the K_Q due to the presence of the laminar flow in the model-scale transition sensitive analysis (again design advance coefficient, $Tu = 1\%$) is compensated by a 9% increase in pressure torque, leading to a 5% higher torque with respect to the corresponding fully turbulent calculation. The intermediate and the highest turbulent intensity values set at the propeller plane realise an earlier transition to the turbulent boundary layer and consequently intermediate values of calculated forces. Limiting streamlines assume a prevalent chordwise orientation, and the flow separation is recognised only at the root of the blade. Increased values

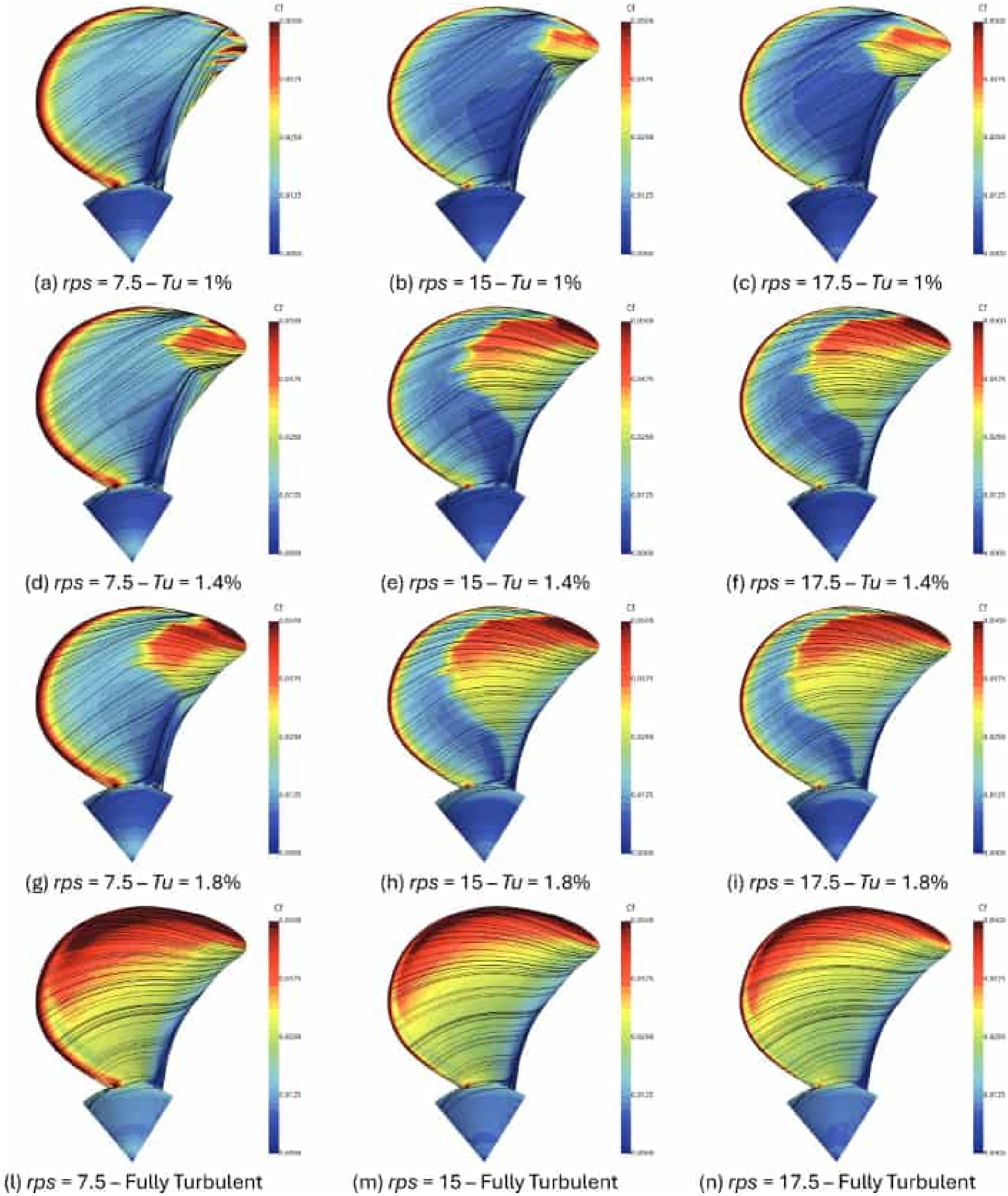

Figure 10. Influence of the turbulence intensity on the laminar to turbulent boundary layer transition (skin friction coefficient distribution and surface streamlines, StarCCM+) at several propeller rates of revolution. VP1304 at $J = 1.2$.

of turbulence make the results from the transition sensitive model closer to the fully turbulent simulations using the *SST k-ω* model (see also Gaggero 2022a on the same test case). With $Tu = 1.4\%$, transition to the turbulent boundary layer is predicted from $r/R > 0.6$, starting from the midchord of the blade. At the higher turbulence level, the first hints of transition can be recognised at r/R of about 0.4, and the onset to the turbulent boundary layer is moved towards the leading edge of the blade. The gain in frictional resistance is

Table 6. Comparison of performance (15 rps) for VP1304.

		Fully Turb.		$Tu = 1\%$		$Tu = 1.4\%$		$Tu = 1.8\%$	
J	K_T Exp.	OF	StarCCM+	OF	StarCCM+	OF	StarCCM+	OF	StarCCM+
0.6	0.629	−0.6%	−0.6%	0.5%	1.2%	0.4%	1.2%	0.0%	0.8%
0.8	0.510	−2.0%	−2.2%	1.0%	1.3%	−0.5%	0.9%	−1.4%	−1.3%
1.0	0.399	−5.2%	−5.5%	1.1%	0.9%	−3.2%	−1.5%	−4.1%	−4.0%
1.2	0.295	−9.4%	−10.1%	−1.6%	−0.8%	−6.9%	−7.3%	−7.8%	−7.8%
1.4	0.188	−17.4%	−18.5%	−11.9%	−11.0%	−13.7%	−13.5%	−14.9%	−14.8%
		Fully Turb.		$Tu = 1\%$		$Tu = 1.4\%$		$Tu = 1.8\%$	
J	$10K_Q$ Exp.	OF	StarCCM+	OF	StarCCM+	OF	StarCCM+	OF	StarCCM+
0.6	1.396	2.0%	2.0%	2.2%	3.2%	2.5%	3.4%	2.2%	3.2%
0.8	1.178	1.4%	1.1%	3.4%	3.4%	2.3%	3.7%	1.5%	1.4%
1.0	0.975	−0.3%	−0.8%	3.1%	2.8%	0.3%	1.7%	−0.1%	−0.5%
1.2	0.776	−2.4%	−3.3%	0.6%	1.3%	−2.3%	−3.5%	−2.2%	−2.9%
1.4	0.559	−6.7%	−7.9%	−6.7%	−6.9%	−5.2%	−5.8%	−5.5%	−6.1%

consequently reduced. Larger portions of the blade under turbulent flow mean higher frictional resistance. Compared to $Tu = 1\%$, the increase in thrust ascribable to the reduction of frictional forces is limited to no more than about 1% (1.1% and 0.7%, respectively, at $Tu = 1.4\%$ and 1.8%, StarCCM + calculations). This is the result of a reduction in the frictional component of about 30% ($Tu = 1.4\%$) and 18% ($Tu = 1.8\%$). The pressure component of the thrust is responsible for another 2% increase, leading to an overall 3% higher thrust with respect to the model-scale, fully turbulent case when the transition sensitive model is applied. Torque exhibits the same trend: the reduction of friction is limited when larger portions of the blade are under a fully developed turbulent boundary layer (on average, only a 2% reduction of the frictional component of the torque) and it is perfectly balanced by the 2% increase in the pressure component, still associable with the different pressure distributions due to viscous-inviscid interactions and (limited) separation. The result is a torque that is almost unchanged for any turbulence intensity higher than 1%.

These trends, discussed for the design advance coefficient, are also true in off-design, with limited differences case by case and again regardless of the adopted CFD solver. They can be appreciated in the open water diagrams of Figure 9. Thrust appears more susceptible to the variations of the turbulent boundary layer onset. Both OpenFOAM and StarCCM + show variations in the order of 7–10% (increase) of thrust on the entire range of advance coefficients when using $Tu = 1\%$ with respect to the fully turbulent simulations. On average over the range of advance coefficients, only a 2% increase is observable when using higher turbulence levels. Torque, instead, is more 'stable': at the lowest turbulence intensity level, when the laminar boundary layer is more extended on the propeller blades, the increase of K_Q is only 3–4%. It is negligible at any advance when the 1.4% or 1.8% turbulence intensity levels are considered. A turbulent boundary layer (or larger zones under the turbulent boundary layer), indeed, results in higher friction and lower pressure, both negatively impacting the thrust. But while friction has a negative (increasing) effect, the lower pressure observable in the case of the turbulent boundary layer contributes to a reduction of the torque, explaining the different sensitivity of the propeller performance to the boundary layer regime. Compared to experiments, the choice of the most appropriate parameter for the transition-sensitive model based only on propeller performance is not trivial. As seen in many similar simulations, the use of transition-sensitive models improves comparison with experiments. Current calculations confirm this observation. Especially for thrust, differences with experiments are significantly reduced by the use of the γ -Re_θ model together with a small value of the turbulence intensity. A turbulence intensity of $Tu = 1\%$ has, for instance, been adopted by several researchers (Rubino and Abdel-Maksoud 2024), based also on the limited available measurements and on the most reasonable estimates of this parameter in towing tanks (Marinet 2014).

Under this assumption, the underestimation of thrust (5–10%) seen with fully turbulent simulations is almost nullified (less than 1% using both CFD codes). Torque, on the contrary, suffers from a slight overestimation since it changes from an averaged −2% (fully turbulent, model-scale) to a + 3% (transition sensitive, model-scale). The prediction of torque slightly improves at the intermediate and higher values of turbulence intensity at which, instead, the predicted thrust becomes more similar and then significantly underestimated compared to the values obtained with the fully turbulent model.

The results for the tip-raked P1727 propeller show the very same trend observed for VP1304. The comparison with model-scale experiments (propeller rate of revolution equal to 18, Figure 13 and Table 7) highlights the positive influence of transition sensitive models. Model-scale fully turbulent calculations, indeed, are substantially underestimated, in terms of both thrust and torque. Regardless of the CFD tool, thrust is 2–9% (OpenFOAM) and 3–10% (StarCCM+) underpredicted in the range of advance coefficient between $J = 0.3$ and $J = 0.7$. Predicted torque is slightly better, with differences (underestimation) not greater than 3%. Switching to the γ -Re_θ substantially reduces the gap with measurements.

At 1% turbulence level, thrust and torque are only slightly overestimated, in particular the OpenFOAM results (Figure 13). A turbulence level of 1.4% realises the best match with experiments since both thrust and torque are within 1% of deviation (except the zero-thrust point, which is in any case less significant and, by its nature, highly susceptible to high percentage errors). Increasing the turbulence intensity to 1.8% leads to results closer to fully turbulent calculations, as a consequence of the more extended turbulent boundary layer observable on the blade.

The trend of the turbulent boundary onset with turbulence intensity is not different from what observed in the case of VP1304. Increased values of turbulence intensity foster the earlier transition to the turbulent boundary layer on a blade that, by its nature (very small expanded area ratio, very small chord-based Reynolds number at the design functioning, not greater than $5.0\ 10^5$), is more prone to laminar flow. At the default value of Tu (1%), the entire suction side of the propeller (Figure 14) is under laminar flow conditions: streamlines are completely radially oriented, and flow separation at trailing edge is evidenced by their clustering. Only at the highest turbulence intensity, at the tip of the blade, there is a stable and developed turbulent boundary layer, still with a severe flow separation from blade root to about $r/R = 0.6$.

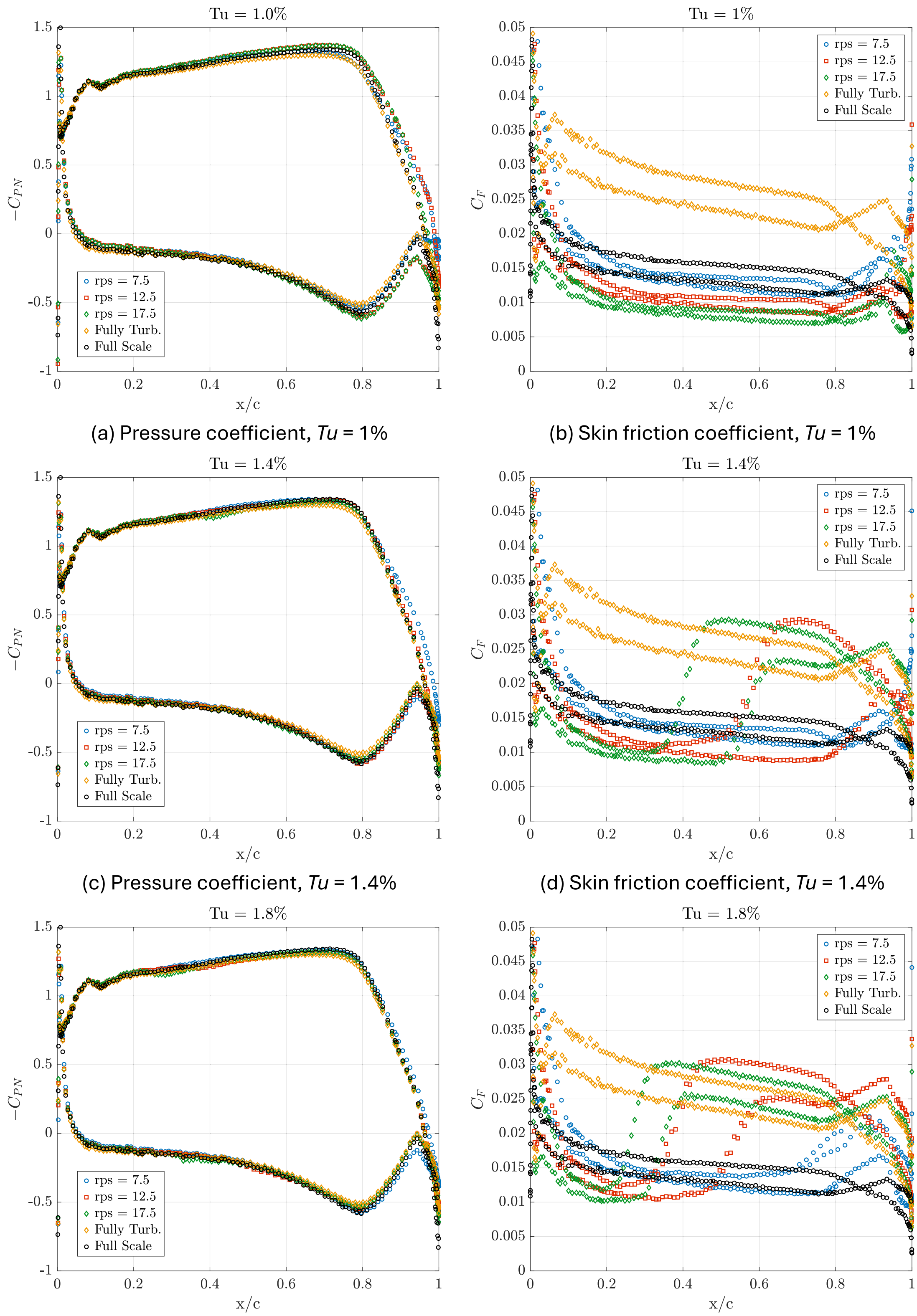

(a) Pressure coefficient, *Tu* = 1%
(b) Skin friction coefficient, *Tu* = 1%
(c) Pressure coefficient, *Tu* = 1.4%
(d) Skin friction coefficient, *Tu* = 1.4%
(e) Pressure coefficient, *Tu* = 1.8%
(f) Skin friction coefficient, *Tu* = 1.8%

Figure 11. Pressure and skin friction coefficient (StarCCM+) on a radial section ($r/R = 0.7$) of the VP1304 propeller ($J = 1.2$).

The frictional component has a very negligible influence on the thrust of the propeller, as seen in Figure 15. Compared to the total thrust, the shear contribution (resistance) is less than 1% (fully turbulent case). When the laminar boundary layer has the maximum extension, the shear component is reduced by more than 60%, but in terms of overall performance, its contribution is less than 0.5%. As a consequence of the different streamlines ('cambering effect', as described in Shin and Andersen 2017, and flow separation) induced by the laminar boundary layer and a different viscous-inviscid interaction, the pressure contribution has the highest influence. Under

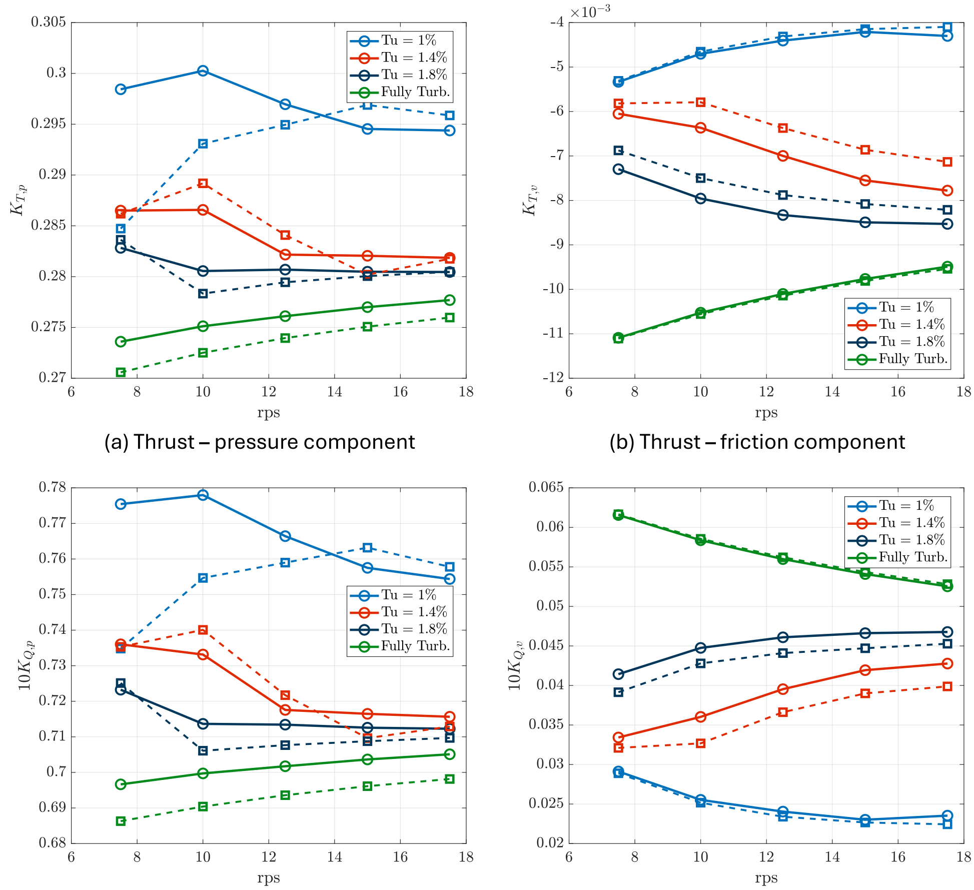

(a) Thrust – pressure component

(b) Thrust – friction component

(c) Torque – pressure component

(d) Torque – friction component

Figure 12. Pressure ($_p$) and shear ($_v$) components of propeller thrust and torque at the design advance coefficient for VP1304. Influence of the turbulence intensity level and of the rate of revolution. Solid lines: OpenFOAM calculations. Dotted lines: StarCCM + calculations.

Table 7. Comparison of performance (18 rps) for P1727.

		Fully Turb.		Tu = 1%		Tu = 1.4%		Tu = 1.8%	
J	K_T Exp.	OF	StarCCM+	OF	StarCCM+	OF	StarCCM+	OF	StarCCM+
0.6	0.353	−1.1%	−1.7%	3.3%	0.7%	1.6%	0.0%	0.6%	−0.2%
0.8	0.283	−2.5%	−3.2%	2.5%	0.9%	1.5%	−0.2%	0.1%	−0.9%
1.0	0.209	−6.3%	−7.1%	0.8%	−0.5%	−1.4%	−2.3%	−3.2%	−3.4%
1.2	0.116	−8.9%	−9.9%	2.2%	0.6%	−1.2%	−1.8%	−5.3%	−5.7%
1.4	0.007	−65.3%	−97.9%	112.0%	−1.3%	20.9%	−14.3%	−1.4%	−21.7%
		Fully Turb.		Tu = 1%		Tu = 1.4%		Tu = 1.8%	
J	$10K_Q$ Exp.	OF	StarCCM+	OF	StarCCM+	OF	StarCCM+	OF	StarCCM+
0.6	0.39	0.7%	1.4%	4.5%	2.6%	2.7%	1.6%	1.8%	1.4%
0.8	0.338	−0.7%	−1.3%	1.8%	0.8%	1.3%	−0.3%	0.0%	−0.7%
1.0	0.275	−1.9%	−2.9%	0.9%	−0.3%	−1.2%	−2.5%	−2.2%	−2.9%
1.2	0.181	−1.8%	−3.0%	0.2%	−1.0%	−2.2%	−3.1%	−4.4%	−5.4%
1.4	0.053	−0.5%	−4.3%	12.9%	−2.2%	−2.6%	−6.2%	−2.8%	−5.1%

laminar flow, increments higher than 3% (Tu of 1.4%, about 7% with Tu equal to 1%) are the most important factors responsible for the increase in thrust from the very underestimated values calculated in fully turbulent conditions.

Given the dominant nature of laminar flow, even at relatively high turbulence intensities (at least compared to the VP1304 case), the pressure increments remain relevant under any conditions under investigation, explaining the overall better agreement of transition-sensitive analysis at any turbulence intensity with the experiments.

The pressure component plays the most important role also for the torque. The pressure drag associated with flow separation predicted by the γ-Re_θ determines increments in the torque with respect to the fully turbulent case of the order of 4–8%. As for VP1304, with the exception of the lowest turbulence intensity case, these increments are totally balanced by the reduction of the frictional component of the torque due to the lower friction associated with the laminar boundary layer, leading also for this propeller to torque curves that are almost overlapped when $Tu > 1\%$.

At the design advance coefficient, trends of the propellers' performance with the model-scale Reynolds number (i.e. rate of revolution) are given in Figure 15. Pressure and shear contribution to thrust and torque are given separately, using both OpenFOAM and

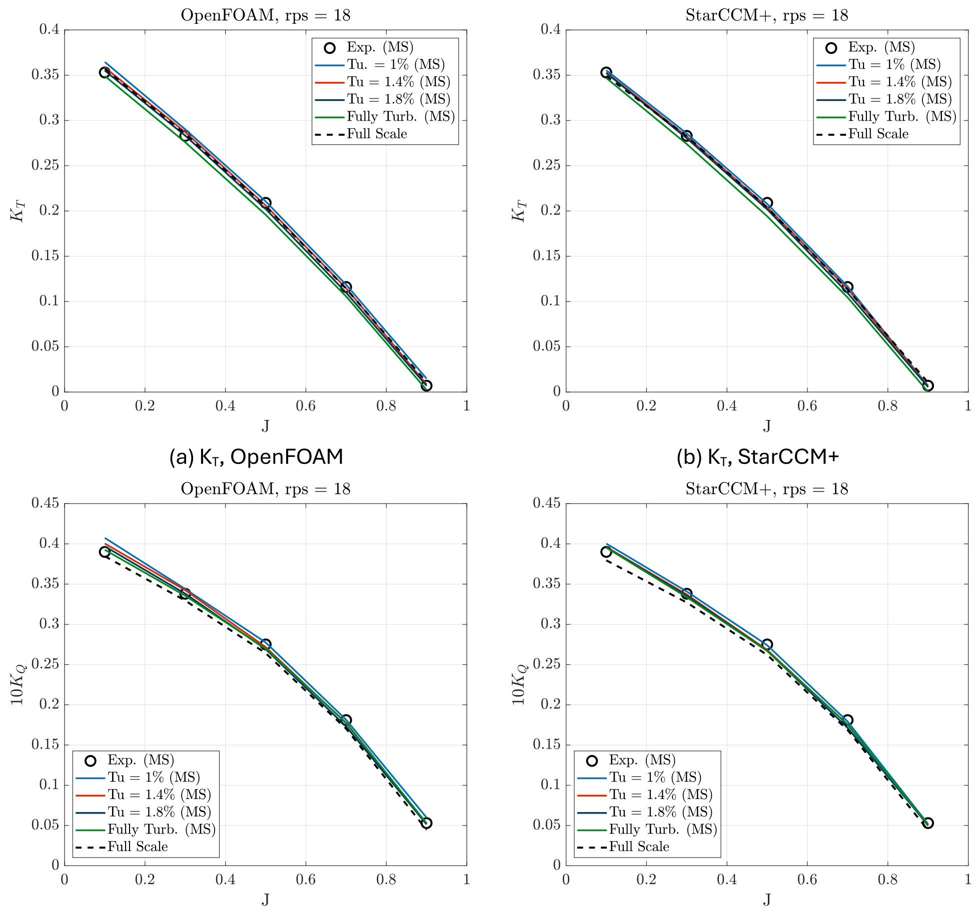

Figure 13. Model-scale open water propeller performance of P1727. Comparison of different turbulence models and turbulence intensities using OpenFOAM (left) and StarCCM + (right) with model-scale experiments (18 *rps*).

StarCCM+. The frictional parts ($K_{T,v}$ and $K_{Q,v}$) clearly highlight the usual influence of the Reynolds number on the frictional component of forces, which is very similar for both the geometries. First, it is worth noting that results from OpenFOAM and StarCCM + are very close to each other, regardless of the rate of revolution or the turbulence intensity level at which the simulation is carried out. Limiting cases are those represented by the fully turbulent calculations and those at a turbulence intensity of 1%, which show a continuous reduction of the friction with the increase of the propeller rate of revolution. The increase of the Reynolds number, overlooking the influence on the pressure distribution, naturally reduces the friction coefficient. This is true in fully turbulent boundary layer conditions (i.e. simulations using the fully turbulent model, or full-scale functioning) as well as in the case of laminar boundary layer over the entire surface under investigation. For transitional cases, a reduction of the frictional forces with the increase of the Reynolds number depends on how much friction increases due to the transition to the turbulent boundary layer (and its extension). For cases with 1% turbulence intensity, propellers (VP1304 in Figure 10, P1727 in Figure 14) exhibit a clear predominance of laminar boundary layer. The localised appearance of spots of turbulent flow associated with a local increase in friction is not sufficient to compensate for the friction reduction provided by the dominant laminar boundary layer at very high Reynolds numbers. Intermediate turbulence intensity levels lead instead to non-monotonic trends. The decrease of the laminar friction coefficient with increasing Reynolds number is outweighed by the growth of extended turbulent – boundary – layer regions: on the blade surface, these turbulent zones expand more rapidly than the reduction in both laminar and turbulent friction coefficients achieved at higher Reynolds numbers. On VP1304, the presence of the turbulent boundary layer for $Tu \geq 1.4\%$ also at the lowest Reynolds number is such that the reduction of the friction coefficient is always compensated by the increase of the turbulent flow. Overall, then, there is an increase in the frictional forces with the increase of the propeller rate of revolution. For P1727, which by its nature is more prone to laminar boundary layer, some intermediate conditions ($12 < rps < 15$) exist in correspondence with which the growth of the turbulent boundary layer is not sufficient to compensate for the reduction of friction due to the increase of the Reynolds number. In this range of functioning conditions, as for the lowest turbulence intensity case (or the fully turbulent one), an increase of the Reynolds number still corresponds to a reduction in friction. At the highest rates of revolution, instead, the presence of a relevant portion of the blade under turbulent flow makes the frictional component of forces increase.

Trends are not so obvious and are partially in disagreement between the two CFD codes when the pressure component is addressed. In the case of VP1304 (and also P1727 when OpenFOAM results are considered), the consequences of much more severe separation at very low Reynolds numbers are well visible since they correspond to the increase in thrust and torque just discussed in the comparison with the experiments. StarCCM+ calculations at the lower rates of revolution of P1727 have instead an opposite trend,

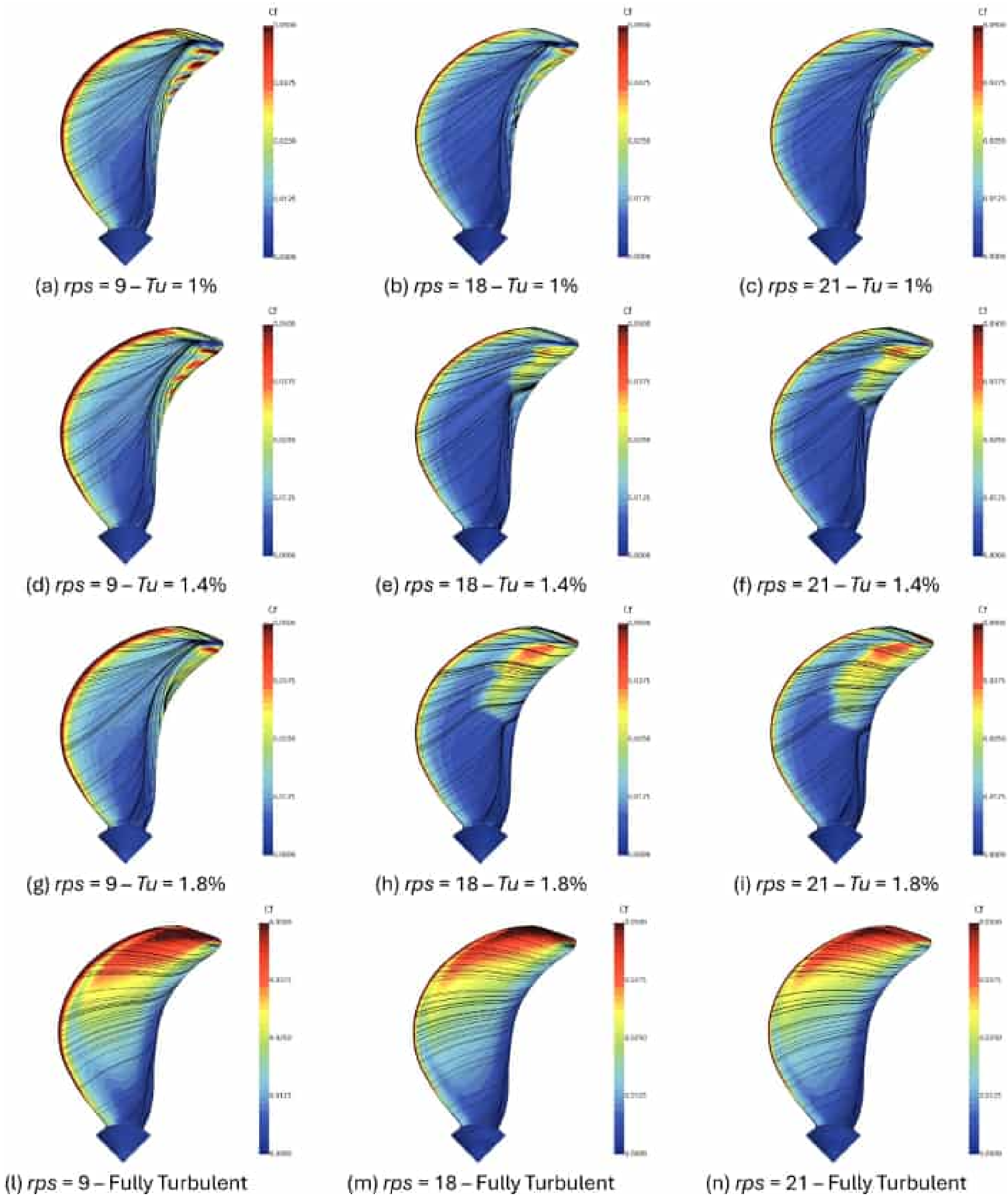

Figure 14. Influence of the turbulence intensity on the laminar to turbulent boundary layer transition (skin friction coefficient distribution and surface streamlines) at several propeller rates of revolution. P1727 at $J = 0.5$.

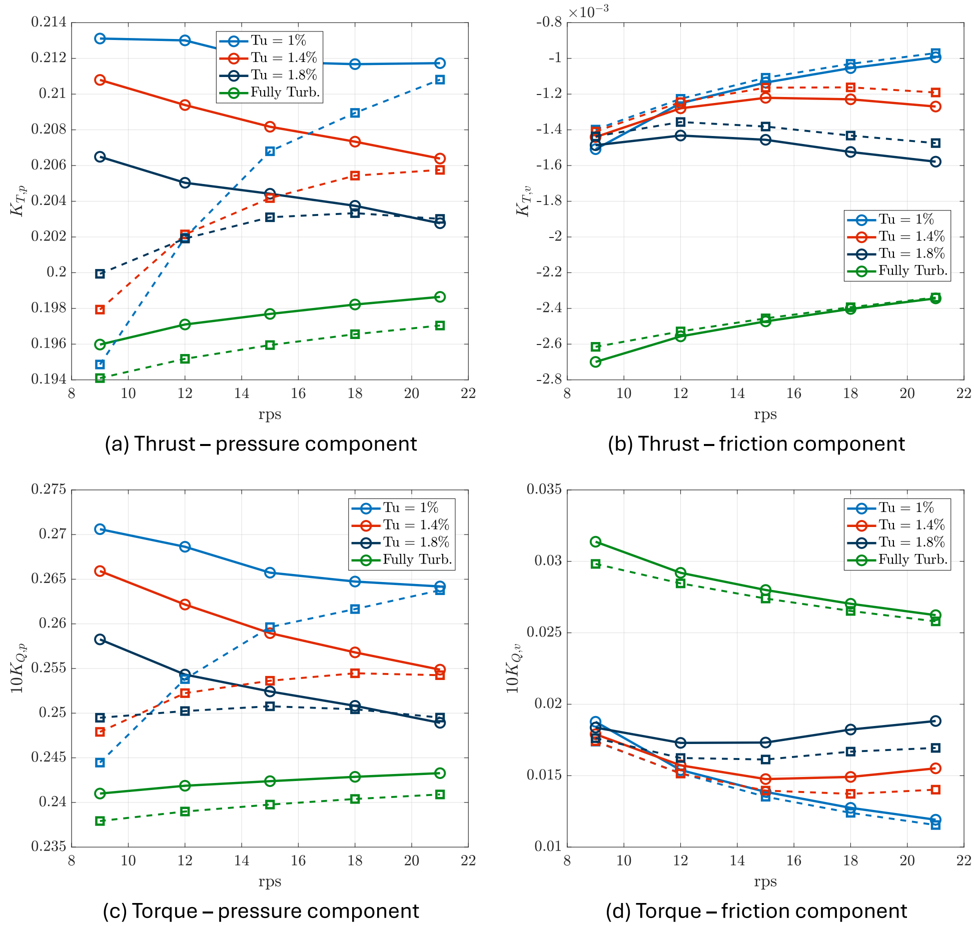

Figure 15. Pressure (p) and shear (v) components of propeller thrust and torque at the design advance coefficient for P1727. Influence of the turbulence intensity level and of the rate of revolution. Solid lines: OpenFOAM calculations. Dotted lines: StarCCM + calculations.

with the lowest values of both thrust and torque for the lower rate of revolution equal to 9 *rps*.

An overview of the scale effects of these two open propellers, considering simultaneously the influence of the Reynolds number and the turbulence intensity levels, is provided in Figures 17 and 19. For the comparisons, scale effects are computed in accordance with Equation (4):

$$\Delta K_T\% = \frac{K_T^{fs} - K_T^{ms}}{K_T^{ms}}$$
$$\Delta K_Q\% = \frac{K_Q^{fs} - K_Q^{ms}}{K_Q^{ms}} \qquad (4)$$

It is worth noting that, with respect to the definition provided by ITTC (1978, 2014), in current formulation positive values of Δ always mean that the full-scale performances are higher than model-scale ones. Reference values for the scaling are exactly those given by the ITTC formulation. They are collected in the diagrams of Figure 16 (VP1304) and 18 (P1727). Since the ITTC formulae directly provide the increments from model- to full-scale, for a fair comparison with current numerical results, these data have been made non-dimensional with respect to the model-scale experimental values. Bars, for any advance coefficient, represent the minimum (ITTC formulae using the highest model-scale rps) and the maximum (ITTC formulae using the lowest model-scale rps) value of the scaling effect to be compared with the values from the CFD calculations at the various model-scale rate of revolution. Different values of surface roughness (the one suggested by the ITTC, 3010^{-6}, and a smaller one) are considered as well to be more coherent with the CFD analyses which do not account for any roughness in full-scale.

ITTC scaling reflects the theoretical assumptions of the Lerbs method: an increase of the Reynolds number due to full-scale corresponds to a reduction in the friction coefficient that always determines an increase of the thrust (positive values of Δ) and a decrease of the torque (negative values of Δ). Trends are monotonic with the advance coefficient since no additional effects like flow separation and influence on the pressure components of the forces due to very off-design functioning are accounted in the ITTC formulation. The magnitude of the model-to-full-scale corrections, regardless of the model-scale rate of revolution, is modest. For VP1304, when a very low full-scale roughness is considered, the maximum thrust correction is lower than 1.5% at the highest advance coefficient. Torque reaches −2%.

Full-scale CFD extrapolations are less obvious, even if some common trends with the ITTC can be identified. As expected from the discussion of model-scale performances at different rates of revolution and turbulence intensity levels, a significant influence of these two parameters can be observed in the scaling effects. At intermediate and design loadings, indeed, the scale effects of thrust depend on the turbulence intensity level. With the lowest value of *Tu*, sometimes also with $Tu = 1.4\%$, model-scale thrust is higher than full-scale performance (negative values of Δ). This is a behaviour opposite to what is expected from the standard ITTC procedure. The reason, again, is the dominance of the model-scale pressure-related phenomena associated with the interaction with the dominant laminar boundary

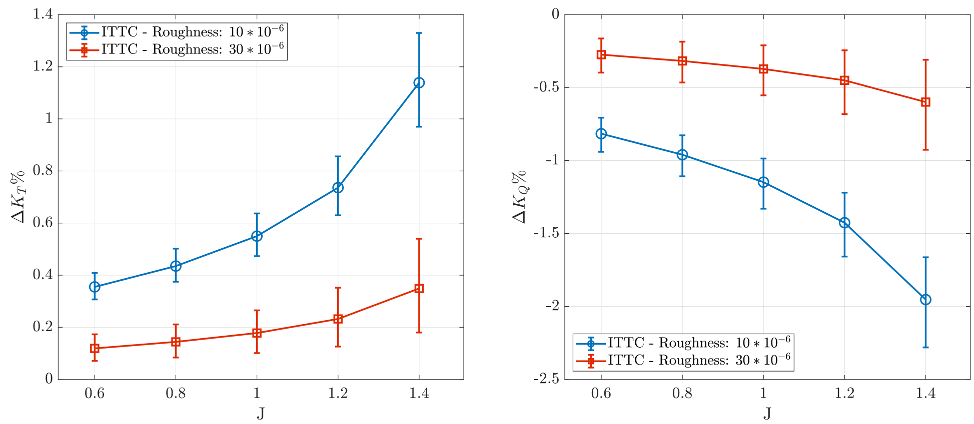

(a) ITTC based thrust coefficient correction

(b) ITTC based torque coefficient correction

Figure 16. 'Average' full-scale corrections from the standard ITTC procedure for VP1304 propeller. Vertical bars represent minimum and maximum values of the ITTC corrections changing the model-scale propeller rate of revolution. Values as a percentage of the model-scale performance from the experimental campaign.

layer not accounted by the traditional scaling methodologies. As seen discussing model-scale performance at various turbulence regimes, 'cambering' and separation exaggerate the pressure components of the model-scale forces, leading to model-scale thrust significantly higher than full-scale, where the reduction of the frictional components for Reynolds effect plays the major role, being the influence on the pressure field is less influenced by a proportionally thinner and non-separated boundary layer. Through the viscous-inviscid interaction taking place in case of dominant laminar boundary layer, indeed, pressure distributions have higher values of suction on the back side compared to fully turbulent (full-scale) conditions, and the flow is naturally more prone to separation, which increases the suction as well. For instance, at $J = 1$, the full-scale contribution (i.e. resistance) of shear thrust to the total delivered thrust is less than 1.5% ($K_{T,\nu} = -0.0059$). Due to the particular flow regime established at model-scale (almost completely laminar flow), when the turbulence intensity is very low ($Tu = 1\%$), the model-scale shear forces are smaller than full-scale since the Reynolds effect, i.e. the reduction of the frictional resistance with increasing Reynolds number, is overbalanced in model-scale by the dominance of laminar flow, which produces much lower friction. On average over the range of propeller rates of revolution at $Tu = 1\%$, they contribute to less than 1% of resistance ($K_{T,\nu} = -0.0043$), then less than full-scale. Pressure components contribute to a 3% higher thrust on average in model-scale. Less friction in model-scale combined with higher pressure forces determines the negative values of the scale effects of thrust.

Increasing the turbulence intensity of model-scale calculations (any advance coefficient, any propeller rate of revolution) determines an increase in the scale effects, which are due to the decrease in thrust in model-scale as a result of the combined effect of pressure and shear components of the forces observed in Figure 12. When the turbulent boundary layer is sufficiently extended over the blade ($Tu = 1.4\%$ and 1.8%), the relative contribution of shear thrust to the total delivered force of the propeller increases to about 2%. With respect to the full-scale $K_{T,\nu}$, model-scale shear thrust is about 20–30% higher (model-scale $K_{T,\nu}$ between -0.006 and -0.0078, depending on the rate of revolution and turbulence intensity), and the pressure contribution to thrust is lower than in full-scale, determining lower model-scale total thrust coefficients and, consequently, positive values of the scaling effect according to the definition given in Equation (4).

The same trend is recognisable when considering, at a constant advance coefficient, the influence of the rate of revolution. Higher *rps* in model-scale foster turbulent boundary layers, mitigate separation-related phenomena, and determine lower values of thrust corresponding to higher scale effects. At intermediate values of turbulence intensity (with the exception of very off-design conditions, $J = 0.6$, and very low rates of revolution, $rps < 10$), scale effects increase with the increase of the advance coefficient, in accordance with the ITTC suggestion, guaranteeing a full-scale increase of thrust of about 1.5–3% (OpenFOAM calculations), which is significantly higher than the values provided by the traditional scaling approach. Frictional forces, indeed, are less dependent on the loading and, at high advance values where their relative importance is higher compared to the pressure contribution, Reynolds effects applied to friction explain the higher improvements of the full-scale propeller performance.

Without the complexity added by the transition-sensitive turbulence models in model-scale, the scale effects computed using only fully turbulent models (then, without most of the viscous-inviscid interactions evidenced in model-scale with the presence of dominant laminar flow) have clearer and more stable trends. The relative full-scale increase of thrust is higher at higher advance coefficients and an increase in the rate of revolution of the propeller determines a reduction of the scale effect. Since mainly shear forces suffer Reynolds effects (at $J = 1$, there is an almost constant increase of the pressure components, +2.5%, from 0.386 of model-scale to 0.3956 of full-scale for thrust regardless of the model-scale *rps*), this trend is easily ascribable to the reduction of the shear forces of fully turbulent model-scale calculations at different Reynolds numbers (from $K_{T,\nu} = -0.01$ at 7.5 *rps* to -0.0087 at 17.5 *rps* versus -0.0059 in full-scale). This corresponds to higher values of thrust in model-scale and, consequently, in smaller differences with respect to the fully turbulent full-scale performance. This behaviour, associated with higher scale effects (3–6% for the thrust), is the same evidenced in Kerkvliet et al. (2024), where it served to introduce the idea of model-scale tests (as well as simulations) tripped to turbulence to ease the scaling procedure of propeller performance.

Similar conclusions can be drawn for the scale effects of torque, again with some important differences in trends compared to traditional scaling rules. At intermediate loadings, full-scale torque is always lower than the value calculated in model-scale. This is true regardless of the turbulence intensity of the model-scale calculations. The maximum variations of the scale effects correspond to the lowest value of Tu (1%) in model-scale. Again, this is the result of the very high torque predicted in model-scale when severe laminar flow induced separation is present, contributing to about a + 4.5% higher torque in model-scale compared to the full-scale data. Nullifying the pressure component increase of torque in full-scale thanks to the fully turbulent flow determines the 2-4% scale effects evidenced in Figure 17. For the intermediate values of turbulence intensity, those that seem to realise a better agreement with model-scale experiments (Figure 9), scale effects seem modest and closer, with respect to thrust, to the ITTC predictions. At the highest loading ($J = 0.6$), scale effects on torque are always much lower than those on thrust, confirming the observation of Kerkvliet et al. (2024), who evidenced a dominance of thrust effects in the increase of the full-scale propeller efficiency. At $J = 0.8$, or $J = 1$, the relative weight of thrust and torque effects on the full-scale efficiency depends on a combined effect of loading, turbulence intensity and rate of revolution. For these advance coefficients and turbulence intensities of 1.4% or 1.8%, the full-scale predicted reduction of torque (abt. −1.5%, OpenFOAM calculations) is more important than the small increase (in some cases, even decrease) of thrust when the model-scale propeller rate of revolution is lower than 12.5. When, instead, model-scale simulations are carried out at higher rps, the increase of thrust (between 1 and 2%) has a higher relative importance for the increase of the propeller efficiency than the small reductions (0–0.75%) of torque. In no cases, anyhow, the increase of thrust is nullified, in terms of full-scale efficiency, by an equivalent increase of full-scale torque, as seen in some cases by Rubino and Abdel-Maksoud (2024). Only at the lightest loading condition the full-scale predicted torque is higher than the corresponding model-scale values regardless of the rate of revolutions and the turbulence intensity (with the exception of $Tu = 1\%$). This change in sign of ΔK_Q is the result of a trend that shows progressively smaller scale effects with the increase of the advance coefficient, then completely opposite to what is foreseen by the ITTC procedures. These tendencies, discussed using OpenFOAM data, are almost replicated also if StarCCM + calculations are considered, with only small discrepancies associated with the differences between the CFD codes already observed (Figures 9 and 12) for identical model-scale conditions.

As for the thrust, the scale effects of torque predicted using only fully turbulent analyses confirm the conclusions of Kerkvliet et al. (2024). Torque is only slightly influenced by the propeller scale: it increases (contrary to the ITTC trend) on average by 0.5%, and the changes in the propeller loading conditions, which have a role in the scale effects of thrust even when solely fully turbulent calculations are considered, are almost uninfluential (Figure 18).

Similar conclusions can be drawn when analysing the scale effects (from different model-scale rps and turbulence intensity levels) computed for the P1727. Trends are quite similar to the previous case, sometimes simply shifted towards higher values of *rps* or turbulence intensity due to the nature of the geometry under investigation. For instance, negative values of the scale effect of thrust (Figure 19) are seen also for values of turbulence intensity (1.4%) that in the case of the conventional propeller already granted positive corrections. P1727 has a very low expanded area and the functioning Reynolds numbers in model-scale consequently are reduced. Also at relatively high values of turbulence intensity the dominance of the laminar boundary layer in model-scale when transition-sensitive models are employed has been observed (Figure 14), and all the laminar flow-related phenomena (importance of the pressure components of forces, and smaller frictional forces than full-scale) explain model-scale performance (thrust) higher than full-scale. For this propeller too, to higher values of J correspond higher values of scaling effects for thrust (when the turbulence intensity is high enough to grant a certain relevance of the turbulent boundary layer in model-scale, $Tu = 1.8\%$), as well as an increase in rps (at constant J) determines higher scaling effects in accordance with usual ITTC procedures. This is particularly true when OpenFOAM calculations are addressed. In the case of StarCCM + simulations, the differences in pressure components of forces evidenced at model-scale (Figure 15) makes the trends not so obvious, in particular for cases at very low turbulence intensity and rates of revolutions, but the qualitative behaviour at intermediate and high rate of revolutions is exactly replied also when using this CFD tool.

Scale effects for torque have a completely different tendency with respect to what is observed for the conventional VP1304. In agreement with the parametric scaling rules of ITTC (with the only exception of the highly loaded cases), the scale effect generally tends to increase with the advance coefficient (Figure 18), reaching values close to 4–5% regardless of the turbulence intensity or the model-scale Reynolds number when J is equal to 0.7. For this tip raked propeller, then, the major contributor to the full-scale increase of efficiency when model-scale transition sensitive models are employed is described by the reduction of the full-scale absorbed torque.

When the fully turbulent model is employed in model-scale, instead, trends are much more stable, as already seen for the VP1304. Increase in full-scale thrust (up to 10% at intermediate and lightly loaded conditions) appears to be the major factor responsible for the full-scale higher efficiency. Contrary to what is evidenced by VP1304 and several literature analyses (Baltazar et al. 2023; Kerkvliet et al. 2024), the scaling of torque still plays a certain role since a full-scale reduction in the order of 3–4% is foreseen at $J = 0.5$ and 0.7.

Ducted propellers: accelerating and decelerating nozzles

The analysis of scale effects of ducted propellers, as in the case of open propellers, starts from the comparison with the available experiments. Also in this case, no paint tests can be used for a thorough discussion of the influence (or the correct tuning) of the turbulence intensity level on the laminar-to-turbulent boundary layer transition, which is addressed comparatively based only on numerical results. Calculations are presented in Figure 20 and Figure 28 (Tables 8 and 9), respectively, for the propeller in the accelerating and the propeller in the decelerating duct. As for the open propellers, the contributions to blades and duct thrust and torque of the pressure and the frictional components of the forces are presented in Figure 21 and Figure 29 for a selected advance coefficient, while streamlines, frictional coefficient distributions, representative of the occurrence of different types of boundary layer, are shown on the blades' suction side and on the external surface of the nozzle in Figures 22 and 23 (accelerating ducted propeller) and 30 and 31 (decelerating ducted propeller). Non-dimensional velocity distributions at trailing edge (Figure 24 and Figure 32) as well as distributions of pressure and skin friction coefficients on a longitudinal section of the nozzle (12 o'clock position) are included as well (respectively Figure 25 and Figure 33) to sustain the trends evidenced by thrust and torque coefficients at different scales.

The comparison with model-scale experiments (carried out at 15 *rps*) shows some substantial differences with the trends observed for the open propellers changing the turbulence intensity level. These differences may be partially attributed to some numerical uncertainty, since no dedicated convergence studies have been carried out specifically for these geometries, even if the influence of the leakage vortex (Gaggero et al. 2014), the only peculiar phenomenon that would have deserved a dedicated grid study, is not deemed sufficient to justify the observed discrepancies of any numerical simulations with respect to the available experiments. They resemble the differences highlighted in many different calculations, using different tools and grid arrangements also aimed at characterising the leakage vortex. The observed consistency of these discrepancies regardless of the adopted mesh and models indirectly confirms the rationality of the grid selection for the scope of current analyses (Gaggero 2023).

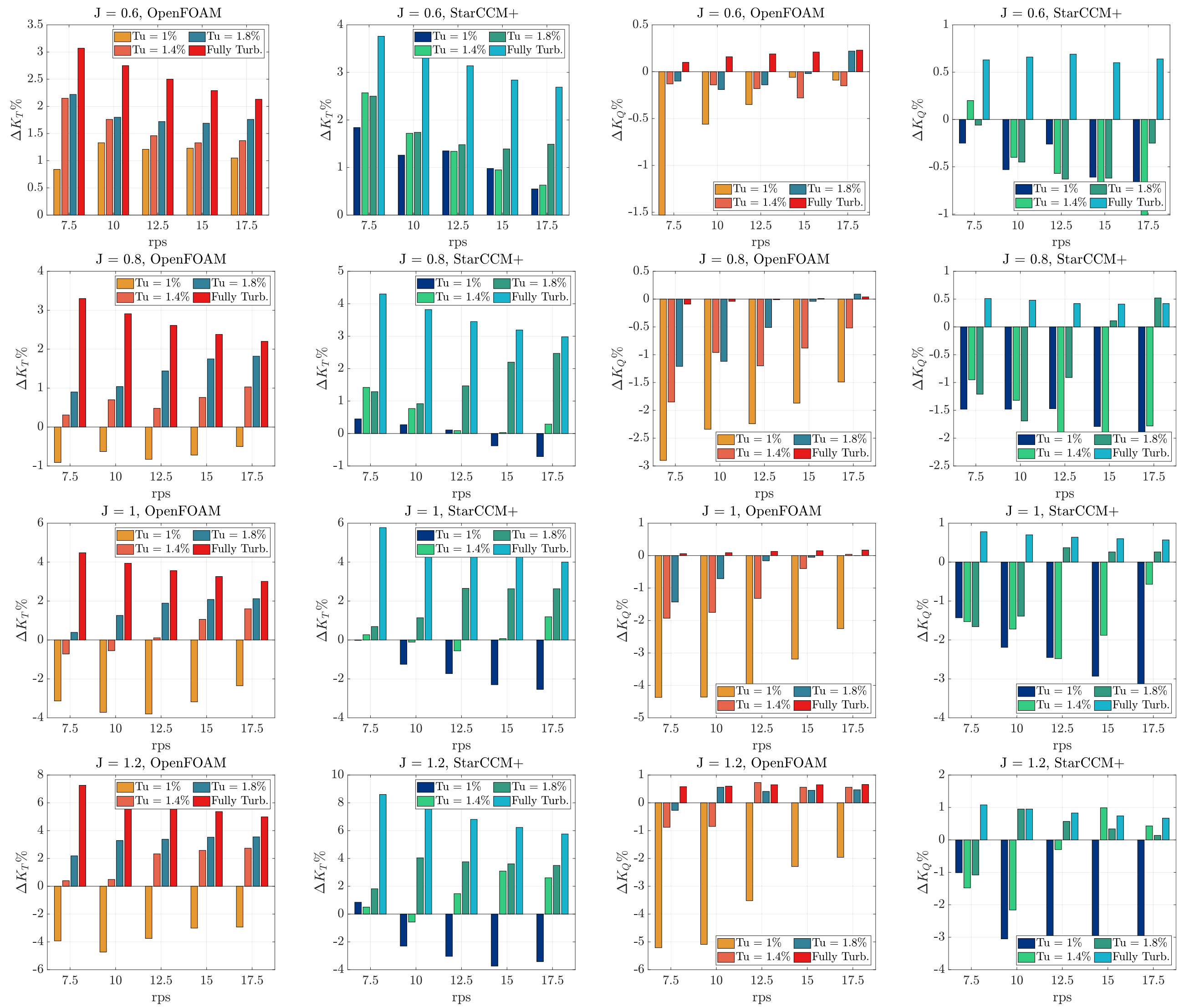

Figure 17. Scale effects for VP1304 propeller as a function of the propeller loading, the model-scale rate of revolution and turbulence intensity level. OpenFOAM (left) and StarCCM + (right) calculations.

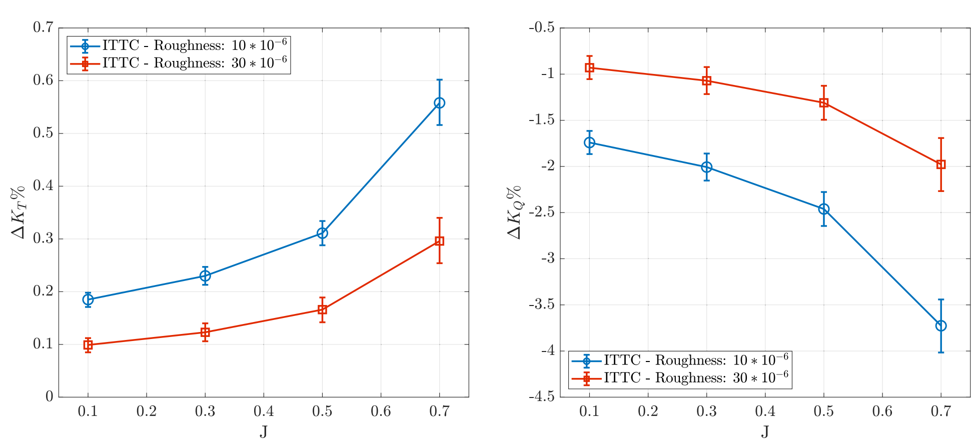

(a) ITTC based thrust coefficient correction

(b) ITTC based torque coefficient correction

Figure 18. 'Average' full-scale corrections from the standard ITTC procedure for P1727 propeller. Vertical bars represent minimum and maximum values of the ITTC corrections changing the model-scale propeller rate of revolution. Values as a percentage of the model-scale performances from the experimental campaign.

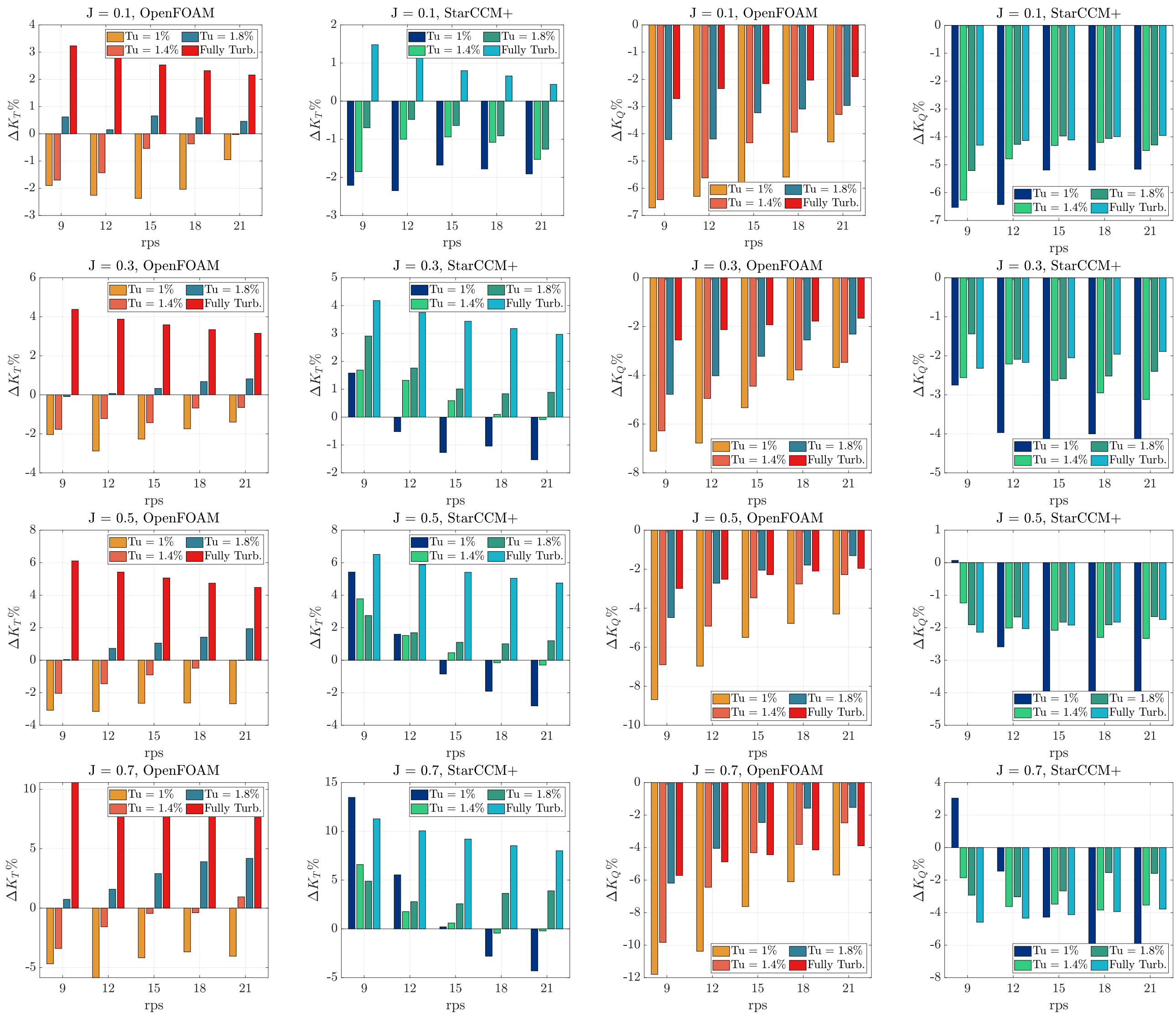

Figure 19. Scale effects for P1727 propeller as a function of the propeller loading, the model-scale rate of revolution and turbulence intensity level. OpenFOAM (left) and StarCCM + (right) calculations.

Table 8. Differences with respect to experiments (15 rps) for the accelerating ducted propeller.

	$K_{Tblades}$				K_{Tduct}			
J	Fully Turb.	Tu = 1%	Tu = 1.4%	Tu = 1.8%	Fully Turb.	Tu = 1%	Tu = 1.4%	Tu = 1.8%
0.2	−1.3%	1.0%	1.0%	1.0%	0.3166	14.1%	17.5%	19.0%
0.4	−1.7%	0.7%	0.6%	0.0%	0.2019	23.2%	23.2%	23.1%
0.6	−1.8%	0.5%	0.2%	−0.3%	0.1165	27.5%	27.5%	27.1%
0.8	−0.9%	1.8%	1.2%	0.4%	0.0414	77.1%	77.1%	75.6%
1	1.4%	5.6%	2.8%	2.3%	−0.0472	−77.7%	−77.7%	−76.3%

	K_{Ttot}				$10K_Q$			
J	Fully Turb.	Tu = 1%	Tu = 1.4%	Tu = 1.8%	Fully Turb.	Tu = 1%	Tu = 1.4%	Tu = 1.8%
0.2	5.2%	7.9%	8.6%	8.6%	−0.3%	−0.3%	−0.3%	−0.3%
0.4	5.0%	8.1%	8.0%	7.5%	−0.3%	−0.6%	−0.6%	−0.9%
0.6	3.7%	6.9%	6.7%	6.0%	−0.1%	−0.9%	−1.0%	−1.1%
0.8	6.9%	10.7%	10.0%	9.0%	1.0%	0.2%	0.0%	0.3%
1	16.7%	27.9%	24.1%	23.8%	3.4%	3.3%	1.8%	2.6%

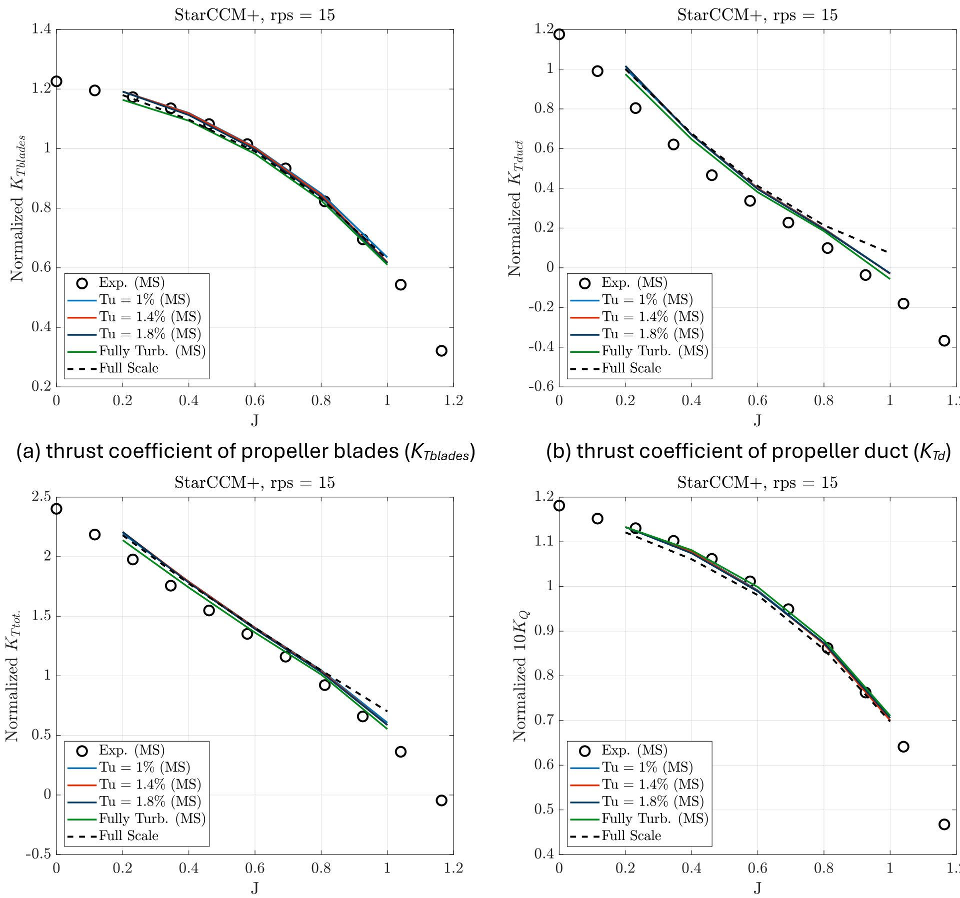

(a) thrust coefficient of propeller blades ($K_{Tblades}$) (b) thrust coefficient of propeller duct (K_{Td})

Figure 20. Model-scale open water propeller performance of the accelerating ducted propeller. For confidentiality reasons, data are normalised with respect to reference values of thrust and torque (experimental performance of propeller blades at the design advance coefficient). Comparison of different turbulence models and turbulence intensities using StarCCM + with model-scale experiments (15 *rps*).

Table 9. Differences with respect to experiments (15 rps) for the decelerating ducted propeller.

	$K_{Tblades}$				K_{Tduct}			
J	Fully Turb.	Tu = 1%	Tu = 1.4%	Tu = 1.8%	Fully Turb.	Tu = 1%	Tu = 1.4%	Tu = 1.8%
0.6	0.3%	3.0%	2.5%	2.1%	8.1%	18.7%	16.1%	13.8%
0.8	0.5%	4.2%	3.3%	2.7%	6.7%	6.7%	5.5%	8.5%
1.0	1.5%	7.1%	5.3%	4.4%	9.6%	9.6%	9.0%	9.8%
1.2	6.1%	15.3%	12.1%	10.7%	8.6%	8.6%	9.2%	10.2%

	K_{Ttot}				$10K_Q$			
J	Fully Turb.	Tu = 1%	Tu = 1.4%	Tu = 1.8%	Fully Turb.	Tu = 1%	Tu = 1.4%	Tu = 1.8%
0.6	0.8%	4.0%	3.4%	2.9%	3.4%	2.6%	2.6%	3.2%
0.8	−0.2%	4.1%	3.2%	2.4%	4.3%	3.7%	4.1%	4.5%
1.0	−0.3%	6.6%	4.6%	3.4%	6.1%	6.3%	6.7%	7.0%
1.2	4.2%	18.0%	13.3%	10.8%	11.4%	13.3%	13.6%	13.5%

In terms of thrust provided by the blades, in the case of the accelerating ducted propeller it is possible to observe the positive influence of the transition sensitive turbulence model. At high and moderate loading ($J < 0.6$), the predicted thrust at any turbulence level is almost identical and closer to experiments than fully turbulent simulations, which slightly underestimate it. This is the result of a very large extent of the laminar boundary layer which covers, as seen in Figure 22, almost all the blade suction side (advance coefficient of 0.6) at any turbulence intensity level (and rate of revolution/Reynolds number). Only at very high turbulence levels is a non-negligible turbulent boundary layer, confined at the tip of the blade, visible. It is not sufficient, in any case, to alter the predicted thrust, which diverges from low and intermediate turbulence intensity cases only at very high and off-design functioning conditions. Compared to open propellers, the massive separation at trailing edge seems avoided, even if some streaks in the frictional coefficient distributions, symptoms of instability of the flow, are visible.

On the contrary, the analyses of the decelerating ducted propeller show a relevant overestimation of the blade thrust when the γ-Re_θ model is employed. Fully turbulent simulations agree very well with experiments while the typical behaviour of transition-sensitive models discussed for open propellers is observable: the highest values of predicted thrust correspond to the lowest values of turbulence intensity, i.e. to the occurrence of a large portion of the laminar boundary layer over the blades that influences through viscous-inviscid interaction the suction on the back. As seen at the design advance

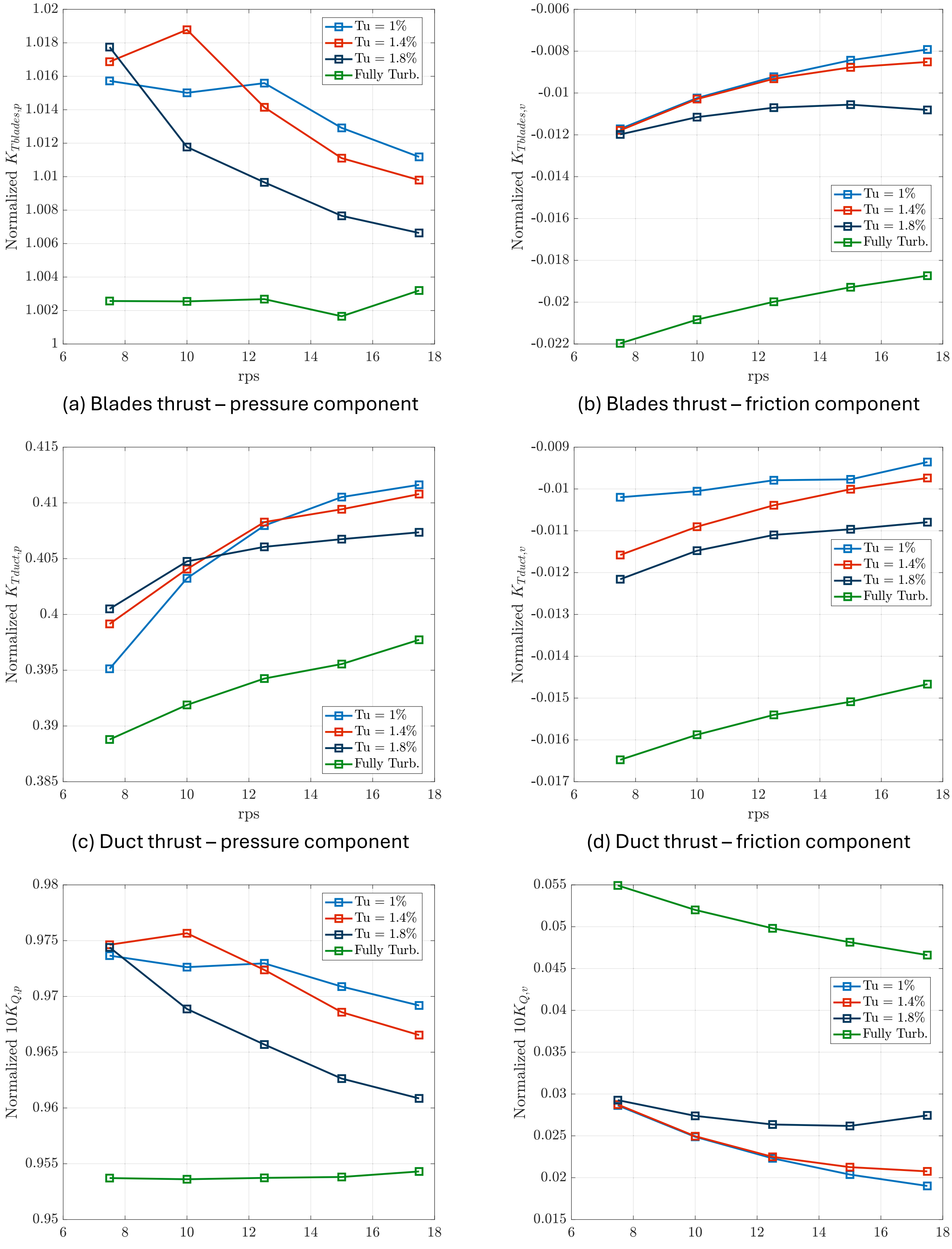

(a) Blades thrust – pressure component

(b) Blades thrust – friction component

(c) Duct thrust – pressure component

(d) Duct thrust – friction component

(e) Torque – pressure component

(f) Torque thrust – friction component

Figure 21. Pressure ($_p$) and shear ($_v$) components of blades and nozzle thrust, and torque at the design advance coefficient ($J = 0.6$) for the accelerating ducted propeller. For confidentiality reasons, data are normalised with respect to reference values of thrust and torque (experimental performance of propeller blades at the design advance coefficient). Influence of the turbulence intensity level and of the rate of revolution.

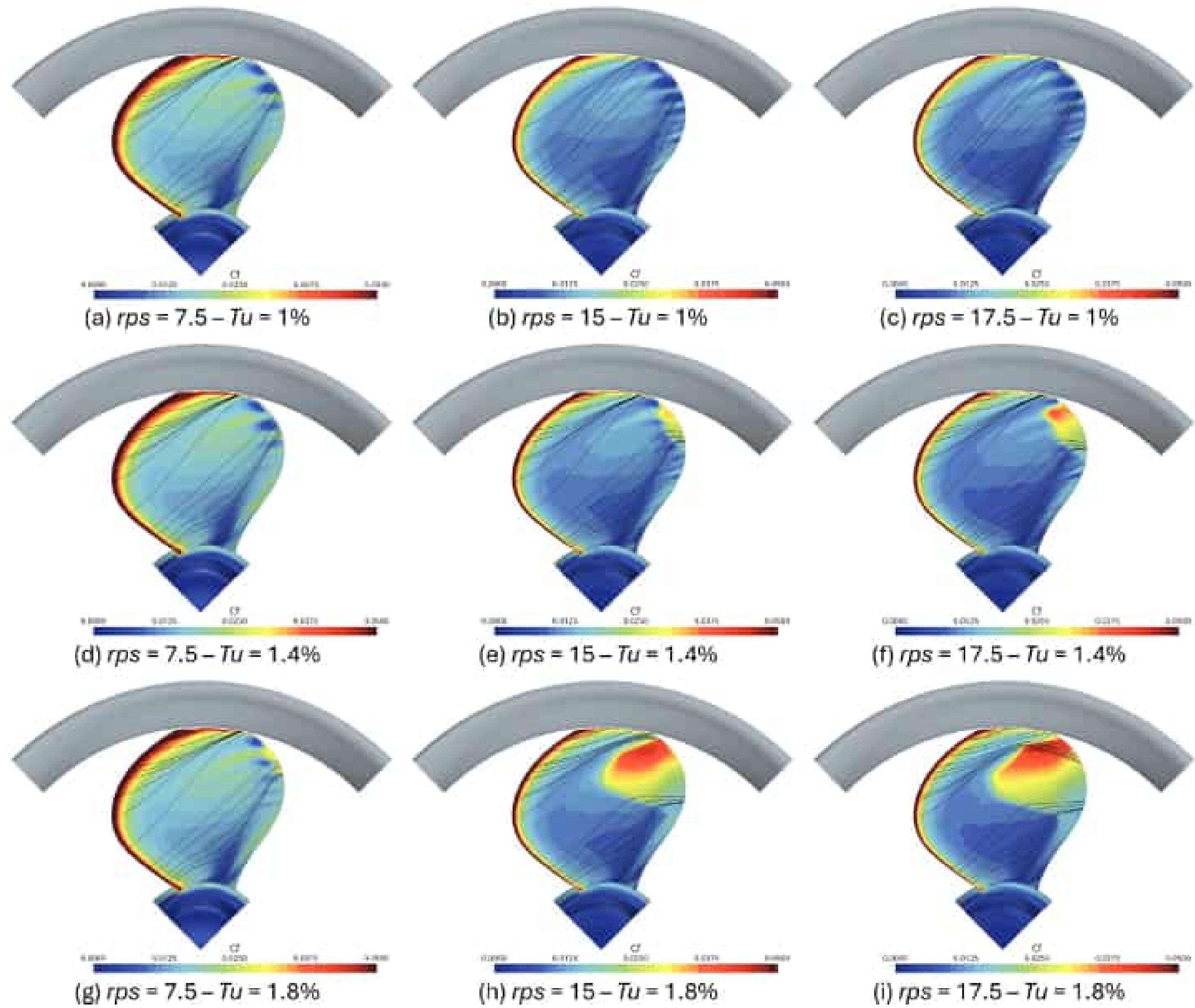

Figure 22. Influence of the turbulence intensity on the laminar to turbulent boundary layer transition (skin friction coefficient distribution and surface streamlines) at several propeller rates of revolution. Accelerating ducted propeller at $J = 0.6$.

coefficient, the decelerating ducted propeller is more sensitive to the transition to turbulent flow over the blade's surface (Figure 30) compared to the accelerating nozzle configuration. The portion of the blade under turbulent boundary layer rapidly increases with the turbulence intensity level and the predicted force follow a trend already well described in the case of open propellers. The induced velocities are likewise affected by the turbulence model, and they play a fundamentally different role in the scaling due to the specific operating principles of the nozzles. This behaviour is directly linked to the associated 'induced-velocity scale effects' (Figure 27), first discussed by Bulten and Nikland (2011) through axial-pump analogies and later examined by Bhattacharyya et al. (2016a). When transition sensitive models are used, overall, the induced velocities of the propeller equipped with the accelerating nozzle are increased. Based on the discussion of Bhattacharyya et al. (2015b, 2016a), this increase is mainly due to the higher duct thrust, observable also in current calculations (Figures 20 and 21). The increase of thrust, expected by the lower turbulence intensity level (lower frictional drag, cambering effect and role of flow separation on the pressure distribution, as discussed in the case of open propeller) is then mitigated by a decrease of the effective angle of attack due to faster inflow. For the decelerating ducted propeller, instead, the use of the γ-Re_θ or the fully turbulent model has no substantial (or mostly negligible) effects on the model-scale velocities in front of the propeller (Figure 27). This is also associable to the very different type of nozzle that, at the design advance coefficient under investigation, produces a very small resistance, and small variations associated with different turbulent regimes are almost ineffective in changing the induced flow. At an unchanged effective angle of attack, the increase of the blade thrust is completely associable to the different flow due to the laminar nature of the boundary layer.

The forces exerted by the ducts (thrust for the accelerating ducted propeller, mainly drag for the decelerating configuration) have an opposite behaviour. They are overall overestimated in the case of the accelerating ducted propeller and are very close to experiments in the case of the decelerating nozzle configuration. Especially in the case of the decelerating nozzle propulsor, the use of the transition-sensitive model and the different levels of turbulence intensity have a negligible influence on the thrust of the duct (see the almost overlapped pressure distributions of Figures 25 and 33 for both the propulsors),

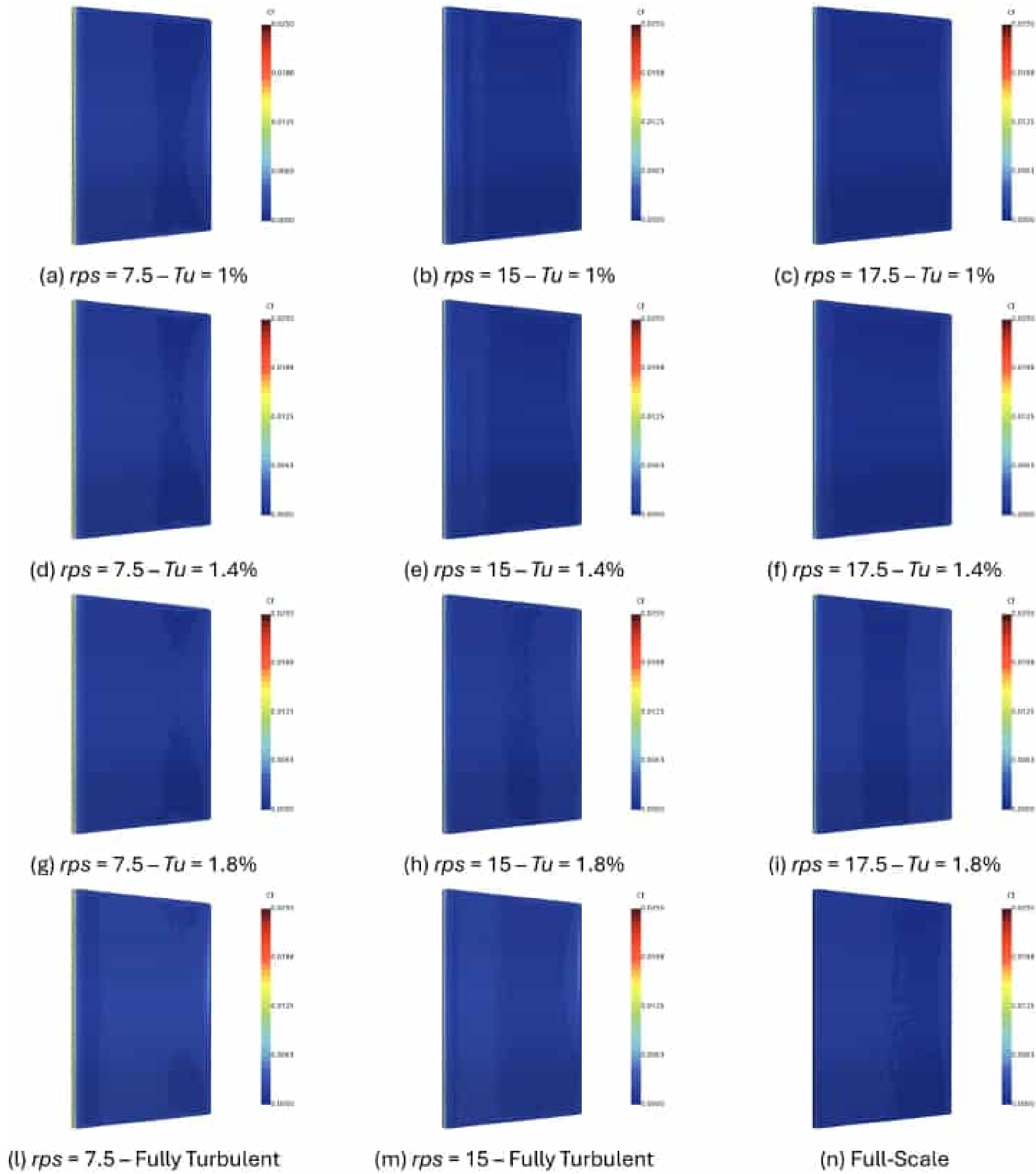

Figure 23. Influence of the turbulence intensity on the laminar to turbulent boundary layer transition (skin friction coefficient distribution) on the external nozzle surface at several propeller rates of revolution. Accelerating ducted propeller at the design advance coefficient ($J = 0.6$).

even if some differences in terms of predicted occurrence of laminar to turbulent transition can be seen on the friction distributions over the duct (Figures 23 and 31, or the sectional distributions of Figures 25 and 33). At about 60% of the nozzle chord (Figure 31), the increase in the friction coefficient can be associated with the occurrence of transition, also seen from the sectional distributions of the skin friction coefficient of Figure 33, which is more evident at higher Reynolds numbers and turbulence intensities. In these functioning conditions, the risk of flow separation, guessable from the 'wavy' pressure distributions (Figure 33a) and the very low values of velocity on the outer part of the nozzle at the trailing edge (Figure 32a), is mitigated. On the contrary, over the nozzle of the accelerating duct

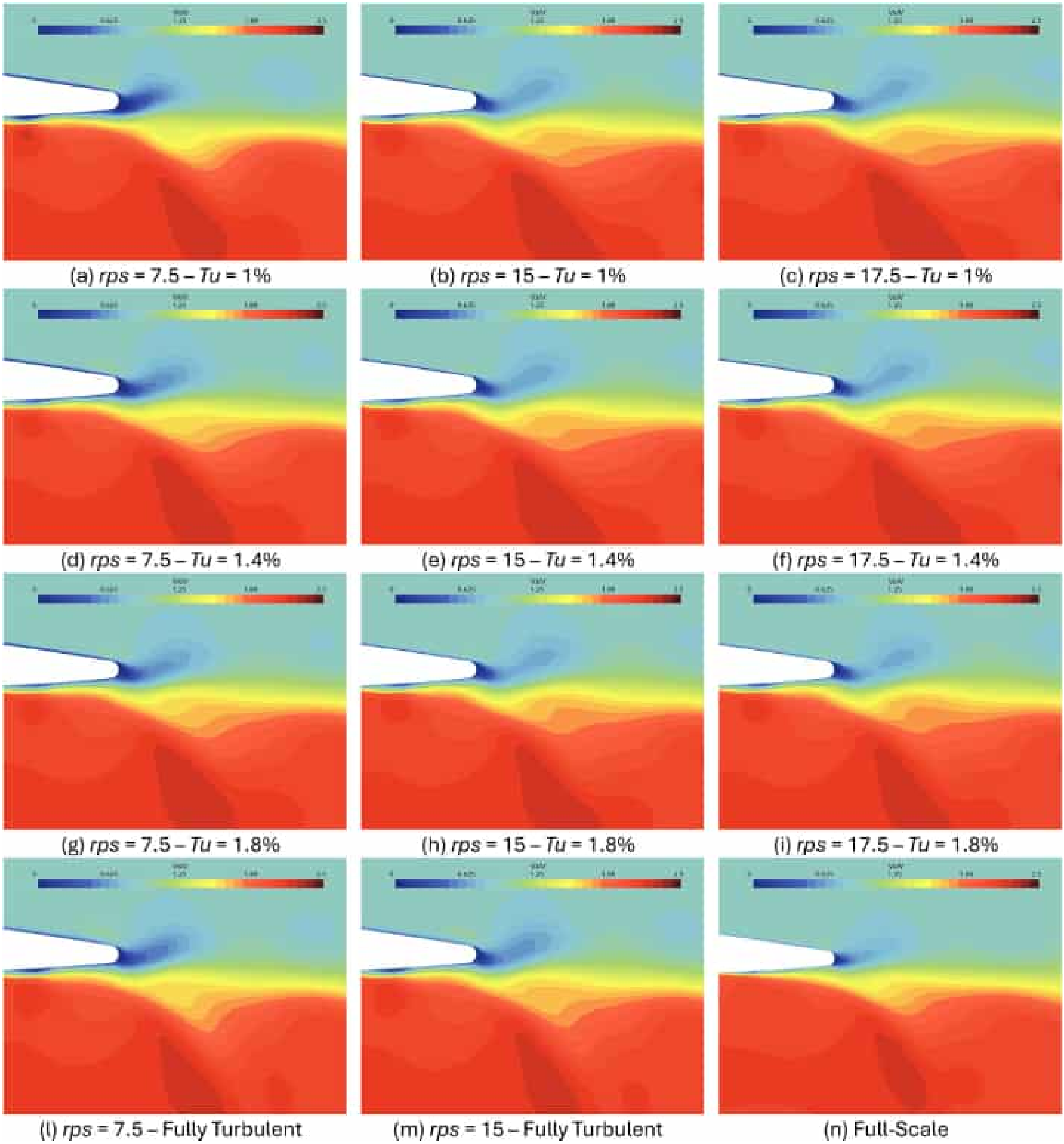

Figure 24. Influence of the turbulence intensity on the non-dimensional axial velocity at the nozzle trailing edge. Longitudinal plane of the accelerating ducted propeller case at the design advance coefficient ($J = 0.6$).

(Figures 23 and 25), an almost constant (and very low) value of the coefficient implies that the boundary layer maintains its dominant laminar nature, especially on the outer surface of the duct, where velocities and turbulence are less influenced by the action of the propeller. This can also be appreciated by comparing the shear component of forces on the duct, which are very close to each other in the case of the accelerating ducted propeller regardless of the Reynolds number and the turbulence intensity level. The combination of blade and duct thrust leads to a total thrust which is slightly overestimated in both cases.

Unlike open propellers, the use of transition sensitive turbulence models seems not crucial for accurate model-scale predictions since results (thrust) generally are better in agreement with experiments when the fully turbulent model is employed. Torque, finally, is slightly overestimated in the case of the decelerating ducted propeller (Figure 28, Table 9), as already seen in several calculations of the

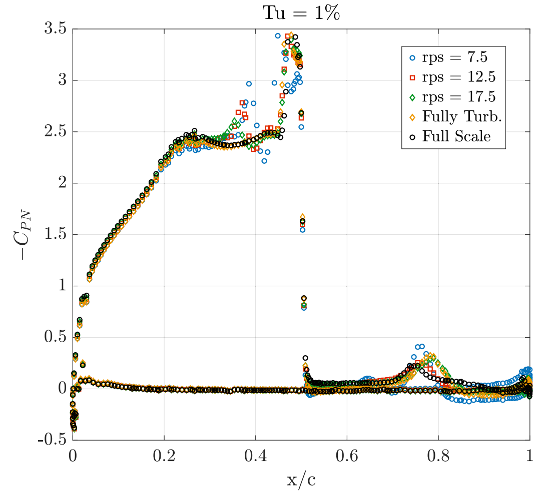

(a) Pressure coefficient, *Tu* = 1%

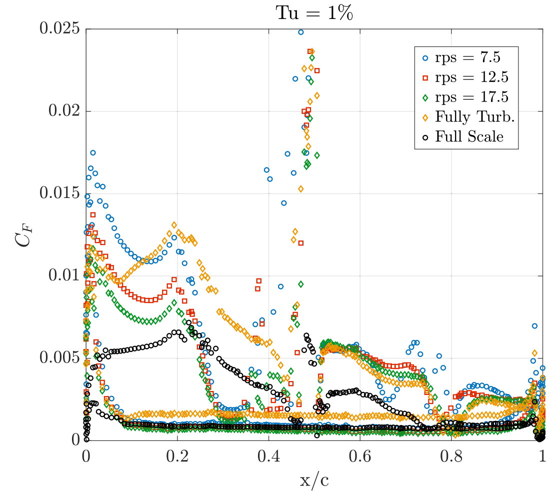

(b) Skin friction coefficient, *Tu* = 1%

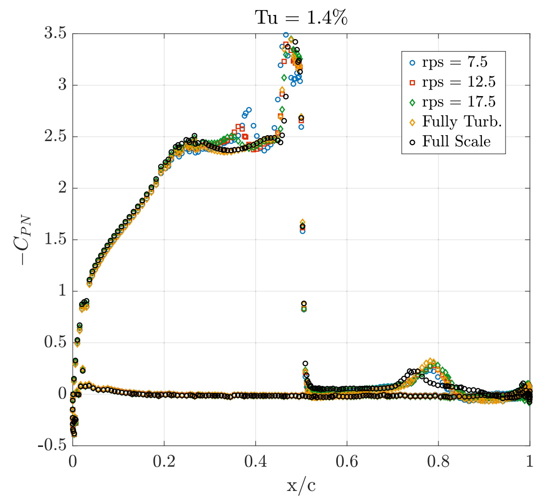

(c) Pressure coefficient, *Tu* = 1.4%

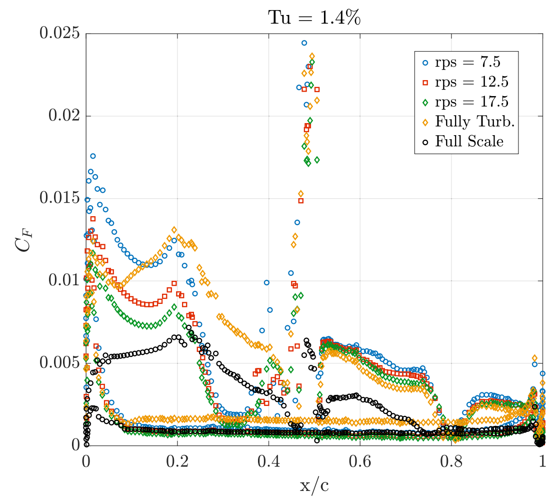

(d) Skin friction coefficient, *Tu* = 1.4%

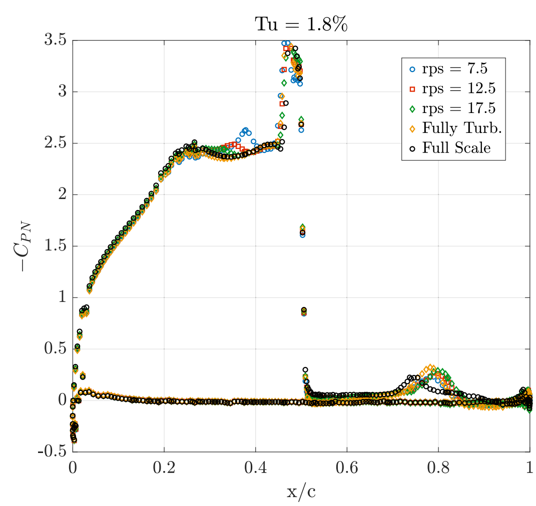

(e) Pressure coefficient, *Tu* = 1.8%

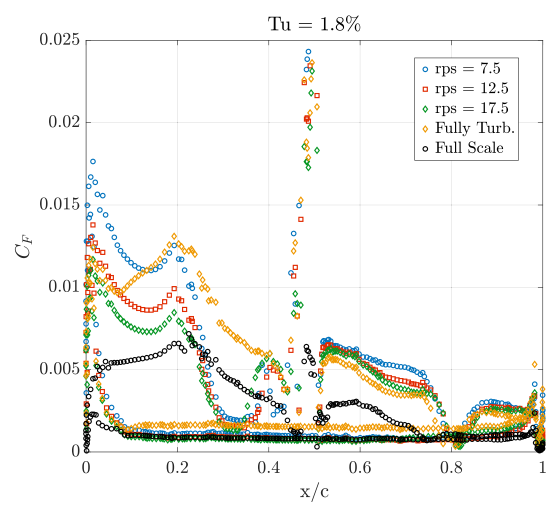

(f) Skin friction coefficient, *Tu* = 1.8%

Figure 25. Pressure and skin friction coefficient on the nozzle of the decelerating ducted propeller. Longitudinal section ($J = 1.0$).

performance of this propulsor (Gaggero et al. 2014; Villa et al. 2020). Unlike the thrust of the same propulsor, the influence of turbulence intensity is much more limited since the calculated performance is very close to each other and very similar to the fully turbulent cases too.

Also in the case of the accelerating nozzle, the influence of the model-scale turbulence model does not seem crucial for improving the predicted performance. Fully turbulent simulations are those closer to the measurements and the inclusion of the laminar-to-turbulent transition capability determines only a slight reduction in torque, which is ascribable to the substantial reduction in friction when moving from a model-scale fully turbulent condition to a model-scale almost completely laminar boundary layer condition (Figure 21 at the design advance and the boundary layer behaviour on the suction side of Figure 22).

While the relative importance of pressure and frictional components of the forces is similar to what is observed in the case of open propellers, trends with the rate of revolutions at the fixed advance coefficients used for the analyses of Figures 21 and 29 are slightly different among the two nozzle configurations. In the case of the accelerating ducted propeller, thrust and torque change, mainly due to the pressure component, with the Reynolds number exactly as with VP1304 (or P1727, when OpenFOAM calculations are considered). At very low rates of revolutions, when the laminar boundary layer is more extended, and its influence on the pressure distribution is more evident, the pressure components of forces, due to separation and cambering, are higher. Their decrease with the increase of the model-scale Reynolds number is balanced by the reduction of the frictional forces, which is almost monotone regardless of the turbulence intensity level. Similarly to the P1727, where the boundary layer is laminar at almost any functioning regime under consideration, friction decreases for the Reynolds effect, and since no relevant turbulent boundary layer (with increased friction coefficient) appears on the blades (with the exception of the case with $Tu = 1.8\%$, well visible at the highest rate of revolution in Figure 22), the increase of the rate of revolution determines a continuous decrease of friction forces.

For the decelerating ducted propeller, trends are opposite, at least for what concerns blade thrust and torque due to the pressure component of forces: they increase with the propeller rate of revolutions, regardless of the increments of the pressure components that may be expected at very low Reynolds number due to separation and cambering. A possible explanation for this behaviour lies in the Reynolds-number effects associated with the induced velocities generated by different nozzle geometries. In the case of the accelerating duct, the increase in propeller thrust at higher Reynolds numbers increases the duct thrust, which in turn leads to greater flow acceleration (Bhattacharyya et al. 2015b, 2016a) and higher inflow velocities (see Figure 27 for a representative case at $Tu = 1.4\%$). This increased induction produced by the duct slightly reduces the propeller thrust, as the higher induced velocities correspond to a higher effective advance condition for the propeller, consistent with the trend observed (for the same Tu) in Figure 21(a). The decelerating ducted propulsor, on the contrary, shows a different Reynolds influence on the induced velocities in front of the propeller. Higher propeller rps determines again higher values of duct thrust (lower duct resistance at the given functioning point for the decelerating ducted propeller), but the flow in front of the blades is marginally slower, and this may contribute to the increasing values of thrust and torque observed in Figure 29(a,e).

Scale effects, for any combination of model-scale rates of revolution and turbulence intensity levels, are shown in Figure 26 (accelerating ducted propeller) and Figure 28 (decelerating nozzle). All together, they provide a complete overview of the phenomena occurring on the propulsors and of the role of the model-scale type of calculations based on which scale effects are determined. Overall, for the accelerating ducted propeller, the scale effect (absolute value) of the thrust coefficient (blade) is relatively small compared to the results seen for the open propellers. It is not higher than 1.5% on average and quite constant with respect to the model-scale rate of revolution (in some cases also with respect to the turbulence intensity level). It shows a certain dependency on the loading of the propulsor (decreasing with the increase of J), which is not coherent with what is observed, using the same nozzle but a different blade shape, by Bhattacharyya et al. (2015a, 2016a, 2016b). Usually, indeed, at lighter loading, the relative contribution to lift and drag (i.e. thrust and torque) of shear forces is higher, being shear forces less influenced by loads. This would result in higher (not lower) scale effects merely due to the reduction of the frictional component of forces in full-scale (see, for instance, current calculations in the case of the open propellers).

The sign of the correction is negative (full-scale thrust lower than model-scale), then opposite to the usual Reynolds effect associated with purely frictional phenomenon. Only when the fully turbulent model-scale calculations are considered is the scale effect coherent with the usual expectations. This result ($\Delta K_{Tblade} < 0$) agrees with the analyses of Bhattacharyya et al. (2016a, 2016b), which evidenced negative scale effects for heavily loaded propulsors mostly as a consequence of a Reynolds influence on the induced velocities. As already discussed in the analyses of model-scale performance at different Reynolds numbers and turbulence regimes (but with respect to full-scale results this phenomenon is much clearer), higher Reynolds numbers correspond to faster inflow velocities to the propeller (Figure 27), which are responsible for the reduction (higher effective J, lower angle of attack) of the full-scale thrust and then of the negative scale correction, as shown by the analyses of Bulten and Nikland (2011) using axial pump analogies. Model-scale fully turbulent simulations, which have in model-scale the lowest velocities (theoretically, the highest blade forces) because of the lowest duct thrust, and which should then determine the highest negative scale effects do not confirm this trend. Reynolds influence on velocities plays a role that, case by case, is balanced or exaggerated by the influence of the combined laminar and turbulent boundary layers on the model-scale pressure distributions on blades and ducts.

The scale effect observed for the duct thrust agrees with the conclusions of Bhattacharyya et al. (2016a, 2016b). With the exception of the very highly loaded condition ($J = 0.2$), where the scale effects computed with the transition-sensitive model are negative for most of the model-scale rates of revolutions, full-scale duct thrust is relatively higher than model-scale and a clear increasing trend with the increase of the advance coefficient is observable. There are no substantial differences (in this range of J) among calculations using different turbulence levels, and this is coherent with the model-scale results used for comparison with experiments (Figure 20): the analysed levels of turbulence are not capable of determining a substantial transition on the nozzle (as well on the blades), resulting in model-scale performance (and then scale effects) almost overlapped. As observed by Bhattacharyya et al. (2016a), also in these analyses, the scale effects predicted using model-scale transition-sensitive turbulence models are lower because of the higher duct performance predicted at small dimensions. Similarly lower scale effects are achieved at higher model-scale rates of revolutions, associable again to the higher model-scale thrust of the duct discussed in Figure 21.

The sudden change of the scale effect at $J = 0.8$ (full-scale thrust 10% higher than model-scale, while at $J = 0.6$ the difference was, on average, 3%), instead, is a symptom of a completely different functioning of the nozzle in full-scale. In lightly loaded conditions, flow separation (as well as the vortex shedding from the blunt trailing edge, as partially observable in Figure 24) on the external accelerating nozzle surface is usual at model-scale. Its occurrence in the current case is proven by the different slope of the duct thrust curves of the open water diagrams of Figure 20. Separation radically modifies the force realised by the nozzle in model-scale, making the scale effects associated with the duct more dependent on the pressure rather than on the frictional component of the forces Bhattacharyya et al. (2015a, 2015b).

Figure 26. Scale effects for the accelerating ducted propeller as a function of the propeller loading, the model-scale rate of revolution and turbulence intensity level.

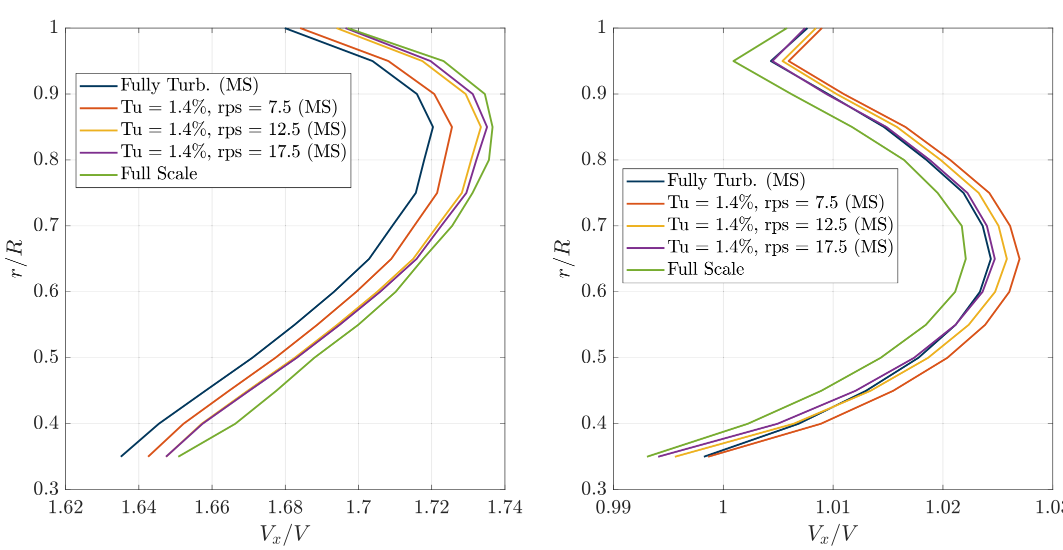

Figure 27. Total axial velocity on a plane in front of the propulsors in model and full-scale.

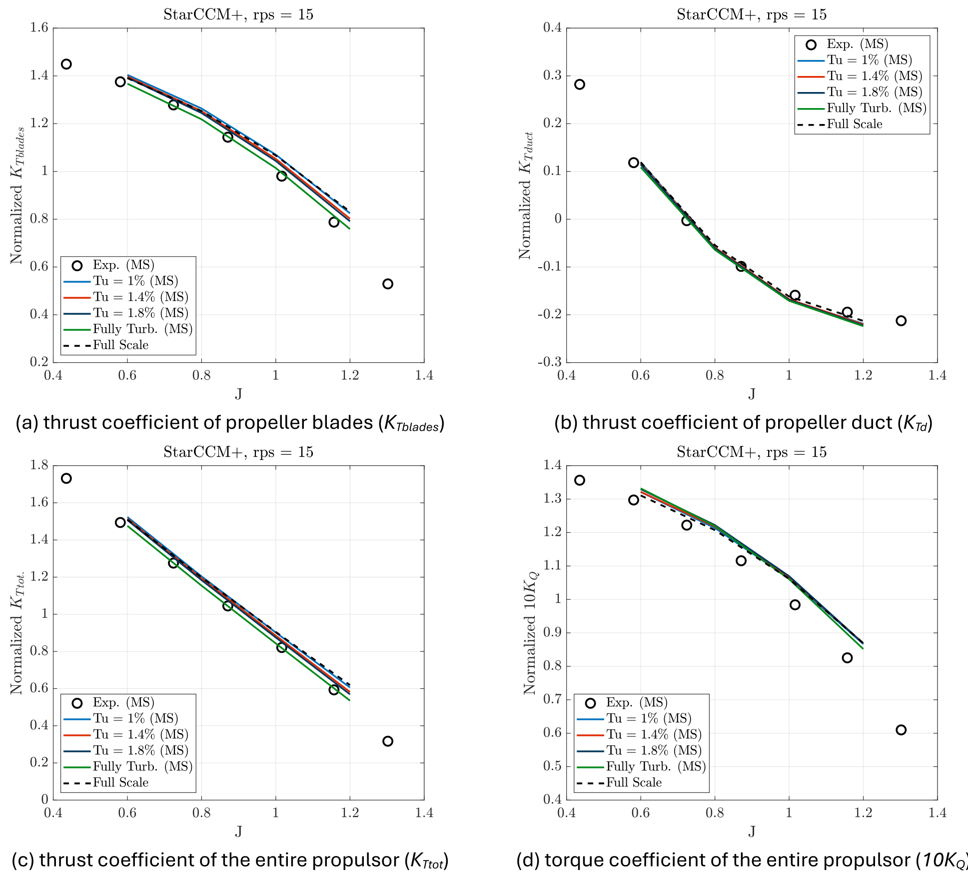

(a) thrust coefficient of propeller blades ($K_{Tblades}$)

(b) thrust coefficient of propeller duct (K_{Td})

(c) thrust coefficient of the entire propulsor (K_{Ttot})

(d) torque coefficient of the entire propulsor ($10K_Q$)

Figure 28. Model-scale open water propeller performance of the decelerating ducted propeller. For confidentiality reasons, data are normalised with respect to reference values of thrust and torque (experimental performance of propeller blades at the design advance coefficient). Comparison of different turbulence models and turbulence intensities using StarCCM + with model-scale experiments (15 *rps*).

Scale effects of the total thrust are merely a combination of blades and nozzle contribution. For this particular case, a balance between the reduction of blade and the increase of nozzle thrust, as in Bhattacharyya et al. (2016a), does not occur, and the scale effect of the total thrust is either positive, negative, and of different strength depending on the loading, the model-scale rate of revolution, and the type of phenomena ('cambering', separation) occurring at model-scale with different turbulence intensity levels and boundary layer regime.

The scale effect of torque is more regular, and trends are clearer over most of the functioning conditions under investigation. The reduction of the torque of the full-scale propulsor is evident, as is its dependency on loading and viscous regime. Compared to the scale effect of thrust, torque plays a more important role in the full-scale increase of efficiency. On average, the reduction of torque (2%) is two times the increase of thrust (if we exclude the fully turbulent simulations, for which the positive combination of the full-scale increased duct thrust with the full-scale increased blade thrust determines a unique increase of the full-scale thrust of the order of 3%). This result agrees with the few data available in the literature even if for the same nozzle (19A) and a family of similar geometries (but different blade geometries) the reductions were of the order of 4%. The influence of the overall blade loading (and, in particular, of the tip loading, in the current case very low for the need of postponing as much as possible the cavitation inception) could explain this difference (Bhattacharyya et al. 2015b). Scale effects estimated from transition-sensitive model-scale calculations are lower, with model-scale torque using the γ -Re_θ usually underestimated with respect to the equivalent fully turbulent simulation. The full-scale reduction of torque is then lower when compared to a lower model-scale value. To the full-scale reduction of torque concurs, as usual, the lower value of friction in full-scale, which has a relative importance on the torque (with respect to the pressure contribution) usually higher than the importance it has on the thrust. As for the thrust, however, a certain responsibility for the reduction of the full-scale torque is ascribable to the modification of the inflow in full-scale, which determines most of the reduction of the pressure component of the torque because of the effectively higher advance seen by the ducted propeller at very high Reynolds number. Scale effects increase from quasi-bollard pull ($J = 0.2$) to free sailing conditions ($J = 0.8$). This time the behaviour is coherent with the literature data, which clearly show this trend for a certain number of relatively different choices of nozzle shapes and blade tip loadings.

The completely different nature of the decelerating nozzle and the very different functioning conditions of this propulsor, not designed for bollard pull, influence the scale effect observed for this propeller. The first difference concerns the sign of the scale effect computed for the blade thrust. With respect to the other ducted propeller, with the decelerating nozzle, the full-scale blade thrust results are generally higher than the value in model-scale, resembling the typical trend of open propellers. Also, the magnitude of the effect is different: the full-scale increment of thrust is of the order of 2% (design advance coefficient, intermediate values of turbulence intensity for model-scale calculations), then almost doubled with respect to the accelerating ducted propeller. Only at the highest loading and with transition-sensitive model-scale calculations does scaling to full-scale correspond to a reduction of propeller performance. Two phenomena may contribute

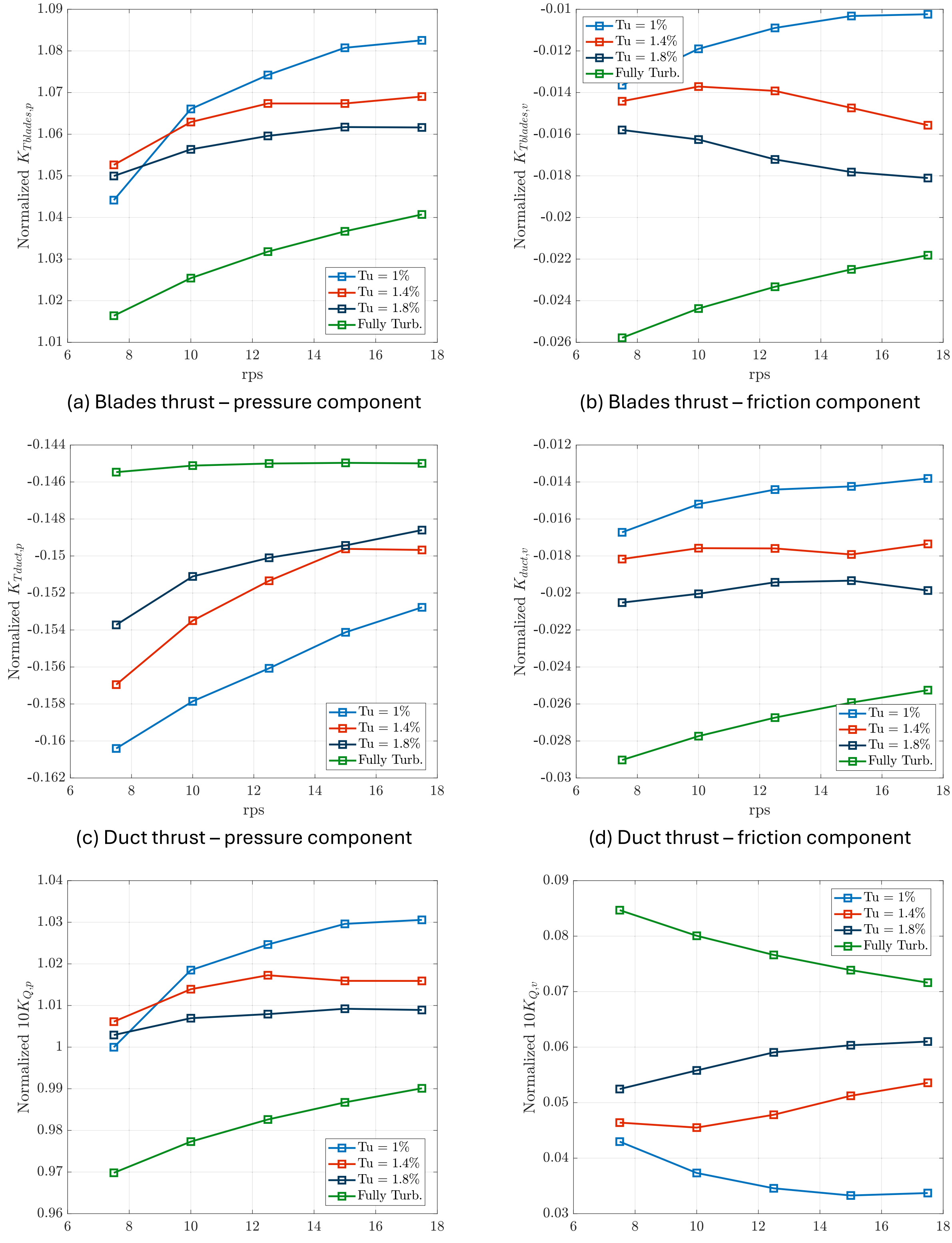

(a) Blades thrust – pressure component

(b) Blades thrust – friction component

(c) Duct thrust – pressure component

(d) Duct thrust – friction component

(e) Torque – pressure component

(f) Torque thrust – friction component

Figure 29. Pressure ($_p$) and shear ($_v$) components of propeller and nozzle thrust and torque at the design advance coefficient ($J = 1$) for the decelerating ducted propeller. For confidentiality reasons, data are normalised with respect to reference values of thrust and torque (experimental performance of propeller blades at the design advance coefficient). Influence of the turbulence intensity level and of the rate of revolution.

to this behaviour. As for open propellers, the turbulent boundary layer in model-scale has a higher importance for this geometry. This can be seen in Figure 30. Moving to full-scale, then, determines a reduction of the shear component of the forces which is higher compared to what would be achieved if the model-scale was mainly under laminar flow with a naturally lower model-scale friction (as seen for the VP1304 and the accelerating ducted propeller).

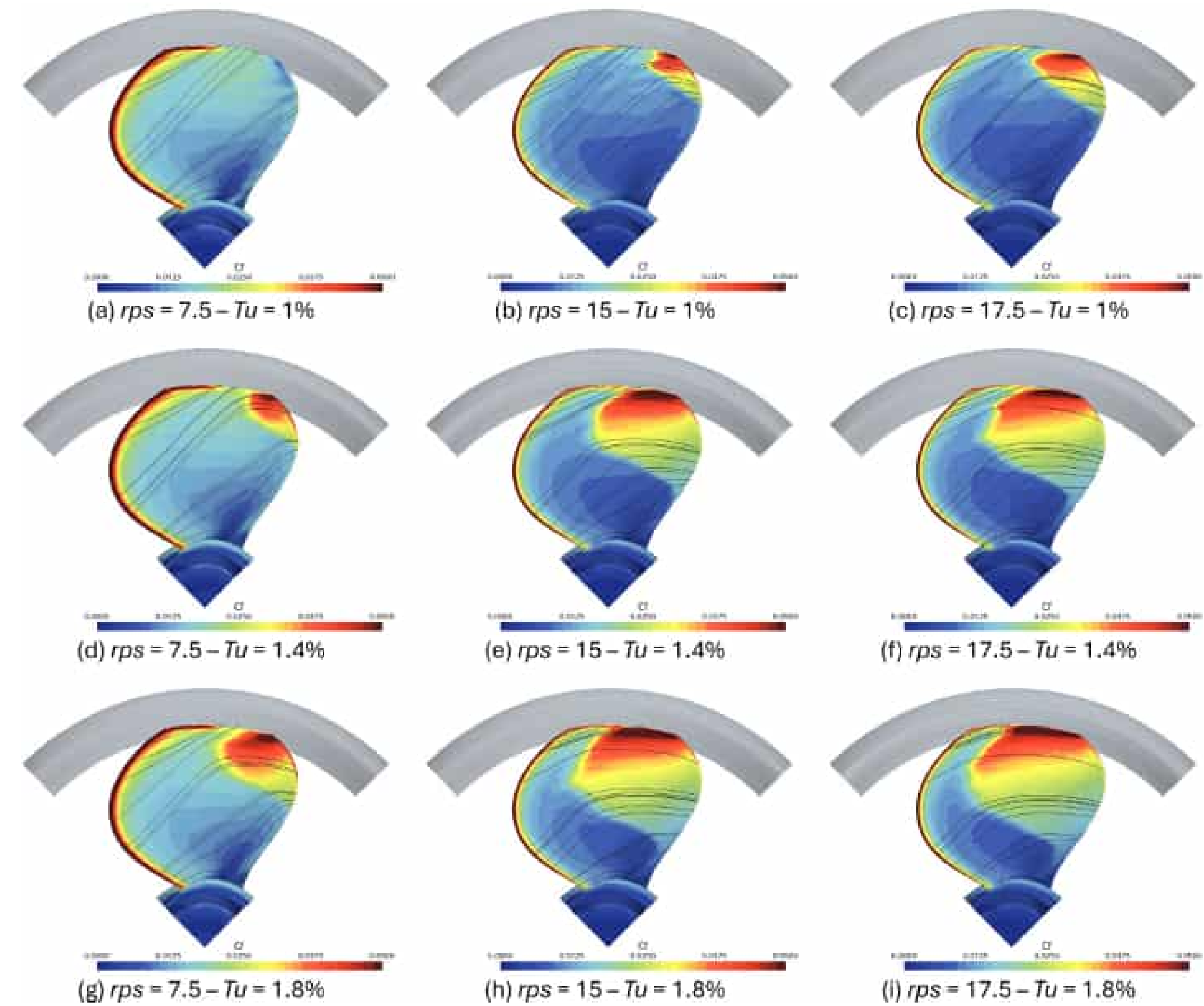

Figure 30. Influence of the turbulence intensity on the laminar to turbulent boundary layer transition (skin friction coefficient distribution and surface streamlines) at several propeller rates of revolution. Decelerating ducted propeller at $J = 1$.

The higher sensitivity to turbulence and the rate of revolution in the model-scale of this propulsor is confirmed by the observable trend of the scale effect with the loading/advance coefficient. In lightly loaded conditions, where the frictional forces are not excessively dependent on the loading, they contribute a higher percentage to the total forces of the propeller, and scale effects are higher because of the full-scale reduction of friction. Moreover, for the decelerating ducted propeller, the Reynolds effect on induced velocities is much reduced (or opposite to the accelerating case), as seen in Figure 27. There is not an increment in the full-scale inflow that contributes to the reduction of the full-scale thrust, and this promotes the positive scale effect seen in Figure 34.

The scale effect of the duct thrust is only apparently opposite to what is observed in the case of the accelerating nozzle. The sign, in this case, is affected by the 'thrust or drag' behaviour of the duct depending on the advance coefficient within the selected range (Figure 28). At the highest loading under investigation ($J = 0.6$) despite the divergent geometry, the decelerating nozzle provides a positive thrust. The positive scale effect indicates a full-scale duct force higher than model-scale. At higher advance coefficients ($J \geq 0.8$), the nozzle provides a negative force (drag), which changes the sign of the scale effect computed accordingly to Equation (4): negative values of the scale effect in Figure 34, for this reason, still denote full-scale forces higher than the corresponding model-scale ones. Globally, this corresponds to a scale effect of the total propulsor thrust, which is positive for most of the conditions under investigation and generally higher than what is observed for the accelerating case, also at comparable loading of the propulsors. The scale effect of torque, finally, shows a pronounced dependency on loading, equally observable regardless of the fully turbulent or transition sensitive nature of the model-scale calculations. At relatively higher loadings, full-scale torque is lower than model-scale. It is true for any turbulence models and turbulence intensity levels, with quite similarly predicted model-to-full-scale differences (starting from the γ-Re_θ) of about a 1% reduction in full-scale. The scale effects, instead, indicate a full-scale torque higher than the model-scale values when lightly loaded conditions are addressed, especially if model-scale data are those from very low rates of revolution. As

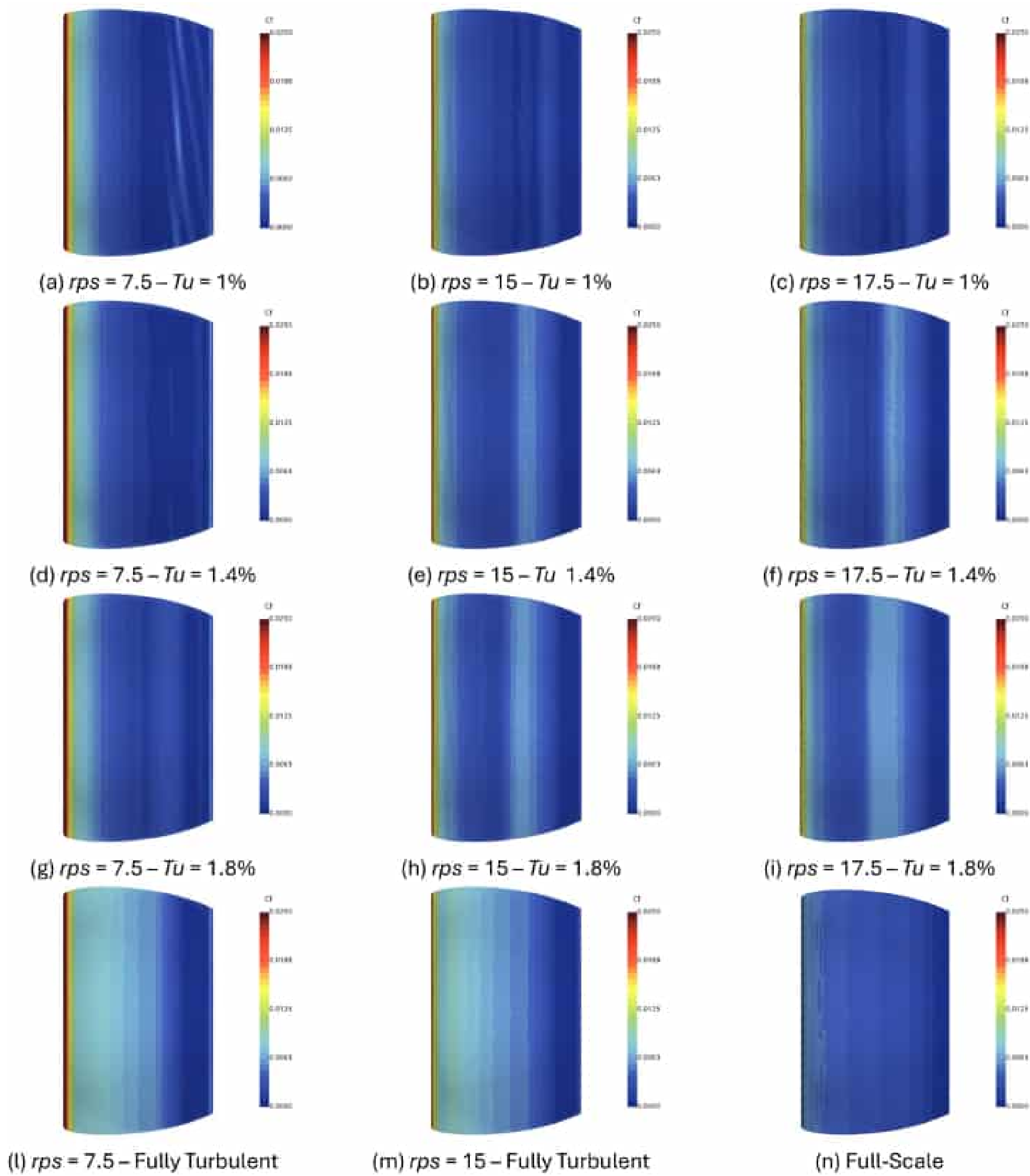

Figure 31. Influence of the turbulence intensity on the laminar to turbulent boundary layer transition (skin friction coefficient distribution) on the external nozzle surface at several propeller rates of revolution. Decelerating ducted propeller at the design advance coefficient ($J = 1$).

for the thrust, for the decelerating ducted propeller, the influence of induced velocities is smaller (and the model - to full-scale trend opposite) compared to the accelerating duct configuration. Lower full-scale induced velocities (as those seen at the design advance in Figure 27) may be responsible for the higher full-scale thrust and torque. The unusual increase with the rate of revolution of the model-scale pressure component of the torque, observed in Figure 29, further contributes to the decreasing trend of the torque scale effect clearly observable at the lowest loading ($J = 1$ and 1.2) (Figures 30–34).

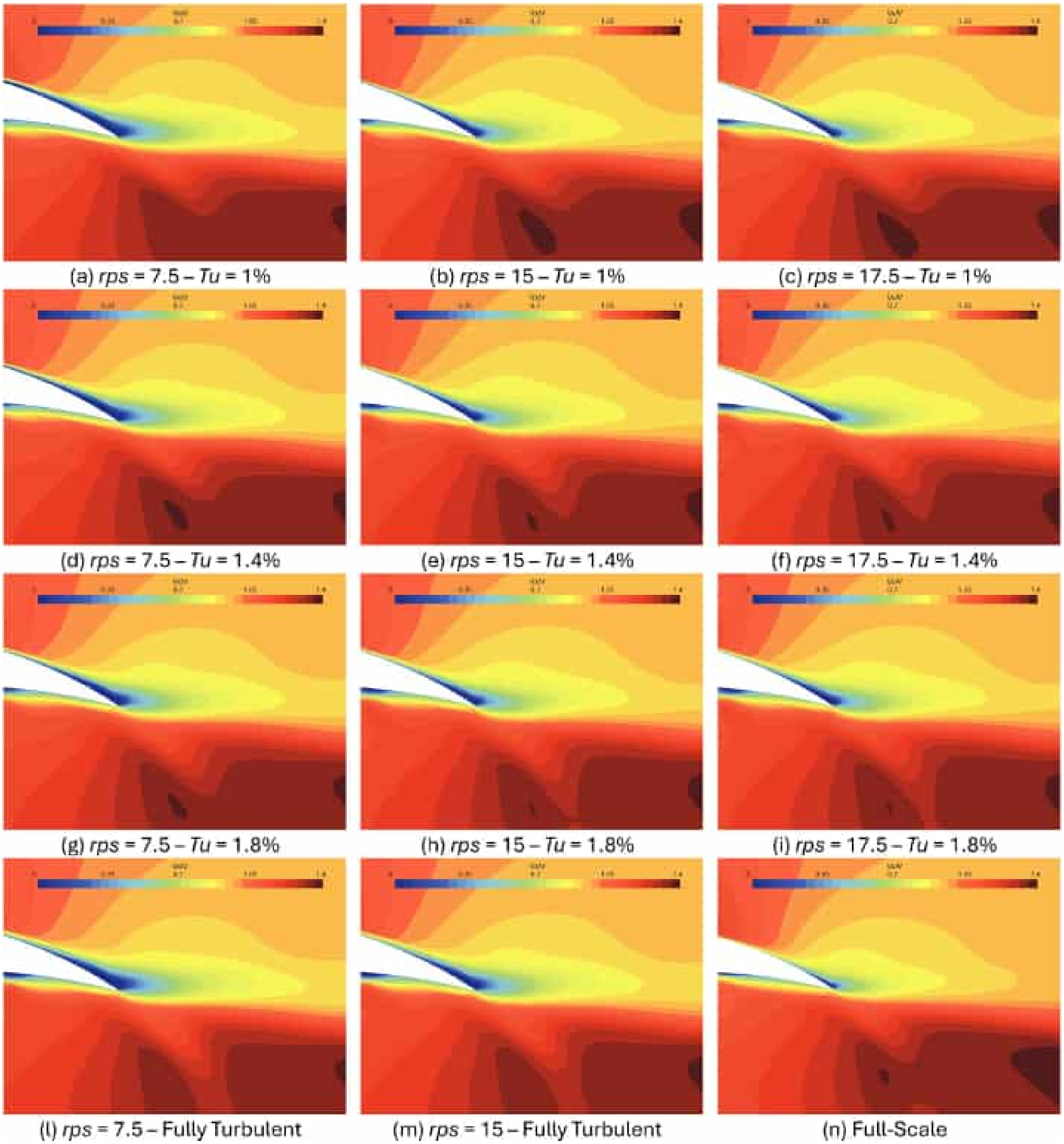

Figure 32. Influence of the turbulence intensity on the non-dimensional axial velocity at the nozzle trailing edge. Longitudinal plane of the decelerating ducted propeller case at the design advance coefficient ($J = 1$).

Conclusions

Current paper enriches the numerical analyses of scale effects of open and ducted propellers by adding to the discussion a systematic investigation into the influence of model-scale Reynolds numbers and turbulence intensity levels for transition-sensitive model-scale calculations, also in the case of less-studied decelerating ducted propulsors, based on which model-to-full-scale corrections are derived.

The model-scale calculations confirmed, at least in the case of the open propeller, that non-negligible gains in accuracy can be achieved using transition sensitive models. Based only on the comparison with model-scale open water performances (then without the additional information provided by paint tests), optimal values of the tuning parameter represented by the turbulent intensity on the propeller plane were identified between 1% and 1.4%, respectively for the VP1304 and the P1727, permitting an overall difference with respect to measurements of about 1% for thrust, 2% for torque, at

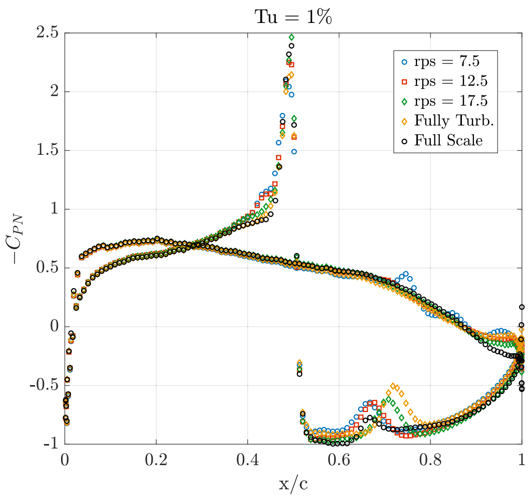

(a) Pressure coefficient, *Tu* = 1%

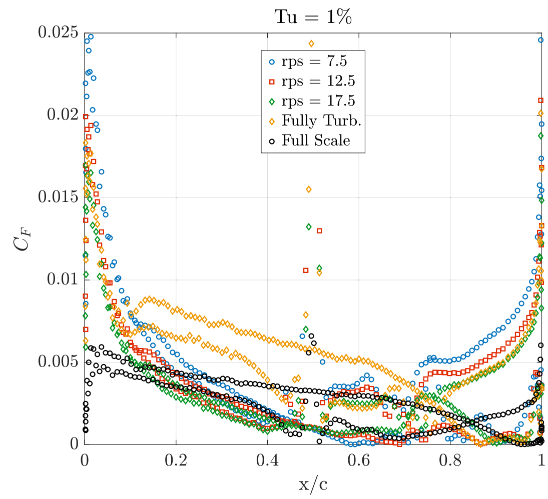

(b) Skin friction coefficient, *Tu* = 1%

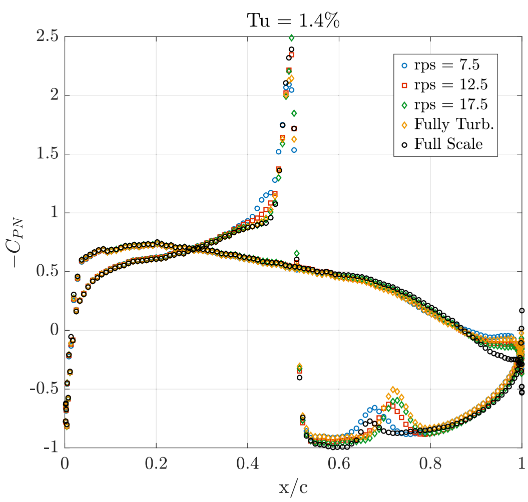

(c) Pressure coefficient, *Tu* = 1.4%

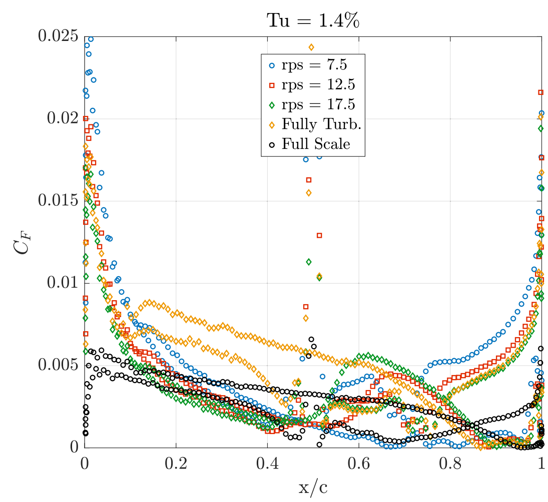

(d) Skin friction coefficient, *Tu* = 1.4%

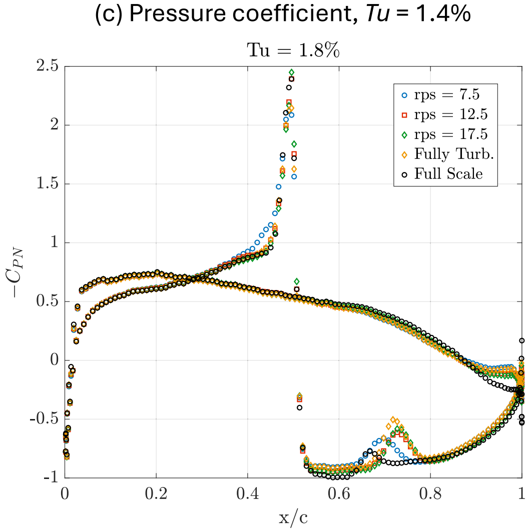

(e) Pressure coefficient, *Tu* = 1.8%

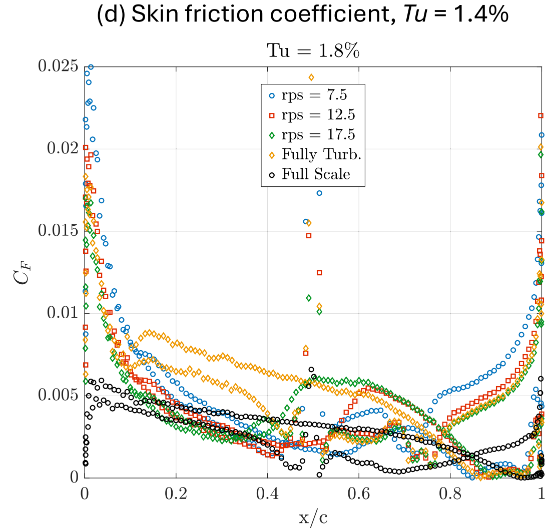

(f) Skin friction coefficient, *Tu* = 1.8%

Figure 33. Pressure and skin friction coefficient on the nozzle of the decelerating ducted propeller. Longitudinal section ($J = 1.0$).

almost any of the loading conditions under investigation. One of the issues related to modelling laminar-to-turbulent transition in model-scale by using Local Correlation Transition Models like the γ-Re_θ is, indeed, the non-negligible influence of the onset to turbulence by the turbulence intensity. This is critical for a priori prediction of model-scale propeller performance because performance is strongly affected by transition and separation, and accurate agreement was achieved only when this parameter was tuned against measurements

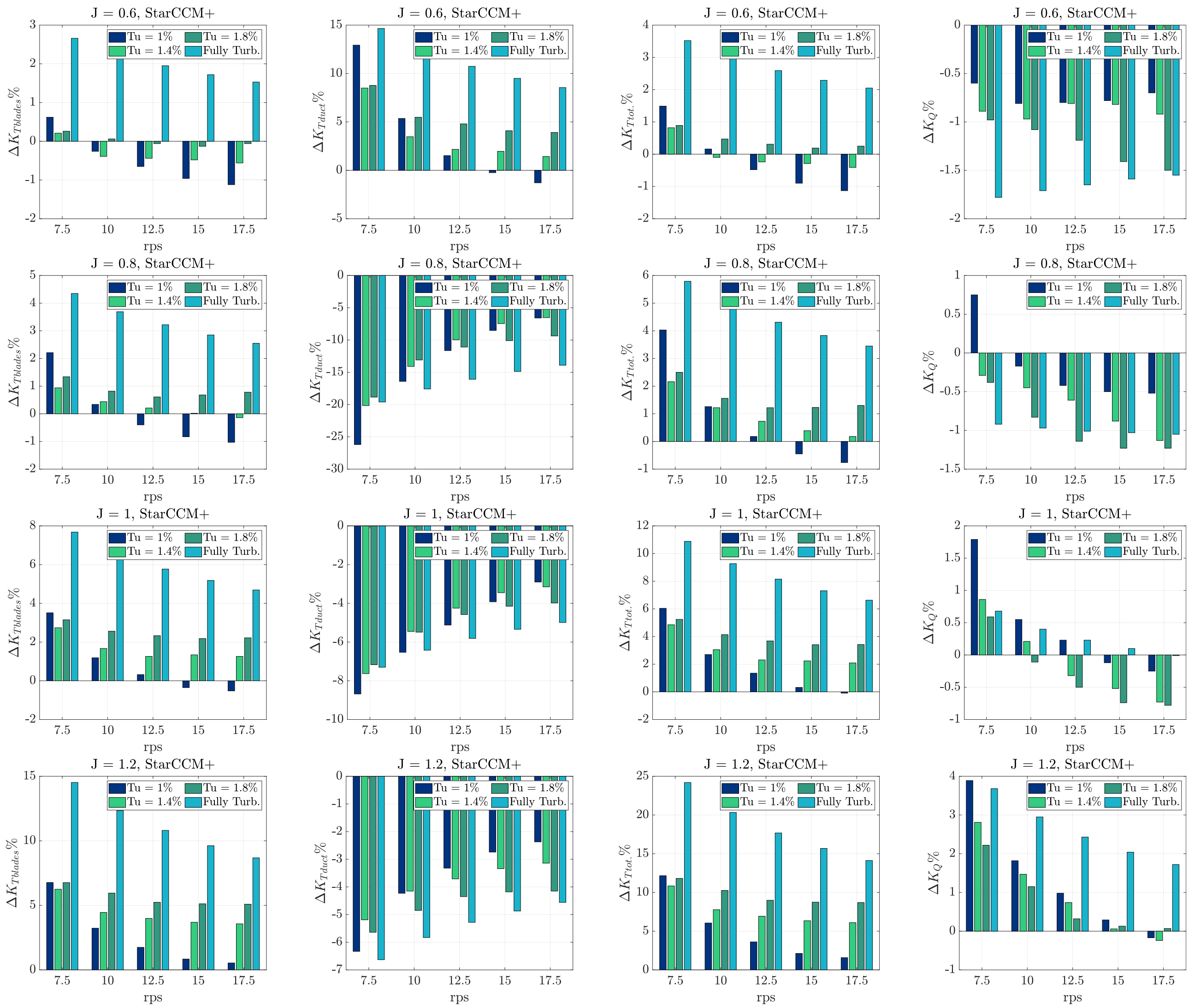

Figure 34. Scale effects for the decelerating ducted propeller as a function of the propeller loading, the model-scale rate of revolution and turbulence intensity level.

or supported by experimental paint tests. Changing simultaneously the turbulence intensity level and the propeller rate of revolution, further to identify the optimal calibration for these specific cases, is also used to collect trends and investigate the influence (or the difference) on the predicted scaling effects when different model test setups are used as references, i.e. under the uncertainty of the boundary layer regime in model-scale. No substantial improvements by the use to the γ -Re_θ model were instead observed in the case of ducted propulsors (except thrust of the blades only in the case of the accelerating nozzle, and marginally torque in the case of the decelerating nozzle), which overall seem better predicted using standard model-scale fully turbulent models.

An abundance of different phenomena, including separation, laminar-to-turbulent transition, and influence on induced velocities (ducted propeller cases), have been observed numerically, and their dependency on Reynolds number, blade loading, and turbulence intensity levels (also used as promotor of different model scale boundary layer regimes) has been discussed to explain the improvements (or small differences) of the predicted model-scale performance. These differences (i.e. the occurrence of such phenomena in model-scale) turned case by case into very different scaling effects. Based on the test cases analysed, the relative importance of thrust and torque for the increase of the full-scale efficiency was largely dependent on the geometry, the loading conditions and the model-scale setup (i.e. flow conditions), more than on the expanded area ratio or Reynolds number as suggested by ITTC procedures. Trends in accordance with the traditional ITTC scaling (relatively small increase of thrust, consistent decrease of torque in full-scale, in magnitude increasing with the reduction of the propeller loading) have mostly been observed, but model-scale simulations at the highest (or at the lowest) rates of revolution evidenced, vice versa, a reduction in scale effects with increasing load. Opposite trends to ITTC have also been observed for very low expanded area ratio propellers, like the P1727. In these cases, full-scale thrust was observed most of the time to be lower than model-scale as a consequence of the unexpectedly high model-scale performance associated with the massive presence of laminar boundary layer (increased pressure component of the thrust, minimal influence of frictional forces due to laminar flow) at any tested model-scale Reynolds number.

This reduction of the full-scale thrust, observed for completely different reasons (Reynolds influence on the induced velocities, not on the friction on the blades), in the case of the accelerating ducted propeller, was not confirmed in the case of the decelerating nozzle. On the contrary, the increase of the full-scale thrust resulted, on average, much higher than the reduction of the torque for most of the loading conditions, while for the accelerating nozzle, the positive scale effect of the duct thrust was almost completely nullified by the lower performance of the blades, resulting in a full-scale efficiency that was mostly increased due to the reduction of the torque.

The systematic analyses of this paper point out once more the complexity of the propeller performance scaling process. It is not only (and probably, not mainly) driven by simple Reynolds effects on friction, but it is influenced in very different, and sometimes unexpected, ways by separation (which is sensitive to the type of boundary layer), viscous-inviscid interactions, loading conditions (from which flow separation depends) and definitely very specific geometrical features of the propeller, not simply the expanded area ratio or some typical characteristics at representative radii. This poses serious issues in defining, especially each time the flow similarity between model and full-scale is not respected (as when separation dominates model-scale performance), also with the aid of CFD calculations, a generalised scaling guideline or formulae to overcome and improve the standard ITTC procedure. At the same time, these numerical findings suggest the need to reconsider model- scale experimental procedures. In particular, they highlight the importance of ensuring the closest possible flow similarity with full- scale conditions, either by conducting measurements at Reynolds numbers consistently higher than those currently recommended, or by artificially triggering the transition to a turbulent boundary layer through appropriate stimulation techniques.

Disclosure statement

No potential conflict of interest was reported by the author(s).

ORCID

Stefano Gaggero http://orcid.org/0000-0001-8470-2955

References

Abdel-Maksoud M, Heinke HJ. 2002. Scale effects on ducted propellers. Proceedings of the 24th Symposium on Naval Hydrodynamics. 744–759.

Allan JF, Couch RB, Lerbs HWE, Telfer EV. 1951. Subject 1 – Reynolds number for model propeller experiments. 6th International Conference of Ship Tank Superintendents, ITTC, Washington, United States of America.

Baltazar J, Rijpkema D, Falcão de Campos J. 2021. Prediction of the propeller performance at different Reynolds number regimes with RANS. J Mar Sci Eng. 9(10):1115. https://doi.org/10.3390/jmse9101115

Baltazar J, Schuiling B, Kerkvliet M. 2023. Modelling of laminar-to-turbulent flow transition on a marine propeller using a RANS solver. 25th Numerical Towing Tank Symposium, NuTTS'23, Ericeira, Portugal.

Barkmann U, Heinke H-J, Lübke L. 2011. Potsdam propeller test case (PPTC). Proceedings of the Second International Symposium on Marine Propulsors, Hamburg, Germany.

Bhattacharyya A, Krasilnikov V, Steen S. 2015b. Scale effects on a 4-bladed propeller operating in ducts of different design in open water. Proceedings of the Fourth International Symposium SMP. 15.

Bhattacharyya A, Krasilnikov V, Steen S. 2016a. Scale effects on open water characteristics of a controllable pitch propeller working within different duct designs. Ocean Eng. 112:226–242. https://doi.org/10.1016/j.oceaneng.2015.12.024

Bhattacharyya A, Krasilnikov V, Steen S. 2016b. A CFD-based scaling approach for ducted propellers. Ocean Eng. 112:116–130. https://doi.org/10.1016/j.oceaneng.2016.06.011

Bhattacharyya A, Neitzel JC, Steen S, Abdel-Maksoud M, Krasilnikov V. 2015a. Influence of flow transition on open and ducted propeller characteristics. In Fourth International Symposium on Marine Propulsors, Austin, Texas, USA.

Brown Met al. 2014. Improving propeller efficiency through tip loading . 30th Symposium on Naval Hydrodynamics, Hobart, Tasmania, Australia.

Bulten N, Nikland M. 2011. On the development of a full-scale numerical towing tank Reynolds scaling effects on ducted propellers and wakefields. Second International Symposium on Marine Propulsors, Hamburg, Germany, 2011.

Eça L, Hoekstra M. 2008. The numerical friction line. J Mar Sci Technol. 13(4):328–345. https://doi.org/10.1007/s00773-008-0018-1

Eça L, Hoekstra M. 2014. A procedure for the estimation of the numerical uncertainty of CFD calculations based on grid refinement studies. J Comput Phys. 262:104–130. https://doi.org/10.1016/j.jcp.2014.01.006

Eça L, Kerkvliet M, Toxopeus SL. 2023. Comparison of RANS turbulence models for the simulation of smooth wall boundary-layers in pressure gradients at moderate and high Reynolds numbers. 10th International Conference on Computational Methods in Marine Engineering (MARINE 2023), Madrid, Spain.

Falcao de Campos JAC. 1983. On the calculation of ducted propeller performance in axisymmetric flows. PhD. Thesis, Delft University of Technology, The Netherlands.

Gaggero S. 2022a. Influence of laminar-to-turbulent transition on model scale propeller performances. Part I: fully wetted conditions. Ship and Offshore Structures. 17(4):715–727. https://doi.org/10.1080/17445302.2020.1863658.

Gaggero S. 2022b. Influence of laminar-to-Turbulent transition on model scale propeller performances. Part II: cavitating conditions. Ship and Offshore Structures. 17(4):772–791. https://doi.org/10.1080/17445302.2020.1866819.

Gaggero S. 2023. A study on the wake evolution of a set of RIM-driven thrusters. J Mar Sci Eng. 11(9):1659. https://doi.org/10.3390/jmse11091659

Gaggero S, González-Adalid J, Sobrino MP. 2016. Design and analysis of a new generation of CLT propellers. Appl Ocean Res. 59:424–450. https://doi.org/10.1016/j.apor.2016.06.014

Gaggero S, Rizzo CM, Tani G, Viviani M. 2012. EFD and CFD design and analysis of a propeller in decelerating duct. Int J Rotating Mach. 2012(1):1–15. https://doi.org/10.1155/2012/823831.

Gaggero S, Tani G, Viviani M, Conti F. 2014. A study on the numerical prediction of propellers cavitating tip vortex. Ocean Eng. 92:137–161. https://doi.org/10.1016/j.oceaneng.2014.09.042

Gaggero S, Villa D. 2018. Improving model scale propeller performance prediction using the $k-kL-\omega$ transition model in OpenFOAM. Int Shipbuild Prog. 65(2):187–226. https://doi.org/10.3233/ISP-180146.

González-Adalid Jet al. 2016. New generation of CLT® propellers. Proceedings of the 3rd International Conference on Maritime Technology and Engineering, MARTECH 2016, Lisbon, Portugal.

González-Adalid J, Sobrino MP, Gaggero S, Gennaro G, Moran-Guerrero A. 2018. The use of modern computational tools in the design process of unconventional propellers for performance prediction and full scale extrapolation. Proceedings of the 19th Conference on Ship and Maritime Research, Trieste, Italy.

Grlj CG, Degiuli N, Farkas A, Martić I. 2022. Numerical study of scale effects on open water propeller performance. J Mar Sci Eng. 10(8):1132. https://doi.org/10.3390/jmse10081132

Hasuike N, Okazaki M, Okazaki A, Fujiyama K. 2017. Scale effects of marine propellers in POT and self propulsion test conditions. Proceedings of the 5th International Symposium on Marine Propulsors, SMP. 17.

Hellsten H. 2005. New advanced k-w turbulence model for high-lift aerodynamics. AIAA J. 43(9):1857–1869. https://doi.org/10.2514/1.13754

Helma S. 2016. A scaling procedure for modern propeller designs. Ocean Eng. 120:165–174. https://doi.org/10.1016/j.oceaneng.2015.10.009

Helma S, Streckwall H, Richter J. 2018. The effect of propeller scaling methodology on the performance prediction. J Mar Sci Eng. 6(2):60. https://doi.org/10.3390/jmse6020060

Hughes G, Allan JF. 1951. Turbulence stimulation on ship models. Trans. SNAME. 59:281–314.

ITTC. 1978. Final report and recommendations of the propulsion committee to the 15th ITTC. in: Proceedings of the 15th ITTC.

ITTC. 2014. Testing and extrapolation methods propulsion, propulsor open water test. Recommended Procedures and Guidelines, 7.5-02-03-02.1.

ITTC. 2017a. 1978 Powering prediction method. Recommended procedures and guidelines, 7.5-02-03-01.4.

ITTC. 2017b. Scaling of conventional and unconventional propeller, open water data. Report of the Propulsion Committee of the 28th ITTC.

ITTC. 2017c. ITTC Benchmarking Test Case (https://www.sva-potsdam.de/en/ittc-benchmark/). Report of the Propulsion Committee of the 28th ITTC.

ITTC. 2024. Final report and recommendations of the resistance and propulsion committee to the 30th ITTC, in: Proceedings of the 30th ITTC (https://ittc.info/downloads/proceedings/30th-conference-hobart-2024/).

Kerkvliet M, Baltazar J, Schuiling B, Eça L. 2024. A numerical study on model propeller performance prediction including transitional and passively controlled boundary layer considerations. Proceeding of the Eight International Symposium on Marine Propulsors, Berlin, Germany.

Khraisat Q, Alves Lopes R, Persson M, Vikstrom M, Bensow R. 2023. Assessing scale effects on a propeller in uniform inflow condition. 25th Numerical Towing Tank Symposium.

Krasilnikov VI, Sun J, Zhang Z, Hong F. 2007. Mesh generation technique for the analysis of ducted propellers using a commercial RANSE solver and its application to scale effect study. Proceedings of the 10th Numerical Towing Tank Symposium (NuTTS'07).

Kuiper G. 1978. Scale effects on propeller cavitation inception (1978). Proceedings of the 12th Symposium on Naval Hydrodynamics, Office of Naval Research, Washington, D.C., United States of America.
Kuiper G. 1981. Cavitation inception on ship propeller models. PhD Thesis, Delft University of Technology, The Netherlands.
Langtry RB, Menter FR. 2009. Correlation-based transition modeling for unstructured parallelized computational fluid dynamics codes. AIAA J. 47(12):2894–2906. https://doi.org/10.2514/1.42362
Li DQ, Lindell P, Werner S. 2019. Transitional flow on model propellers and their influence on relative rotative efficiency. J Mar Sci Eng. 7(12):427. https://doi.org/10.3390/jmse7120427
Lopes R. 2021. Simulation of transition from laminar to turbulent regime in practical applications of incompressible flow. PhD thesis, Universidade de Lisboa – Instituto Superior Tecnico, Lisbon, Portugal.
Lücke T, Streckwall H. 2017. Experience with small blade area propeller performance. In Proceedings of the 5th International Symposium on Marine Propulsors, SMP. 17.
MARINET. 2014. Work package 2: marine energy system testing – standardisation and best practice – deliverable 2.23: Review of Tow Tank Limitations, MARINET – Marine Renewables Infrastructure Network, European Commission within the Call FP7, 7th Framework Program, Grant Agreement No. 262552, 2014.
Menter FR. 1994. Two-equation eddy-viscosity turbulence models for engineering applications. AIAA J. 32(8):1598–1605. https://doi.org/10.2514/3.12149
Menter FRet al. 2006. A correlation-based transition model using local variables—Part I:Model Formulation. J Turbomach. 128(3):413–422. https://doi.org/10.1115/1.2184352
Menter FR, Esch T. 2001. Elements of industrial heat transfer predictions. 16th Brazilian Congress of Mechanical Engineering (COBEM). 109.
Menter FR, Esch T, Kubacki S. 2002. Transition modelling based on local variables. 5th International Symposium on Turbulence Modeling and Measurements, Mallorca, Spain.
Menter FR, Kuntz M, Langtry R. 2003. Ten years of industrial experience with the SST turbulence model. Turbulence, Heat Mass Trans. 4(1):625–632.
Meyne K. 1968. Experimentelle und theoretische Betrachungen zum Maßstabseffekt bei Modellpropeller-Untersuchungen. Schiffstechnik, Vol 15.
Moran-Guerrero A, Gonzalez-Gutierrez LM, Oliva-Remola A, Diaz-Ojeda HR. 2018. On the influence of transition modeling and crossflow effects on open water propeller simulations. Ocean Eng. 156:101–119. https://doi.org/10.1016/j.oceaneng.2018.02.068
Müller SB, Abdel-Maksoud M, Hilbert G. 2009. Scale effects on propellers for large container vessels. First International Symposium on Marine Propulsors.
Rijpkema D, Baltazar J, Falcao de Campos J. 2015. Viscous flow simulations of propellers in different Reynolds number regimes. Proceedings of the Fourth International Symposium on Marine Propulsors, Austin, TX, USA (Vol. 31).
Rubino G, Abdel-Maksoud M. 2024. Model-and full-scale tip-raked marine propellers: analysis of the scale effects in open water conditions. Proceedings of the Eighth International Symposium on Marine Propulsors, Berlin, Germany.
Schuiling B, Kerkvliet M, Rijpkema D. 2024. An experimental study on visualisation and passive control of model propeller boundary layers. Proceeding of the Eight International Symposium on Marine Propulsors, Berlin, Germany.
Shin KW, Andersen P. 2017. CFD analysis of scale effects on conventional and tip-modified propellers. Fifth International Symposium on Marine Propulsors. VTT Technical Research Centre of Finland.
Siemens PLM. 2021. StarCCM+ Version 16.04.007 Users Guide.
Spalart PR. 2000. Strategies for turbulence modelling and simulations. Int J Heat Fluid Flow. 21(3):252–263. https://doi.org/10.1016/S0142-727X(00)00007-2
Streckwall H, Greitsch L, Muller J, Scharf M, Bugalski T. 2013. Development of a strip method proposed as new standard for propeller performance scaling. Ship Technol Res. 60(2):58–69. https://doi.org/10.1179/str.2013.60.2.002
The OpenFOAM Foundation. 2020. OpenFOAM 8.0 Users Guide.
van Lammeren WPA. 1939. Propulsion scale effects. North East Coast Institution of Engineers and Shipbuilders, Volume 56, pp. 115-152, London, The United Kingdom.
Villa D, Gaggero S, Tani G, Viviani M. 2020. Numerical and experimental comparison of ducted and non-ducted propellers. J Mar Sci Eng 8(4):257. https://doi.org/10.3390/jmse8040257
Walters DK, Leylek JH. 2002. A new model for boundary-layer transition using a single-point RANS approach. ASME 2002 International Mechanical Engineering Congress and Exposition. American Society of Mechanical Engineers, pp. 67–79.